

Arm-based control of a lower limb exoskeleton

Proof of concept of a novel approach based
on the shoulder kinematics

Fabio Izzi

Biomechanical Design Department - 3mE

Arm-based control of a lower limb exoskeleton

Proof of concept of a novel approach based on the shoulder kinematics

by

F. Izzi

to obtain the degree of Master of Science
at the Delft University of Technology,
to be defended publicly on Friday 10/05/2019 at 3:00 PM.

Student number: 4505050
Project duration: April 1, 2018 – February 1, 2019
Thesis committee: Prof. dr. ir. H. van der Kooij, TU Delft, supervisor
Prof. dr. ir. H. Vallery, TU Delft
Dr. L. Peternel, TU Delft

An electronic version of this thesis is available at <http://repository.tudelft.nl/>.

Abstract

Recognising the user's locomotive intentions is crucial for the correct functionality of exoskeletons and active orthoses. For gait applications, extrapolating control inputs from the arm swing may be worthwhile, since arm oscillations naturally occur during human locomotion. A similar method would be unaffected by severe impairments of the lower limbs, and there is evidence suggesting enhanced results of gait rehabilitation when arms and legs exercise together. In this thesis, we propose a control algorithm to drive online a lower limb exoskeleton through the arm swing. Contrary to a previous EMG-based approach by La Scaleia et al. (2014), our algorithm exploits shoulder kinematic data to mimic "single swinging", a natural mode of human interlimb coordination which is characterised by each arm swinging in-phase with the contralateral leg. Our proposed control architecture relies on two major modules: an Arm Observer and a Gait Generator. The Arm Observer consists of an adaptive frequency oscillator which extrapolates the frequency and phase of the arm swing by receiving online measurements of the angular shoulder position in the sagittal plane. This data is used by the Gait Generator to compute lower limb trajectories, based on regression models from a previous study by Koopman et al. (2014). We validated our controller through human-subject experiments, involving three participants walking on a treadmill with and without a lower limb exoskeleton, the Lopes II. When feed by data associated with natural walking, our adaptive frequency oscillator could very precisely replicate the arm swing frequency, stride cadence and timing of shoulder flexion peaks when walking faster than 0.5 m/s. When wearing the exoskeleton, our algorithm allowed the participants to cope with constant and variable treadmill velocities in the range of 0.5-1.25 m/s. As such, the results of this thesis show that our proposed approach can extend the applicability of arm-based control to walking speeds suitable for gait rehabilitation and assistance.

Contents

List of Figures	vii
List of Tables	ix
1 Introduction	1
1.1 Interlimb coordination: current understanding	2
1.2 Arm-based control: state-of-art	4
1.3 EMG-dependent arm-based control: limitation	5
1.4 Thesis objective and novelty	6
1.5 Report structure	6
2 Control architecture	7
2.1 Biomimicking single swinging: moving beyond EMG-based control and its limitations . . .	7
2.2 Control architecture	8
2.2.1 Arm Observer	8
2.2.2 Mapping Function	9
2.2.3 Trajectory Generator	11
2.2.4 Safety Mechanism	11
3 Experimental protocol	13
3.1 Materials	13
3.2 Participants	15
3.3 Walking Tasks	15
3.4 Control Modes	16
3.5 Data Analysis	16
4 Case Studies	19
4.1 Participant 1	20
4.1.1 Natural walking	20
4.1.2 Arm-based control: Task 1	22
4.1.3 Arm-based control: Task 2	24
4.2 Participant 2	29
4.2.1 Natural walking	29
4.2.2 Arm-based control: Task 1	31
4.2.3 Arm-based control: Task 2	34
4.3 Participant 3	38
4.3.1 Natural walking	38
4.3.2 Arm-based control: Task 1	39
4.3.3 Arm-based control: Task 2	42
5 Discussion	47
5.1 Analysis of natural walking	47
5.1.1 Tracking performance	47
5.1.2 Gait estimation	47
5.1.3 Side-differences	48
5.2 Analysis of task 1 and 2	48
5.2.1 Task 1: constant treadmill speed	48
5.2.2 Task 2: variable treadmill speed	49
5.3 Comparison to other techniques	50
5.4 Limitations	50

6	Conclusions	53
A	Mapping Function: Theoretical derivation	55
B	Simulink Implementation	57
B.1	Arm Observer	58
B.2	Gait Generator	58
B.3	Safety Mechanism & Gait Termination modules	59
B.4	Position Controller	60
B.5	Controller Switch	61
C	Consent Form	63
D	Heel-strike detection: algorithm	69
E	Data analysis: metrics formulation	73
E.1	Stride-cycle metrics	73
E.1.1	Arm-cycle metrics	74
E.1.2	Full-trial metrics.	74
F	Results: Additional figures	75
	Bibliography	87

List of Figures

1.1	Generalized control framework for active lower limb prostheses and orthoses	1
1.2	Model of shoulder accelerations transmitted by the trunk during walking	3
1.3	Model of CPG distribution within the CNS	4
1.4	Arm-based controller proposed by La Scaleia et al. [21]	5
2.1	Architecture of our arm-based controller	8
2.2	Key-events selected by Koopman et al. [16]	10
3.1	Our experimental set-up	13
3.2	Treadmill speed profiles for task 2.	15
4.1	Tracking performance, participant 1 - natural walking	20
4.2	Gait estimation, participant 1 - natural walking	21
4.3	Tracking performance, participant 1 - task 1	22
4.4	Gait generation, participant 1 - task 1	23
4.5	$ W $ and θ_{Amp} , participant 1 - task 1	23
4.6	Tracking performance - part 1, participant 1 - task 2	24
4.7	Tracking performance - part 2, participant 1 - task 2	25
4.8	Gait generation, participant 1 - task 2	26
4.9	$ W $ and θ_{Amp} , participant 1 - task 2	27
4.10	Tracking performance, participant 2 - natural walking	29
4.11	Gait estimation, participant 2 - natural walking	30
4.12	Tracking performance, participant 2 - task 1	31
4.13	Gait generation, participant 2 - task 1	32
4.14	$ W $ and θ_{Amp} , participant 2 - task 1	33
4.15	Tracking performance - part 1, participant 2 - task 2	34
4.16	Tracking performance - part 2, participant 2 - task 2	35
4.17	Gait generation, participant 2 - task 2	36
4.18	$ W $ and θ_{Amp} , participant 2 - task 2	37
4.19	Tracking performance, participant 3 - natural walking	38
4.20	Gait estimation, participant 3 - natural walking	39
4.21	Tracking performance, participant 3 - task 1	40
4.22	Gait generation, participant 3 - task 1	41
4.23	$ W $ and θ_{Amp} , participant 3 - task 1	41
4.24	Tracking performance - part 1, participant 3 - task 2	42
4.25	Tracking performance - part 2, participant 3 - task 2	43
4.26	Gait generation, participant 3 - task 2	44
4.27	$ W $ and θ_{Amp} , participant 3 - task 2	45
B.1	Simulink model of the Arm Observer.	57
B.2	Simulink model of the Gait Generator.	59
B.3	Simulink model of the Safety Mechanism.	60
B.4	Simulink model of the Gait Terminator.	60
B.5	Simulink model of the Position Controller.	61
B.6	Simulink model of the Controller Switch.	62
D.1	Representation of foot-off and heel-strike events as displacements of the centre of pressure.	69
F.1	Time trace of actual and estimated shoulder trajectories - participant 1, natural walking .	76

F.2	Average shoulder trajectory per stride cycle - participant 1, natural walking	77
F.3	Time trace of actual and estimated shoulder trajectories - participant 1, task 1	78
F.4	Comparison of right shoulder trajectories across control modes - participant 1	78
F.5	Time trace of actual and estimated shoulder trajectories - participant 2, natural walking .	79
F.6	Average shoulder trajectory per stride cycle - participant 2, natural walking	80
F.7	Time trace of actual and estimated shoulder trajectories - participant 2, task 1	81
F.8	Comparison of right shoulder trajectories across control modes - participant 2	82
F.9	Time trace of actual and estimated shoulder trajectories - participant 3, natural walking .	83
F.10	Average shoulder trajectory per stride cycle - participant 3, natural walking	84
F.11	Time trace of actual and estimated shoulder trajectories - participant 1, task 1	85
F.12	Comparison of right shoulder trajectories across control modes - participant 3	86

List of Tables

3.1	Lopes II joint degrees of freedom (actuated and/or measured)	14
B.1	Input-output to the Simulink model of the Arm Observer.	58
D.1	Heel-strike detection with natural walking data: Filtering parameters	70

Introduction

The interest in robotic gait rehabilitation and assistive technologies has noticeably increased over the last few years. A significant reason for that is the consistently increasing number of people who might benefit from such applications, caused by contemporary challenges such as global ageing populations and increments of patients with impaired mobility [4, 37]. Among the proposed solutions, the design of exoskeletons and active orthoses is a popular topic under investigation. In principle, these devices are expected to tackle crucial problems of gait rehabilitation and assistance. For instance, they could enable intense and repeatable training sessions without imposing an excessive physical burden on the therapists [4]. Furthermore, these devices can empower the end-users to partake in daily activities that require net-positive energetic outputs (e.g. stair climbing, running, jumping) [9, 37].

Designing an exoskeleton is not simple, and it requires to address problems belonging to a wide range of engineering disciplines [4, 47]. Among the many design challenges, the development of proper control architecture is crucial to promote a reliable human-machine interaction. As shown in figure 1.1, the general schematic of a controller for a lower limb exoskeleton is usually organised as a hierarchical structure composed of three main parts: the high, mid and low levels [37]. The high level is responsible for perceiving the user's locomotive intents. The mid level maps these detected

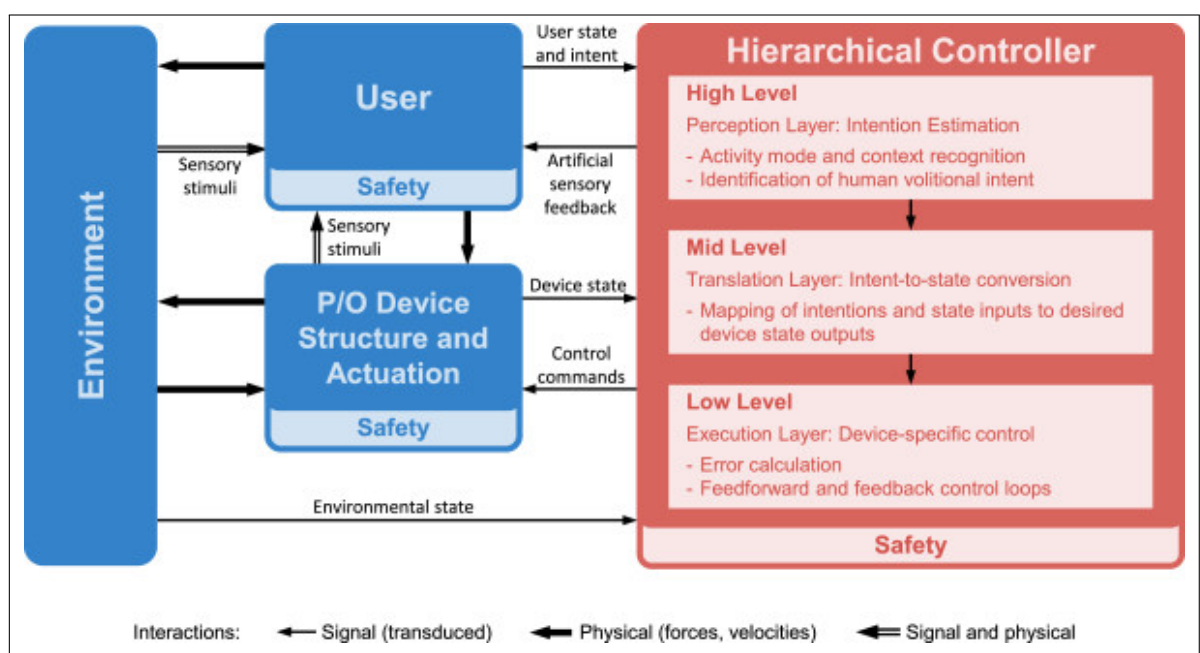


Figure 1.1: Generalized control framework for active lower limb prostheses and orthoses (P/O device). "Safety" includes all possible mechanisms (mechanical passive and actively controlled) to ensure an user-machine safe interaction. Figure retrieved from [37].

intentions into a set of target states for the robot actuators. The low level sends commands to the robot motor(s) to reduce the error between the desired and current device states. Ideally, the overall control structure should make the user perceive the wearable device as a natural extension of his/her own body, thus allowing a large variety of movements without an excessive cognitive load [37]. To reach this ideal functionality, and according to the just described architecture, the controller needs inputs from the user that are as representative as possible of both the desired motion and the current state of the human-machine interaction.

Biological information is usually redundant, which means that multiple signals from different body regions could be representative of similar control actions [4, 37]. Therefore, there is not a unique choice of user's signals to quantify locomotive intentions. A popular choice among the literature is to pick signals directly from the user's legs [44], often in the form of EMGs [37]. These data are among the most representative of human gait dynamics, because of the primary propulsive role of the lower limbs during bipedal locomotion. However, the main impediment of leg-based signals is that their measurement often requires the residual functionality of at least one of the two limbs. Unfortunately, this condition is not met by patients with a severe motor impairment of the lower body, which in turns are also those individuals who might benefit the most from assisting and rehabilitating technologies.

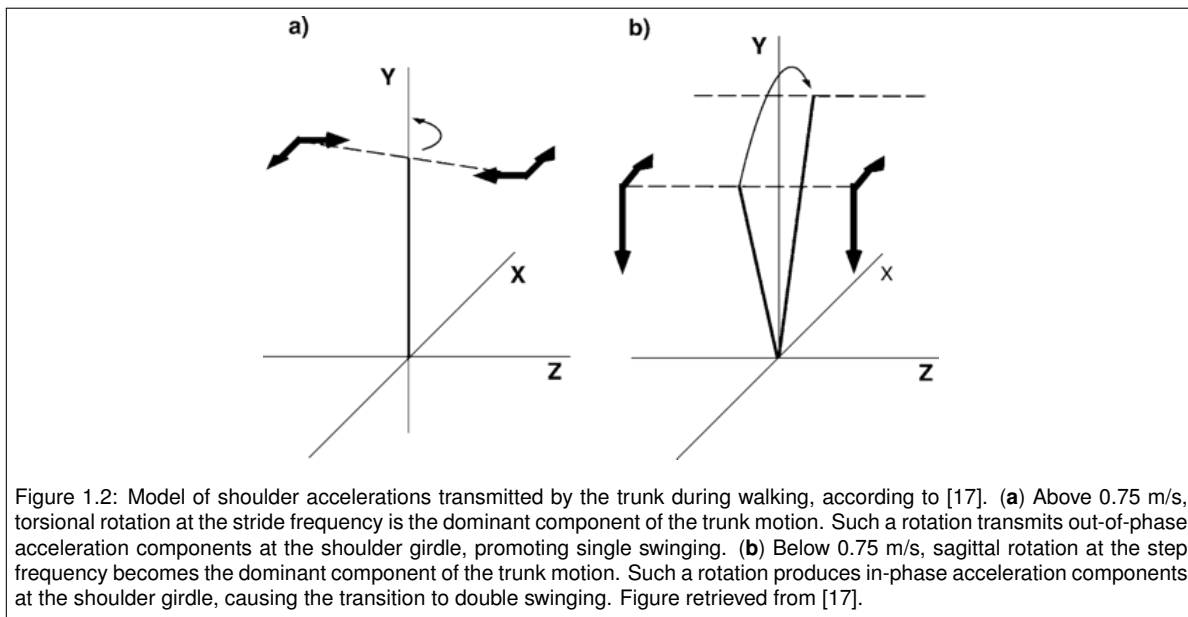
To overcome this problem, Brain-Computer Interfaces (BCIs) are appealing solutions. Brain signals contain the richest amount of information and can be used to extract features relevant to a large variety of locomotive actions [37]. However, this type of biological data is challenging to measure and process, mostly because brain activity is characterised by a dynamic interplay between several conscious and unconscious mental processes [5]. Another complication is that rhythmic movements, such as those of the limbs during bipedal locomotion, are likely primarily generated in the spinal cord [48]. Therefore, a conspicuous rate of gait-related neural information would not be carried by brain signals. Eventually, BCIs usually impose an intense cognitive effort on the user, who also needs extensive training before learning how to operate them correctly [35].

A less bio-inspired, but quite popular approach due to its easy implementation, is the design of "manual controllers". This category includes all those solutions where the user sends commands to the device by performing actions external to natural walking: for instance, by assuming specific trunk postures, moving the fingers into certain positions or pressing buttons on a remote [37]. These control strategies are not constrained to any physiological aspect of the gait. As such, they offer a vast number of design possibilities, seldom limited by the creativity of the designer. However, their "artificial nature" makes them often suboptimal concerning seamlessness and intuitiveness of the command actions [37].

The arm swing is a subtle feature of human locomotion since the upper limbs are not primarily recruited in the gait generation. Nevertheless, the motion of the arms occurs quite naturally while walking and there are reasons to believe that it can serve as a valid source of control signals for an exoskeleton [21]. For instance, the arms share with the legs the property of being a peripheral source of biological data, thus unaffected by concomitant mental activities and likely representative of neuronal computations in the spinal cord [21, 24]. At the same time, an arm-based controller might extend the use of lower limb exoskeletons to patients with entirely lost functionality of the legs, but still in control of the upper body. This control strategy might even benefit gait rehabilitation regarding treatment effectiveness, as many studies suggest that reactivation of neuronal pathways in the lower limbs is facilitated by including the arm swing within the training protocol [10, 24, 50].

1.1. Interlimb coordination: current understanding

For a long time the arm swing was regarded as a passive phenomenon driven by the gait dynamics, and thus merely investigated. From the second half of the twenty-century, the interest in human interlimb coordination increased consistently. This was mostly because of two major findings associated with walking while naturally swinging the arms: a faint muscle activity in the upper limbs [1] and a reduced metabolic cost of locomotion [6, 26, 38, 45]. Nowadays, it is still debated why the arm swing occurs and how it correlates to the movement of the rest of the body [24]. However, a part of the literature suggests that during natural walking upper and lower limbs move following two speed-dependent coordination patterns [7, 11, 17, 42]. The first mode, often referred to as "single swinging" [43], occurs at walking velocities higher than 0.75-0.8 m/s and it is characterised by each arm oscillating in-phase with the contralateral leg. The stride cadence entrains the upper limb oscillations, and thus the fre-



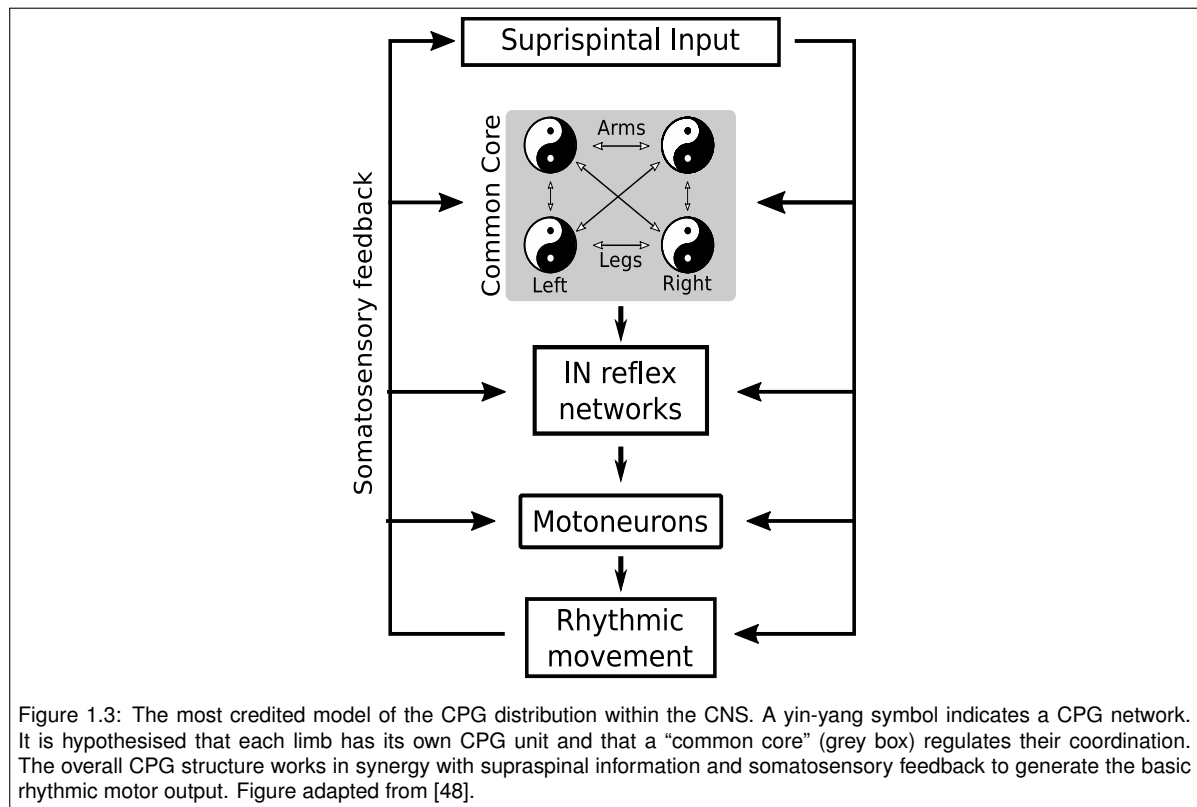
quency ratio between arm and leg rotations is 1:1.

At gait speeds below 0.8 m/s, the arm swing becomes less vigorous, with the upper limbs moving in parallel with each other and twice as fast as the legs. The step cadence now entrains the arm oscillations, making the frequency ratio between the arm and leg movements equal to 2:1. This second mode is often referred to as “double swinging” [43]. However, it is still argued whether it is a consistent feature of interlimb coordination since some experimental studies show that the transition is subject-specific, could involve only one side of the body, or even not occur at all [17]. Even the experimental protocol might influence the occurrence of double swinging: for instance, walking on a treadmill rather than overground was found to promote the preservation of single swinging [3].

Independently of the adopted mode of interlimb coordination, the amplitude of the arm swing is proportional to the walking speed [3, 7, 20, 33], even though some studies argue that this correlation is the artefact from a primary dependence on the step length [8, 22, 36]. Some articles report the presence of side asymmetries in the amplitude of the arm oscillations, but still, the literature is ambiguous about this finding: Gutnik et al. [12] observed the dominant hand swinging more vigorously, while others found the left arm to move with larger rotations, despite any hand dominance and side asymmetries in the lower limbs [2, 20, 25].

There are many hypotheses regarding the mechanism that causes human interlimb coordination. One possibility is that the synchronisation of the upper and lower limbs is analogue to that occurring in a system of coupled compound pendulums. As such, the natural pendulum frequency of each limb was suggested to be the leading factor in determining the existence of two interlimb coordination modes and the associated transition [42, 43]. This view, however, has also received some criticism [7], and more likely, different factors contribute to the generation of interlimb coordination. For instance, the trunk might mediate the relative motion of the limbs, by adjusting its torsional elasticity [18] or, as shown in fig.1.2, by changing the dominant acceleration component transmitted to the shoulder girdles [17].

According to the detected EMG signals in the shoulder and arm muscles during normal walking, the central nervous system (CNS) also seems to play an active role in the generation of interlimb coordination [1, 15, 19]. The muscle activity supporting the arm swing is quite weak (about 5% of maximum voluntary contractions [13]) and predominantly carried by the anterior and posterior deltoids [19]. Because of the observed weakness, it can not be excluded that its primary function is to stabilise the shoulder joints against foot contact with the ground [28]. However, a more leading hypothesis is that rhythmic muscle contractions in the upper and lower limbs are produced by central pattern generators (CPGs) [24]. A CPG consists of networks of oscillating interneurons located in the spinal cord that can produce rhythmic muscle activity without the need of any rhythmic input [48]. Despite their ability to operate as stand-alone units, there is enough evidence supporting a close interplay of CPGs



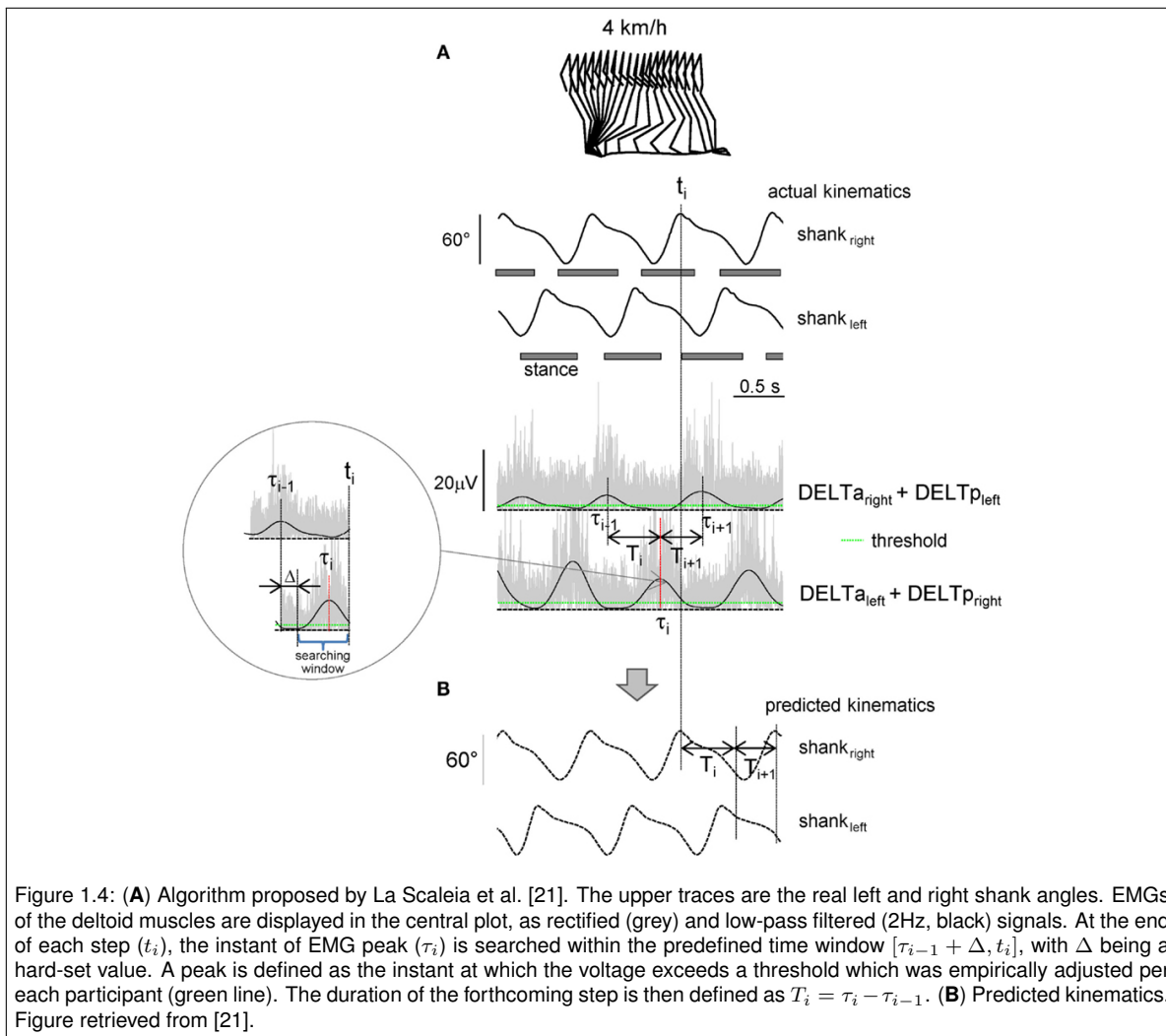
with both supraspinal neuronal activity and somatosensory feedback (see fig.1.3) [48, 49]. However, direct evidence of CPGs in humans is still missing, since impractical and ethically challenging to collect [48–50]. Even more challenging is to identify the exact web of interneurons forming a CPG network, which are often indistinguishable from those controlling peripheral reflexes [48]. Nowadays, the most credited hypothesis is that each limb has one CPG structure and that a “common core” provides their synchronisation (see fig 1.3). The nature of this “common core” is debated: it might be a pool of shared interneurons, a set of propriospinal connections, or even a physiological organ not yet identified [48].

1.2. Arm-based control: state-of-art

Even though very scarce in number, some studies have investigated control algorithms and regression techniques to extract gait dynamics from data associated with the arm swing. For instance, Chéron et al. [5] demonstrated that a dynamic recurrent neural network, composed by 20 hidden units, can reconstruct (offline) the elevation angles of the thigh, shank and foot by using as input the EMG signals of the anterior and posterior deltoids. Yoon et al. [46], instead, developed a full-body rehabilitation robot whose control architecture adapts the training speed based on the interaction torques between the machine upper levers and the user’s arms.

Among this limited group of articles, the work of La Scaleia et al. [21] emerges as the most interesting. This study is the only one which proposes an arm-based controller for piloting in real-time a lower limb exoskeleton. In particular, La Scaleia et al. [21] proposed an algorithm that predicts online the kinematics of a forthcoming step based on EMG measurements of the anterior and posterior deltoids, as shown in fig.1.4. Their arm-based controller first reduces the deltoid EMG data into two signals by combining the activity of the antagonist, contralateral muscle pairs: the activity of the left anterior deltoid is summed to that of the right posterior deltoid, and vice-versa. This sensory fusion technique permits to partially compensate for the weakness of the shoulder muscular activity associated with the arm swing. Then, the two resulting signals are filtered and the time elapsed between two consecutive peaks, one per each signal, is computed. This time variable defines the desired duration of the forthcoming step, and a set of predefined joint trajectories for the lower limbs are stretched accordingly.

First, this arm-based controller was validated offline by feeding pre-recorded deltoid EMGs that



were measured during walking at constant and variable gait speeds. Then, La Scaleia et al. [21] tested two real-time implementations, both including healthy participants. In the first protocol, people were asked to drive an avatar in a virtual reality environment. The majority of the participants could generate stable walking of the avatar for an entire minute, at both constant and variable walking speeds in the range of 3-5 km/h. During the second experiment, one single person was trained to drive an actual exoskeleton with their arm-based controller implemented on. This participant could execute 7 to 10 consecutive steps without interruptions.

1.3. EMG-dependent arm-based control: limitation

Despite reporting two successful implementations involving actual participants, La Scaleia et al. [21] proposes a control algorithm which has a critical limitation: it depends on EMG measurements of the deltoid contractions. Recording appropriately this type of physiological data can be challenging and usually requires extensive signal processing techniques to decode the raw information meaningfully [29]. When dealing with the muscle contractions associated with the arm swing, the situation is made even more challenging by the weakness of this muscular activity. La Scaleia et al. [21] only partly tackled the issue by combining signals of the side-antagonist deltoids. Eventually, they had to ask the participants to emphasise their arm rotations when testing the arm-based controller. Furthermore, the study does not specify the relation of this emphasised arm swing amplitude with the walking speed: participants might have maintained a constant amplitude across the speed conditions, and produced different gait velocities by just changing the swing frequency. During normal walking, however, the amplitude of the arm swing is proportional to the walking speed, with very weak oscillations for the slower

gaits. As such, the proposed EMG-based algorithm might not be suitable for real gait rehabilitation and assistance scenarios, which involve much slower walking speeds (typical range: 0.5-4 km/h [16]) than those tested in [21].

1.4. Thesis objective and novelty

This thesis project aimed to extend the applicability of an arm-based controller for a lower limb exoskeleton to a range of speeds suitable for gait rehabilitation and assistance. The novelty of our study is to propose a method based on the kinematics of the arm-leg coordination. Compared to previous techniques based on the muscle activity of the upper body [5, 21], this method does not require complex signal processing or emphasised rotations of the arms. By not constraining a priori the arm swing amplitude, we also expected our control strategy to promote a more natural adaptation of the arm swing amplitude to the gait velocity.

1.5. Report structure

The current report is organised as follows. Chapter 2 describes the structure of our proposed controller. It contains the explanation of the biological foundation for our algorithm, an overview of the control architecture and the mathematical descriptions of the composing modules. Chapter 3 explains the experimental protocol that we used to validate our algorithm and the metrics that we computed for the result analysis. Chapter 4 reports the results of the experiments, organised in a case-study fashion. Discussion and conclusions are given in Chapters 5 and 6, respectively.

2

Control architecture

This chapter describes the arm-based controller which we propose with this thesis project. The first section explains the biological foundation of the method and the type of interlimb coordination promoted. Later, an overview of the control architecture is given, contextualising the controller role within the human-machine interaction. Eventually, this chapter describes the main modules composing the control structure. The discussion, however, is restricted to the theoretical characterisation of the algorithm, that is on the mathematical representation of its fundamental components. In this way, the description of the algorithm is kept independent from those aspects uniquely related to the actual exoskeleton on which it is applied. The description of the model-based code that we used to validate our algorithm on a physical exoskeleton is given in Appendix B.

2.1. Biomimicking single swinging: moving beyond EMG-based control and its limitations

The work of La Scaleia et al. [21] has shown the feasibility of controlling a lower limb exoskeleton through the arm swing (see Chapter 1). However, the algorithm which they proposed relies on the deltoid muscular activity to generate the gait. Such a design choice is limiting. In particular, it forced emphasised arm swing amplitudes for the range of walking speeds that they studied, 3-5 km/h. During normal walking, the arm swing amplitude is proportional to the gait velocity and approaches quite small oscillations when walking slower than 2.7 km/h. Considering also that gait rehabilitation and assistance involve training speeds much slower than those tested by La Scaleia et al. [21], relying on EMG data weakens the applicability of their proposed algorithm.

Analysis of the literature on the interlimb coordination points out that upper and lower limbs move according to specific coordination modes (single and double swinging), each associated with a specific interlimb frequency- and phase-locking (see Chapter 1). In this thesis, we propose a control architecture that uses arm-related kinematic data to generate the joint trajectories for a lower limb exoskeleton. By moving beyond the use of EMG data, this method has the potential to overcome the limitations in [21], and extend the feasibility of arm-based control to a range of speeds more appropriate for gait rehabilitation and assistance.

The arm-leg coordination established by our algorithm mimics single swinging. In particular, it makes the contralateral upper and lower limbs have the same frequency and phase of rotation, with a peak of shoulder flexion coinciding with the contralateral heel-strike. According to part of the literature [3], the actual phase offset between heel-strikes and peaks of shoulder flexion is speed dependent (but convergent to zero as the walking speed increases). We decided not to implement this dependence on the speed because the literature neither accurately quantifies it, nor describes the influence of wearing an exoskeleton on it. As such, we simplified the design by assuming a perfect coincidence between heel-strikes and flexion peaks. Later, we checked the validity of this assumption through our experimental analysis (see Chapter 4). Because of similar literature uncertainties, we did not implement a transition to double swinging when the walking speed reduces below a certain threshold.

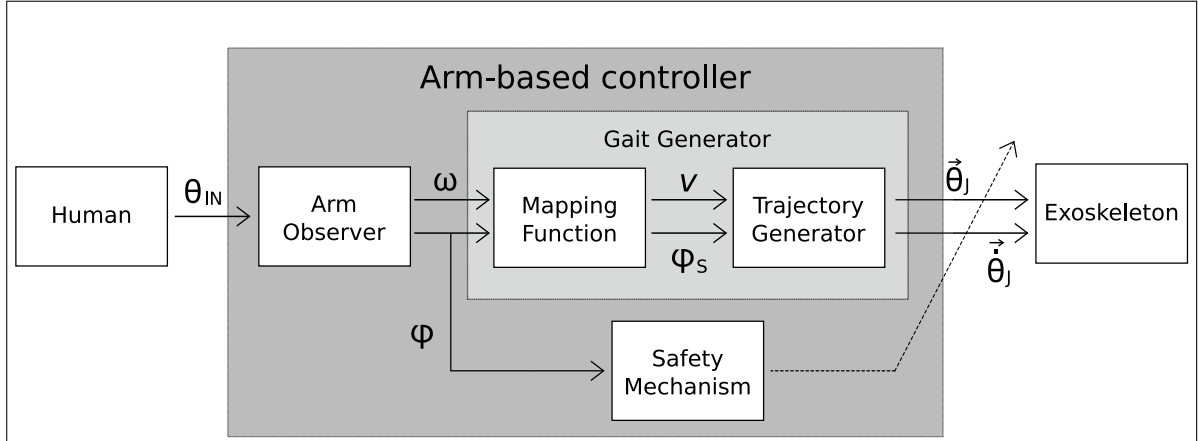


Figure 2.1: Architecture of our arm-based controller (dark grey area) and its function within the human-machine interaction. The controller receives the user's angular shoulder position, θ_{IN} , from which the Arm Observer estimates the frequency ω and phase ϕ of the arm swing. The Mapping Function module estimates the user's desired walking speed v from ω and converts ϕ into the phase of the stride cycle ϕ_S . Then, the Trajectory Generator uses this information to compute two vectors containing joint angular positions, $\vec{\theta}_j$, and velocities, $\vec{\dot{\theta}}_j$. These vectors constitute the target dynamics for the exoskeleton. The Mapping Function and Trajectory Generator compose the Gait Generator module (light grey area). In parallel to the latter, the Safety Mechanism triggers gait termination (decoupling dotted line between the arm-based controller and the exoskeleton) if a faulty estimation of ϕ occurs. All the variables just presented are time-dependent, which was not explicitly illustrated for better readability.

2.2. Control architecture

Figure 2.1 depicts the architecture of our arm-based controller and its interaction with the user and the exoskeleton. The control structure consists of three main components: the Arm Observer, the Gait Generator and the Safety Mechanism. The Arm Observer contains an adaptive frequency oscillator which estimates the frequency, $\omega(t)$, and phase, $\phi(t)$, of the arm swing from real-time measurements of the angular shoulder position in the sagittal plane, $\theta_{IN}(t)$. The Gait Generator converts the two outputs of the Arm Observer into joint reference trajectories for the exoskeleton, expressed as vectors of joint angular positions and velocities, $\vec{\theta}_j(t)$ and $\vec{\dot{\theta}}_j(t)$ respectively. Specifically, it performs this function through two submodules:

- Mapping Function: converts $\omega(t)$ into the expected walking speed, $v(t)$, and $\phi(t)$ into an estimation of the phase of the stride cycle, $\phi_S(t)$;
- Trajectory Generator: receives $v(t)$ and $\phi_S(t)$ as inputs, and by means of regression models inspired by the work of [16], produces the vectors $\vec{\theta}_j(t)$ and $\vec{\dot{\theta}}_j(t)$.

In parallel to the Gait Generator, the Safety Mechanism continuously inspects the estimated phase of the shoulder rotation, looking for a non-monotonic progression of $\phi(t)$. If a similar situation occurs, this module triggers gait termination to prevent dangerous discontinuities in the robot trajectories.

Our proposed control architecture does not require any data processing of its input signal, $\theta_{IN}(t)$, since the adaptive frequency oscillator already embeds filtering properties. The controller needs the data of only one shoulder to work, but it does not allow to start the gait. Also, the adaptive frequency oscillator requires a few arm swing cycles to converge to the shoulder signal. When testing the algorithm on a real-time implementation, we started the gait in position control (see Chapter 3), with the Arm Observer receiving the shoulder rotation signal, but the Gait Generator decoupled from the exoskeleton. Only after convergence of the adaptive frequency oscillator, the control mode was switched from position to arm-based control, as explained in Appendix B.

2.2.1. Arm Observer

The Arm Observer is composed of an adaptive frequency oscillator, which is a non-linear dynamic system capable of synchronising with a given periodic input. The literature contains several articles

proposing techniques to design adaptive frequency oscillators. In this thesis, we considered the work of Ronsse et al. [34], which is in turn based on the adaptation rule described in Righetti et al. [30]. We chose this specific implementation because of its:

1. rapid convergence and excellent tracking of almost harmonic signals, as we expected the shoulder rotation to be during the arm swing;
2. embedded zero-delay filtering properties, and thus intrinsic robustness against input noise;
3. previous records of successful use in rehabilitation/assistance robotics [34];
4. straightforward interpretation of the tunable parameters;

In mathematical terms, this adaptive oscillator consists of the following set of equations, which we present separated into three groups just for allowing a better description:

$$\begin{aligned}\theta(t) &= \alpha_0(t) + \alpha_1(t) \cdot \sin(\phi(t)) \\ \dot{\phi}(t) &= \omega(t) + \nu \cdot F(t) \cdot \cos(\phi(t))\end{aligned}\quad (2.1)$$

$$F(t) = \theta_{IN}(t) - \theta(t) \quad (2.2)$$

$$\begin{aligned}\dot{\omega}(t) &= \nu \cdot F(t) \cdot \cos(\phi(t)) \\ \dot{\alpha}_0(t) &= \eta \cdot F(t) \\ \dot{\alpha}_1(t) &= \rho \cdot F(t) \cdot \sin(\phi(t))\end{aligned}\quad (2.3)$$

where t is the independent time variable and \dot{x} the time derivative of a generic x variable, $\theta(t)$ the oscillator output state, $\alpha_0(t)$ and $\alpha_1(t)$ the offset and amplitude of the oscillations respectively, $\phi(t)$ the oscillator phase, with $\phi(t) \in [0, 2\pi]$, $\theta_{IN}(t)$ the (periodic) driving input, $\omega(t)$ the oscillator natural frequency, and ν , η and ρ learning coefficients.

An intuitive understanding of the behaviour of this dynamical system is as follows. The first two equations (eqs. 2.1) represent the dynamics of a phase oscillator with offset and amplitude that are time-variable, and with frequency $\phi(t)$ that depends on the error between the target signal and the oscillator state, $F(t)$ (eq. 2.2). The remaining equations (eqs. 2.3) ensure that the offset, amplitude and frequency of the oscillator converge to values that minimise this error, thus making $\theta(t)$ converging to $\theta_{IN}(t)$. In a different perspective, this adaptive frequency oscillator can be seen as a sinusoid which adapts its amplitude, offset and frequency so to match a target signal.

The learning behaviour is controlled by the coefficients ν , η and ρ , with higher values producing a faster synchronisation. However, setting high learning parameters comports larger fluctuations of $\alpha_0(t)$, $\alpha_1(t)$ and $\omega(t)$, which are destabilising for the oscillator dynamics and can prevent the synchronisation to occur. Therefore, there is a trade-off to pay between high responsiveness of the system and the stability of its synchronising behaviour. In [34], the following learning parameters were used: 20, 5 and 5 for ν , η , ρ respectively. After some pilot tests, we chose smaller values for our implementation: 6.5, 1.5 and 1.5 respectively. Higher gains comported too aggressive dynamics, often resulting in a non-monotonic progression of $\phi(t)$ and gait termination triggered by the Safety Mechanism.

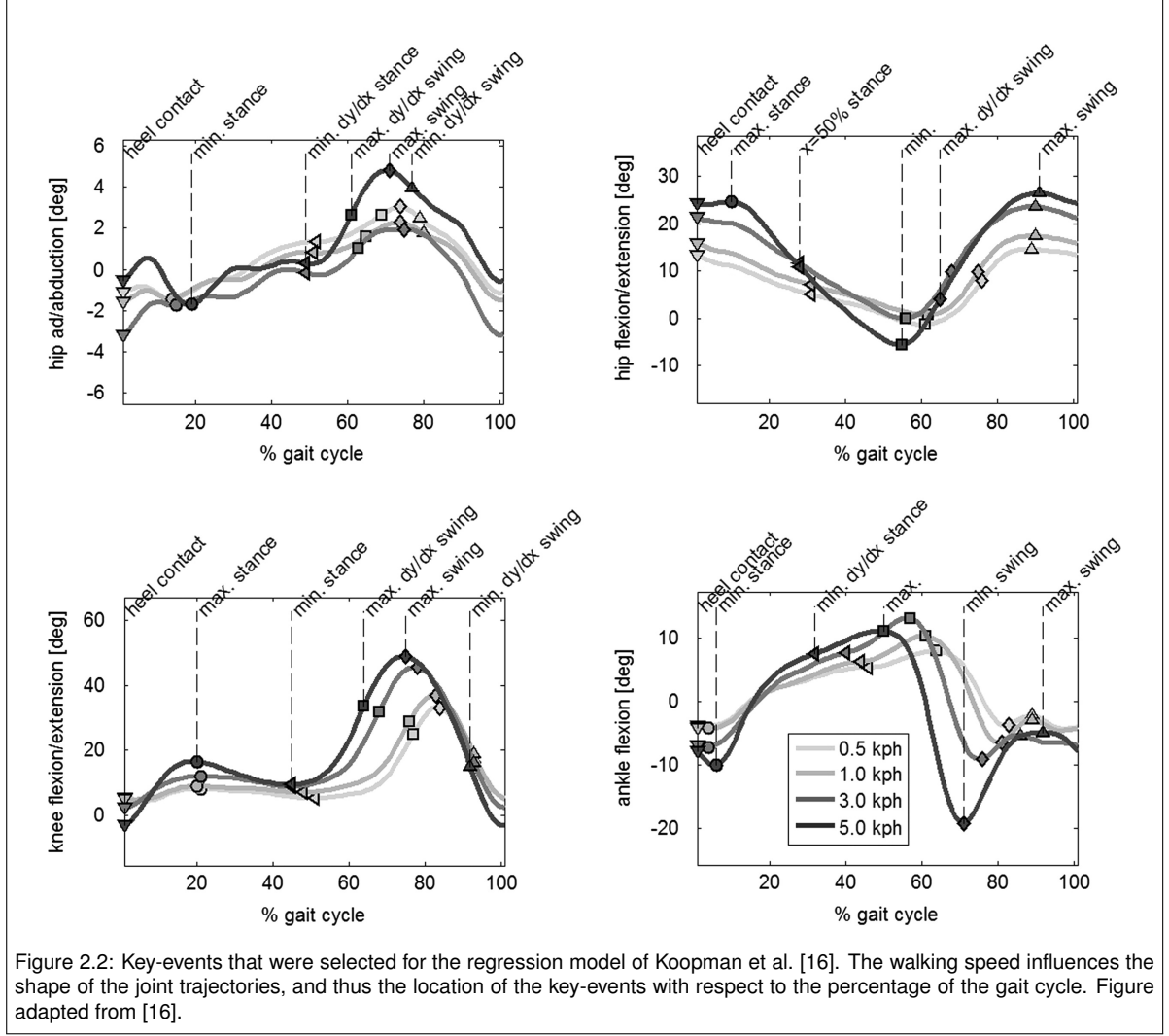
2.2.2. Mapping Function

The role of the Mapping Function module is to convert the outputs of the Arm Observer into inputs for the Trajectory Generator. In particular, this latter module requires two signals: a target walking speed, $v(t)$, and an estimation of the phase of the stride cycle, $\phi_S(t)$.

By rearranging some of the equations described in [16] (see Appendix A), we derived first a relation between $v(t)$, expressed in m/s, and the stride cadence $\omega_S(t)$, expressed in Hz:

$$v(t) = 4 \omega_S^2(t) \cdot \frac{\beta_0 + \beta_2 \cdot h}{1 - 4\beta_1 \cdot \omega_S^2(t)} \quad (2.4)$$

where: h is the patient height, β_0 , β_1 and β_2 regression coefficients measured in [16] and equals to -0.532 , 0.020 and 0.47 , respectively. During single swinging, the stride cadence is equal to the



frequency of the arm swing. By assuming that the parameter $\omega(t)$ of the adaptive frequency oscillator approximates closely the value of the arm swing frequency, in equation 2.4 we replaced $\omega_S(t)$ by $\omega(t)$, with this latter quantity previously converted from rad/s to Hz.

In order to estimate the phase of the stride cycle, we looked once again into the biomechanics of single swinging, which are characterised by contralateral arm and leg oscillating in phase with each other. Thus, we approximated $\phi_S(t)$ with the phase of the adaptive frequency oscillator $\phi(t)$, which in turn estimates the phase of the arm swing. $\phi(t)$ is computed by the Arm Observer in radiant, while the Trajectory Generator needs $\phi_S(t)$ in the percentage of a stride cycle. As such, we implemented the following relation:

$$\phi_S(t) = \frac{100}{2\pi} (\phi(t) - \pi/2) \quad (2.5)$$

where $-\pi/2$ is necessary to match the maximum flexion of the right shoulder, which occurs at $\phi(t) \simeq \pi/2$, with a left heel-strike, which must occur at $\phi_S(t) = 0\%$ according to conventions in the Trajectory Generator. As explained above, our algorithm requires the signal of only one shoulder to work, and the literature does not provide convincing pieces of evidence to prefer one body side (see Chapter 1). We decided to use the right shoulder because easier to match with the stride cycle conventions used in the Trajectory Generator. In our experimental analysis, we partly investigated the dependence of our algorithm functionality on the input shoulder (see Chapters 4).

2.2.3. Trajectory Generator

Based on the method proposed in Koopman et al. [16], the Trajectory Generator produces pre-defined joint trajectories that are eventually sent to the exoskeleton as the vector signals $\vec{\theta}_j(t)$ and $\vec{\dot{\theta}}_j(t)$. Each reference trajectory is generated by interconnecting a number (2 to 6) of key-events with a 3rd or 5th order spline. The key-events consist of the heel-strike, which defines the start of the stride cycle, and a set of extreme values in the joint angular position and velocity profiles (see fig. 2.2). As such, each key-event characterises a specific phase of the stride cycle in terms of joint angle, angular velocity and angular acceleration (for 5th order), or joint angle and angular velocity (for 3rd order). Considering a 5th order spline¹, the i -th key-event of the j -th joint, $K_{j,i}$, is described as:

$$K_{j,i} = \left(\phi_{j,i}, \theta_{j,i}, \dot{\theta}_{j,i}, \ddot{\theta}_{j,i} \right) \quad (2.6)$$

where: $\phi_{j,i}$ is the phase of the stride cycle associated with $K_{j,i}$, and $\theta_{j,i}$, $\dot{\theta}_{j,i}$, $\ddot{\theta}_{j,i}$ are the corresponding joint angular position, velocity and acceleration, respectively. The four parameters defining a key-event can vary according to the gait speed and user's length. This aspect is modelled in the Trajectory Generator by computing the variables in equation 2.6 through the following regression models:

$$\begin{aligned} \phi_{j,i} &= (\Phi_{1,j,i} + \Phi_{2,j,i} \cdot v + \Phi_{3,j,i} \cdot v^2 + \Phi_{4,j,i} \cdot h) \pmod{100} \\ \theta_{j,i} &= Y_{1,j,i} + Y_{2,j,i} \cdot v + Y_{3,j,i} \cdot v^2 + Y_{4,j,i} \cdot h \\ \dot{\theta}_{j,i} &= YY_{1,j,i} + YY_{2,j,i} \cdot v + YY_{3,j,i} \cdot v^2 + YY_{4,j,i} \cdot h \\ \ddot{\theta}_{j,i} &= YYY_{1,j,i} + YYY_{2,j,i} \cdot v + YYY_{3,j,i} \cdot v^2 + YYY_{4,j,i} \cdot h \end{aligned} \quad (2.7)$$

where: $(\pmod{100})$ indicates the phase wrapping ($\phi_{j,i}$ resets to 0 after reaching 100%), h is the patient's body length, $v(t)$ is the target walking velocity, and $\Phi_{j,i}$, $Y_{j,i}$, $YY_{j,i}$ and $YYY_{j,i}$ are regression coefficients determined by measuring several (healthy) gait trajectories [16]. The time dependence of $v(t)$ in the set of equations 2.7 was dropped for better readability only. The Trajectory Generator assumes the gait to be symmetric: the reference trajectories are initially determined for the left leg, and those of the right side are produced by adding/subtracting 50% to the Φ_1 parameter of each key-event. Therefore, the Trajectory Generator fully characterises the robotic gait once it receives as inputs: an estimation of the stride cycle phase, the patient's length and a target walking speed.

2.2.4. Safety Mechanism

The Safety Mechanism controls that the $\phi(t)$ parameter of the adaptive frequency oscillator progresses monotonically. According to equation 2.5, a non-monotonic progression would result in a non-monotonic growth of the gait phase $\phi_S(t)$, a trend that compromises the functionality of the Trajectory Generator. In order to avoid such a scenario, the Safe Mechanisms subtracts the current and previous values of $\phi(t)$:

$$\Delta\phi(t) = \phi(t - \Delta t) - \phi(t)$$

where Δt indicates the integration time between two consecutive algorithm iterations. Then, gait termination is triggered if the following condition is true:

$$\Delta\phi(t) \in (0, \pi]$$

The presence of an upper boundary is crucial since $\phi(t)$ drops from 2π to 0 at the end of a shoulder rotation cycle. Including an upper threshold consents to interrupt non-monotonic progressions of $\phi(t)$ while allowing its phase wrapping.

The Safety Mechanism can trigger gait termination, but can not execute the breaking action directly. This is because the algorithm for executing gait termination usually depends on the exoskeleton in use. As such, we report this part of the controller in Appendix B.

¹The formulation for a 3rd order spline is obtained by removing the acceleration terms.

3

Experimental protocol

This chapter describes the experimental protocol that we used to evaluate the correct functionality of our arm-based controller when applied on real-time implementations. First, the materials are introduced, emphasising on the description of the lower limb exoskeleton that we used in our experiments. After, participants and testing conditions are described. The chapter ends by presenting the metrics that we selected for the result analysis. Appendix E gives more details on the exact formulations that we used to compute these metrics.

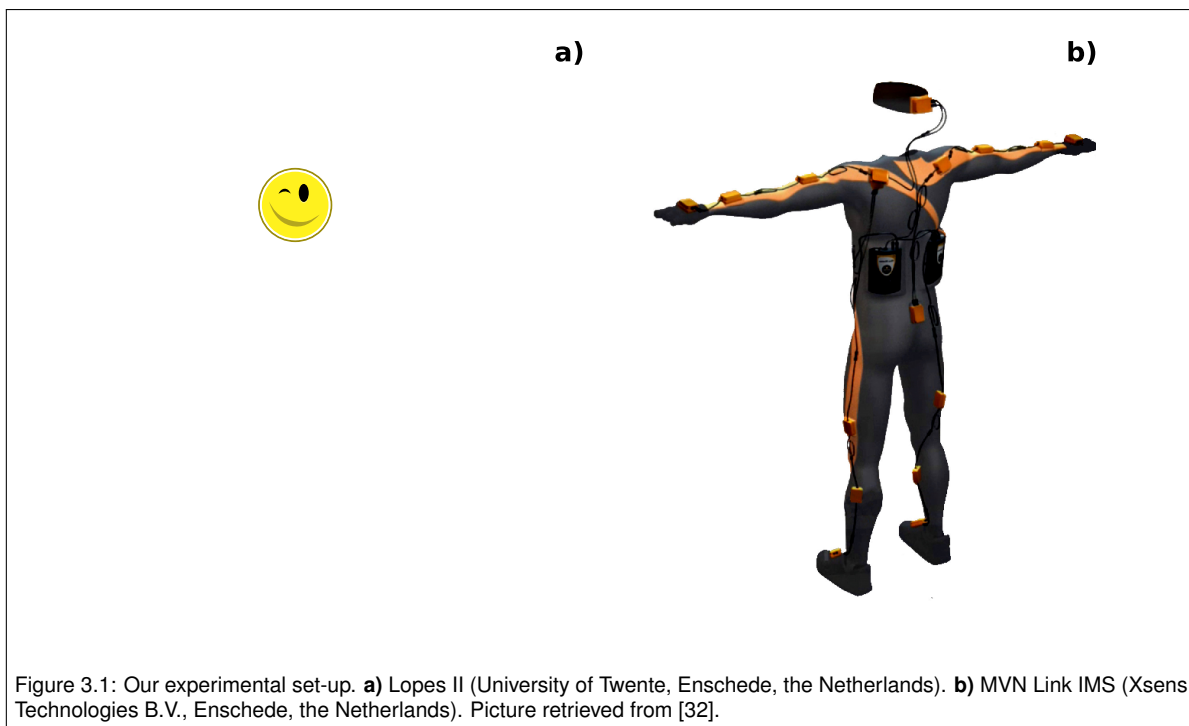


Figure 3.1: Our experimental set-up. **a)** Lopes II (University of Twente, Enschede, the Netherlands). **b)** MVN Link IMS (Xsens Technologies B.V., Enschede, the Netherlands). Picture retrieved from [32].

3.1. Materials

To validate our arm-based controller on a real-time implementation, we implemented the algorithm on the Lopes II (Fig.3.1-a), which is a treadmill-based lower limb exoskeleton developed at the University of Twente [23]. The robot has several degrees of freedom (table 3.1), but only eight are actuated: hip flexion/extension, hip abduction/adduction, knee flexion/extension, pelvis forward/aft and pelvis mediolateral. The Lopes II is driven by admittance control, and thus it can operate by receiving as input target trajectories and stiffness per each actuated degree of freedom.

Table 3.1: Lopes II joint degrees of freedom (actuated and/or measured), with abbreviations as used in the Lopes Development Library. Positive directions refer to the user's point of view.

#	Abbreviation	Joint description	Positive direction (for HLC)	Actuated	Measured
1	PX	Pelvis forwards/backward	Forwards	Y	Y
2	PZ	Pelvis left/right	Right	Y	Y
3	LHA	Left hip abduction/adduction	Abduction	Y	Y
4	LHF	Left hip flexion/extension	Flexion	Y	Y
5	LKF	Left knee flexion/extension	Flexion	Y	Y
6	LAP	Left ankle plantarflexion	Plantarflexion	-	Y
7	RHA	Right hip abduction/adduction	Abduction	Y	Y
8	RHF	Right hip flexion/extension	Flexion	Y	Y
9	RKF	Right knee flexion/extension	Flexion	Y	Y
10	RAP	Right ankle plantarflexion	Plantarflexion	-	Y
11	PY	Pelvis up/down	Up	-	Y
12	PAX	Pelvis axial rotation	Right hip forward	-	Y
13	POB	Pelvis obliquity	Left hip up	-	Y

Setting a stiffness coefficient to zero makes the system renders itself transparent along the degree of freedom associated with that parameter. Setting all joint stiffness coefficients to zero is called “Zero Impedance mode”, and results in the robot minimising the effects of its dynamics on the user. On the contrary, very high stiffness coefficients make the robot tracking the given trajectories while resisting to any perturbation exerted by the user. For our experiments, we chose a very stiff set-up for the hip and knee degrees of freedom, with each corresponding stiffness coefficient equal to about 1300 Nm/rad. This was because of the group of participants involved in our experiments: they were all healthy individuals, and thus potentially able to correct and stabilise wrongly-generated trajectories under more compliant configurations. Furthermore, a stiff response of the Lopes II is more representative of full-motion assistance and early rehabilitation stages, i.e. those critical conditions in which the user's impairment is so severe to make the robot largely in charge of the gait production. On the contrary, we set the stiffness of the pelvis degrees of freedom to zero, in an attempt to imitate the dynamics of mobile exoskeletons, which are usually not actuated at this joint. Still, this is a rough approximation since the Lopes II differs from mobile devices for several aspects: it misses ankle actuation, does not allow to tilt over the ankle with straight leg-trunk complex, and overall provides more support against falls thanks to its rigid structure. Furthermore, reproducing a behaviour typical to all exoskeletons is tricky, or even impossible, considering that every device dynamics are made unique by the specific hardware components and low-level control strategies.

There are multiple sensors instrumented in the Lopes II (and its treadmill), which allow recording both joint kinematics and ground-foot contact dynamics. Sensors and actuators communicate with the Low-level Controller (LLC), a PC which runs on Linux Real-Time and takes care of the low-level control of the system. The high-level control is carried by the High-level Controller (HLC), a Matlab/Simulink - xPC Target (the Mathworks, Natick, MA) in communication with the LLC by a UDP interface. Therefore, to test our arm-based controller with the Lopes II, we implemented our algorithm in a Matlab/Simulink Real-Time model and downloaded it in the HLC. More details on this are given in Appendix B.

To measure the shoulder angular positions, participants wore the full-body inertial motion capture system MVN Link IMS (Xsens Technologies B.V., Enschede, the Netherlands) (see figure 3.1-b). Since we used the software provided by the manufacturer (MVN 2018 0.3) to integrate the raw sensor data,

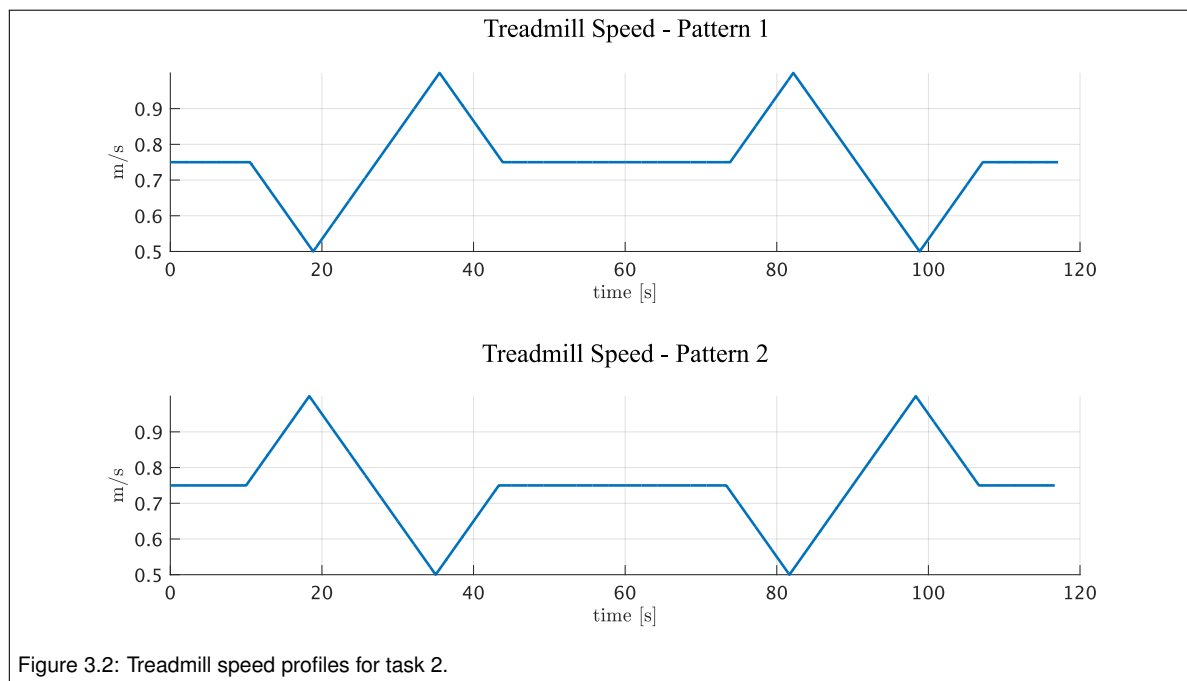


Figure 3.2: Treadmill speed profiles for task 2.

the sagittal angular positions of each shoulder joint was defined according to the in-built Xsens Biomechanical model. We also performed sensor calibration and model scaling according to manufacturer recommendation [32]. Communication between the MVN studio software and the Lopes II xPC-Target was carried by UDP transmission.

3.2. Participants

Three healthy people took part in the experiments: participant 1 (gender: female, age: 28, height: 1.78 m), participant 2 (gender: male, age: 40, height: 1.90 m) and participant 3 (gender: male, age: 30, height: 1.83 m). All the participants were volunteers and signed a consent form before taking part in the research (see Appendix C). None of these people had ever practised with our arm-based controller before, but all of them were acquainted walkers of the Lopes II. This condition was an essential prerequisite because, during a pilot test with people who were new to the Lopes II, we observed users to struggle in maintaining a natural arm-leg coordination when walking wearing the exoskeleton (even with the system in Zero Impedance mode). This is a reasonable finding considering that the device inevitably perturbs the wearer's gait, making a novel user in need of some training sessions before feeling comfortable with the system dynamics.

3.3. Walking Tasks

The experimental protocol included two walking tasks. The first one (task 1) consisted of walking at a constant treadmill speed for two minutes, for a total of five speed-conditions: 0.25, 0.50, 0.75, 1.00 and 1.25 m/s. Considering that 0.75 m/s is the threshold speed below which double swinging might occur (see Chapter 2), and to reduce order effects associated with transitions in interlimb coordination, we sorted the trials into two sequences, to which we assigned the participants randomly:

- Sequence 1 = 0.75 m/s → 0.50 m/s → 0.25 m/s → 0.75 m/s → 1.00 m/s → 1.25 m/s
- Sequence 2 = 0.75 m/s → 1.00 m/s → 1.25 m/s → 0.75 m/s → 0.50 m/s → 0.25 m/s

In this way, it was also possible to gradually increase the difficulty of the task, assuming that 0.75 m/s is a reasonably easy speed to maintain for a user trained with the Lopes II and that the transition to more extreme conditions is increasingly challenging. We included a second trial of 0.75 m/s walking as an intermediate condition, which served as wash-over between velocities that are characteristic of single or double swinging. During this intermediate test, we did not record any data. Failure to complete

one trial comported to skip to the intermediate 0.75 m/s condition, or to terminate the experiment if the latter condition had been already tested. In case a participant found difficult to walk at 0.75 m/s, the experiment would have continued based on the participant's feedback, that is his/her preference for which of the five walking conditions to test. Nevertheless, this scenario never happened, and all participants could always complete two-minute walking at 0.75 m/s.

The second task (task 2) consisted of walking with the Lopes II while the treadmill speed changed according to two possible patterns, as shown in figure 3.2. We randomly assigned each participant to one of the two speed-profiles.

Later on, we will refer to the term "trial" to indicate an attempt to complete either a two-minute walking condition of task 1 or a full profile of speed variation of task 2. For both tasks 1 and 2, we gave to each participant the possibility to repeat a certain trial as many times as desired. We declared a trial failed only if a participant felt uncomfortable in attempting/repeating it, or if time constraints forced us to move forward with the experiment.

3.4. Control Modes

We tested two different control modes for the Lopes II:

- Arm-based control, during which the user drove the exoskeleton with our arm-based controller. The right shoulder was always the limb controlling the system;
- Position control, during which the exoskeleton joint trajectories were only depended on the on-going treadmill speed. This mode was a default controller of the Lopes II (see Appendix B).

Position-control served: (1) as a baseline for some metrics that we used in the result analysis; (2) to understand the arm swing promoted by the Lopes II; (3) to initialise the gait (see Chapter 2).

Each participant completed task 1 and 2 with each controller, with random assignation of tasks and control modes. Participants could ask a few minutes of rest at any moment during the experiments.

Besides walking with the Lopes II, participants also completed task 1 by walking on the Lopes II treadmill without wearing the exoskeleton. For convenience, we will refer to this testing condition as "natural walking". During natural walking, the Arm Observer module (see Chapter 2) was still receiving the shoulder rotation, allowing us to analyse the capacity of the adaptive oscillator in (1) synchronising to healthy data and (2) reproducing stride properties, such as stride cadence and onset of heel-strike. In other words, data from natural walking served to validate the Arm Observer as a method to characterise the arm-leg coordination by exclusively recording shoulder kinematic information.

We asked participants to use their right shoulder to drive the exoskeleton for a matter of practicality when combining the Arm Observer with the Gait Generator (see Chapter 2). Still, the literature suggests that the arm swing presents side asymmetries, and we wanted to evaluate their effects on our controller functionality. Therefore, during natural walking, we ran in parallel two Arm Observer modules, each feed by one of the two shoulder signals.

3.5. Data Analysis

When running the experiments, the Matlab/Simulink - xPC-Target received data from the sensors of both the Lopes II and Xsens suit. Precisely, it logged the following signals, at 1 kHz sampling rate:

- the left/right angular shoulder positions in the sagittal plane, $\theta_{IN}(t)$; (*)
- the left/right adaptive frequency oscillator parameters $\theta(t)$, $\omega(t)$ and $\phi(t)$; (**)
- the joint (angular) velocities, $\vec{\theta}(t)$; (**)
- the joint interaction forces, $\vec{T}(t)$; (**)
- the vertical ground reaction forces and position of the center of pressure; (**)

Signal(s): (*) directly measured by the Xsens suit sensors; (**) directly measured by the Lopes II sensors, or computed online by the HLC/LLC.

where the $\vec{\theta}(t)$ and $\vec{T}(t)$ vectors contain an element per each degree of freedom listed in table 3.1. To remove sensor noise before proceeding with the data analysis, we filtered the angular shoulder position signals and the interaction force signals through a low-pass filter (Butterworth, forward and backward in time, third-order, cutoff frequency of 10 Hz). Filtering of the other data was unnecessary since already performed online by the HLC/LLC of the Lopes II.

Per each participant, control mode and task, we separated each raw sequence of data into accomplished trials. For any trial belonging to task 1, we discarded the first minute of the two-minute walking duration, considering this initial period as adaptation to the walking speed. For both tasks, we further segmented the data into stride and arm cycles, with a left/right stride cycle defined as the interval between two left/right heel-strikes, and a left/right arm cycle as the interval between two consecutive peaks of the left/right shoulder flexion. We detected the shoulder flexion peaks through the Matlab function “findpeak.m”, applied to the filtered $\theta_{IN}(t)$ signals. We visually inspected the correctness of this selection process. The algorithm which we used for the heel-strike detection is described in Appendix D. Per each left/right stride cycle, we computed the following metrics:

1. ω_S = stride cadence, computed as the inverse of the stride duration and assumed constant throughout the stride cycle;
2. \overline{AE}_{ω_S} = mean absolute error between ω_S and the $\omega(t)$ parameter of the adaptive frequency oscillator. This metric was expressed as a percentage of ω_S , which is a percentage of the actual stride cadence. \overline{AE}_{ω_S} is representative of the performance of the adaptive oscillator in estimating the stride cadence, with higher performance reached for values of this metric closer to 0%;
3. ϕ_{HS} = value of the phase $\phi(t)$ of the left/right adaptive frequency oscillator at the instance of right/left heel-strike. This metric was expressed as (1) a percentage of the oscillator cycle, wrapped within [-50%, 50%], and as (2) a time offset, which is the actual number of seconds between a left/right heel-strike and the closest instance of 0% phase of the right/left adaptive oscillator. For both these two versions, the sign convention considers a positive/negative value as indicative of an early/late detection. ϕ_{HS} indicates the performance of our arm-based control algorithm in predicting heel-strikes contralateral to the input shoulder, with higher performance associated with values of this metric closer to 0%.

Per each right/left arm cycle, we computed the following variables:

1. θ_{Amp} = amplitude of the angular shoulder position, $\theta_{IN}(t)$;
2. ω_A = arm swing frequency, computed as the inverse of the arm cycle duration and assumed constant throughout this interval;
3. \overline{AE}_{ω_A} = mean absolute error between ω_A and the $\omega(t)$ parameter of the adaptive frequency oscillator. This metric was expressed as a percentage of ω_A , which is a percentage of the actual arm swing frequency. \overline{AE}_{ω_A} is representative of the performance of the adaptive oscillator in estimating the arm swing frequency, with higher performance reached for values of this metric closer to 0%.
4. ϕ_{PF} = value of the phase $\phi(t)$ of the left/right adaptive frequency oscillator at the instance of maximum flexion of the left/right shoulder. This metric was expressed as (1) a percentage of the oscillator cycle, wrapped within [-50%, 50%], and as (2) a time offset, which is the number of seconds between a left/right peak of shoulder flexion and the closest instance of 0% phase of the left/right oscillator. For both these two versions, the sign convention considers a positive/negative value as indicative of an early/late detection. ϕ_{PF} represents the performance of our arm-based control algorithm in locking its zero phase to the maximum flexion of its input shoulder, with higher performance associated with values of this metric closer to 0%.

In addition, we also computed the offset between a peak of shoulder flexion and the associated contralateral heel-strike, expressed as a percentage of the stride cycle ipsilateral to the shoulder peak. This metric measures the actual shift between these two gait events, permitting to validate whether assuming their coincidence was appropriate when we designed our arm-based controller.

When belonging to trials of task 1, we computed the average and standard deviations of all the

above metrics, and also of the filtered shoulder trajectory $\theta_{IN}(t)$ over a stride cycle - to compute the statistics of this latter quantity, we interpolated the data assigned to each stride segment over 1000 samples. To use the same number of elements, we selected only the first 19 elements of each metric when computing its statistics (for $\theta_{IN}(t)$, the first 19 interpolated stride segments). Across all participants and trials, this number was the minimum amount of data available when considering all the previous metrics. During natural walking at constant 1.25 m/s, participant 2 exhibited an instance of cross stride walking within the first 30 seconds. To exclude such abnormality from the analysis, we computed the statistics of the metrics associated with this condition over their last 19 elements instead.

Per each sequence of data characterising a complete trial, we computed the following variables:

1. \overline{AE}_{SH} = mean absolute error between $\theta_{IN}(t)$ and the $\theta(t)$ parameter of the associated adaptive frequency oscillator. This metric was expressed as a percentage of the average arm swing amplitude adopted during the trial. \overline{AE}_{SH} indicates how well the Arm Observer tracked its input signal, and thus characterises the overall synchronisation error. Higher tracking performance corresponds to values of this metric closer to 0%;
2. $|W|$ = absolute work exchanged between the Lopes II and its user. This measure characterises the level of synergy in the human-machine interaction, with smaller values meaning a higher agreement between the gait desired by the user and the one promoted by the robot.

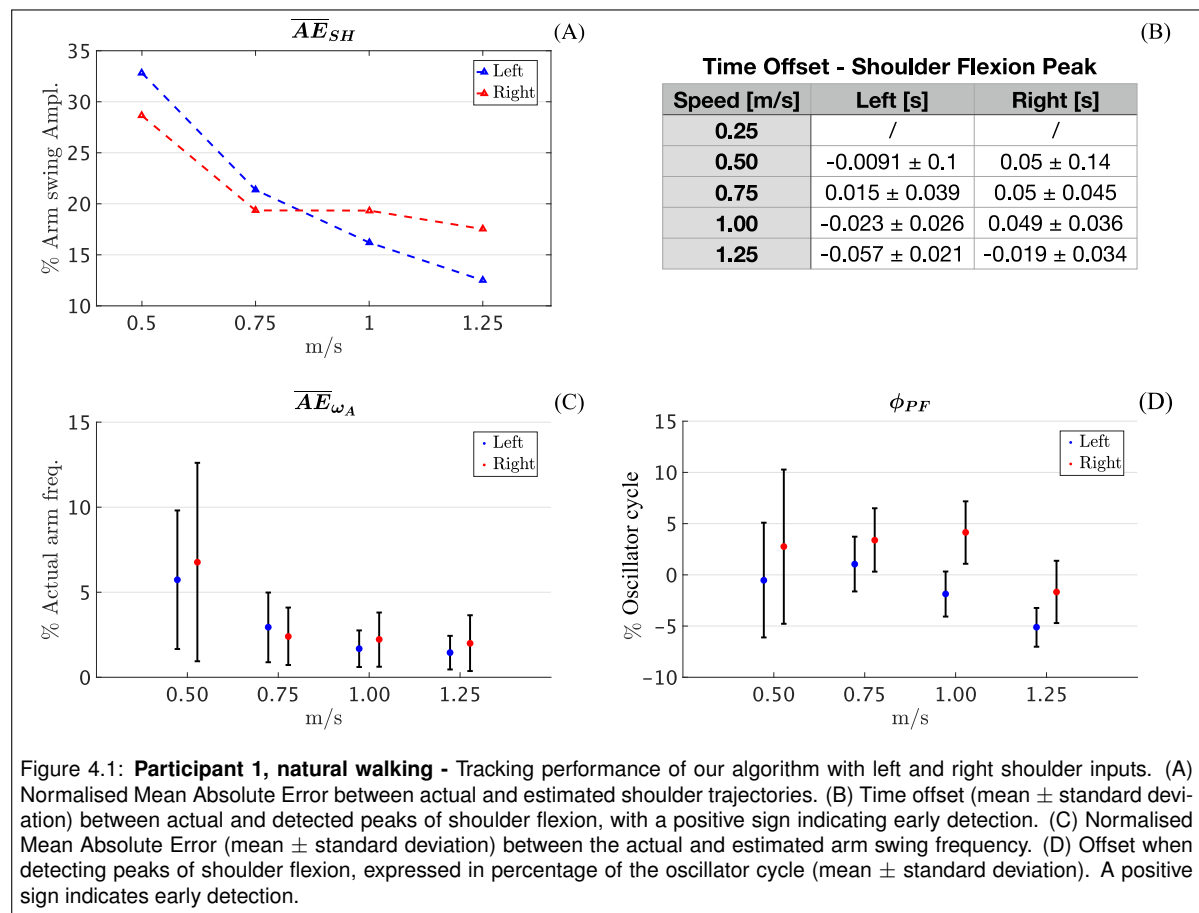
For the trials associated to task 2, \overline{AE}_{SH} was computed within each arm cycle and expressed as a percentage of the arm swing amplitude associated to the same arm cycle. Similarly, $|W|$ was computed within each stride cycle for task 2 data. During natural walking at 0.75 m/s, participant 2 stumbled at about 50 sec. We removed the left and right data associated with this discontinuity, as well as the remaining 10 seconds of the trial. Since more than 19 left and right arm/stride cycles were present in the remaining segment of data, this decision affected only the computation of \overline{AE}_{SH} .

4

Case Studies

This chapter describes the results of our experimental study. The analysis is divided per participant, in a case-study fashion. Within each case study, the results are presented arranged by the walking condition: natural walking, exoskeleton walking during task 1 and task 2. A preliminary analysis of the results showed us that the Arm Observer always failed to synchronise to the shoulder signal during natural walking at 0.25 m/s. Only for participant 2, this failure also occurred for the left adaptive frequency oscillator during natural walking at 0.5 m/s. Therefore, we do not report the performance metrics associated with these conditions in the following analysis. For the seek of objectivity, we still report the corresponding full-time traces of actual and estimated shoulder trajectories (see Appendix F).

4.1. Participant 1



4.1.1. Natural walking

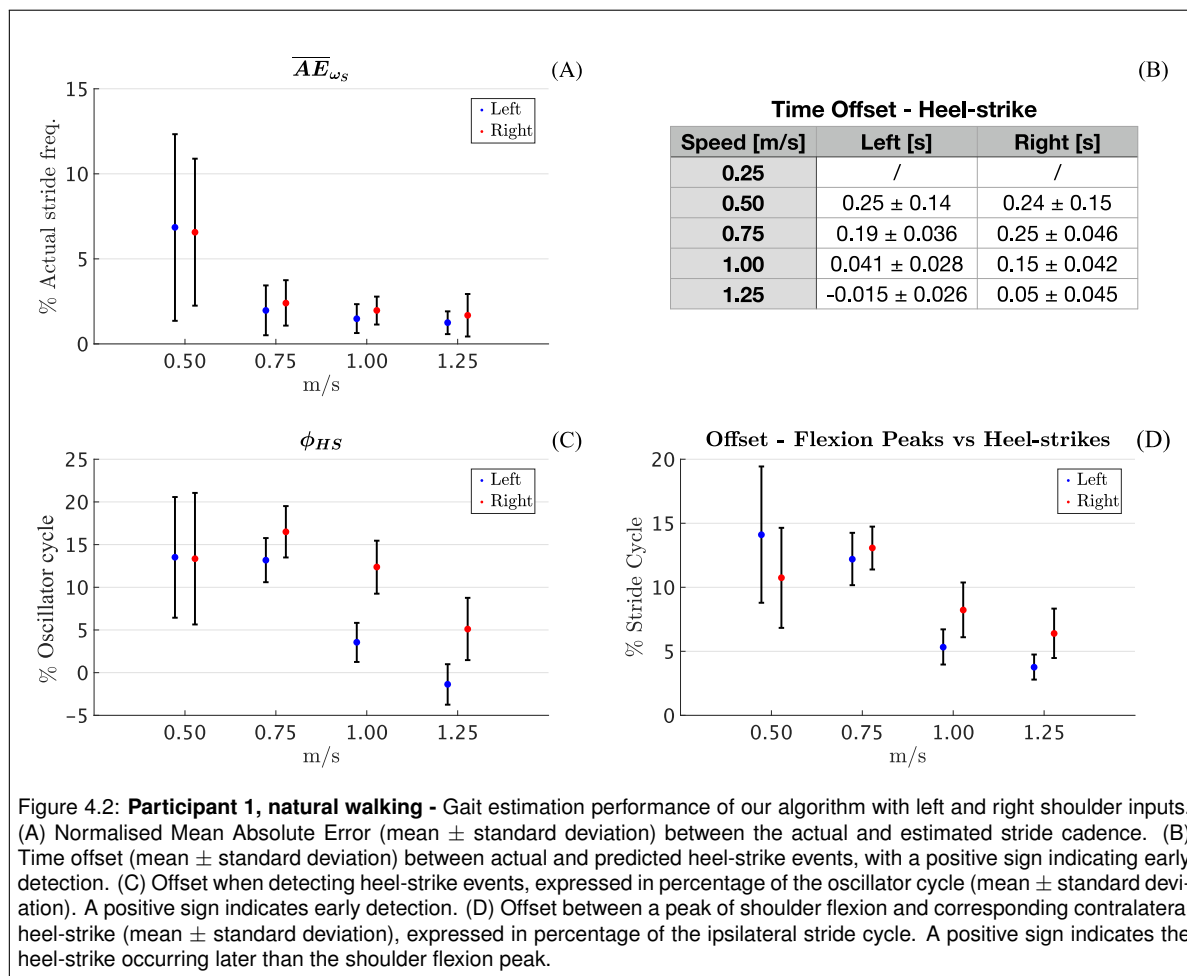
Tracking performance

The performance of each adaptive frequency oscillator in tracking the assigned shoulder rotation improved almost proportionally to the walking speed, as pointed out by the nearly inverse relationship between \overline{AE}_{SH} and the treadmill velocity (figure 4.1, plot A). Inspection of the time traces of actual and estimated shoulder trajectories further confirms that the oscillator synchronisation to the input signal was excellent within the range of 0.75-1.25 m/s, for both body sides (figure F.1, Appendix F). These plots also show that the similarity of the real shoulder trajectories to sinusoidal shapes reduced when walking at 0.5 m/s, mostly because of occasional instances of minor peaks in-between two consecutive maxima of shoulder flexion (especially visible in the left side data). This increased irregularity is a major contributor to the just observed drop in tracking performance.

The $\omega(t)$ parameter of each adaptive oscillator estimated the frequency of the assigned shoulder rotation very well, and especially within the range of 0.75-1.25 m/s, the average mean absolute error did not exceed ~3% of the real frequency value (figure 4.1, plot C). Both precision and accuracy of the frequency estimation dropped at 0.5 m/s, as shown by larger means and standard deviations respectively. This finding is consistent with the reduced oscillator synchronisation occurring at this speed condition.

Peaks of shoulder flexion were predicted with very small time offsets (figure 4.1, Table B), that once converted in the percentage of the oscillator cycle, did not exceed on average $\pm 5\%$ (figure 4.1, figure D).

Concerning side asymmetries, none of the plots in figure 4.1 suggest that one of the adaptive frequency oscillators outperformed the other consistently.

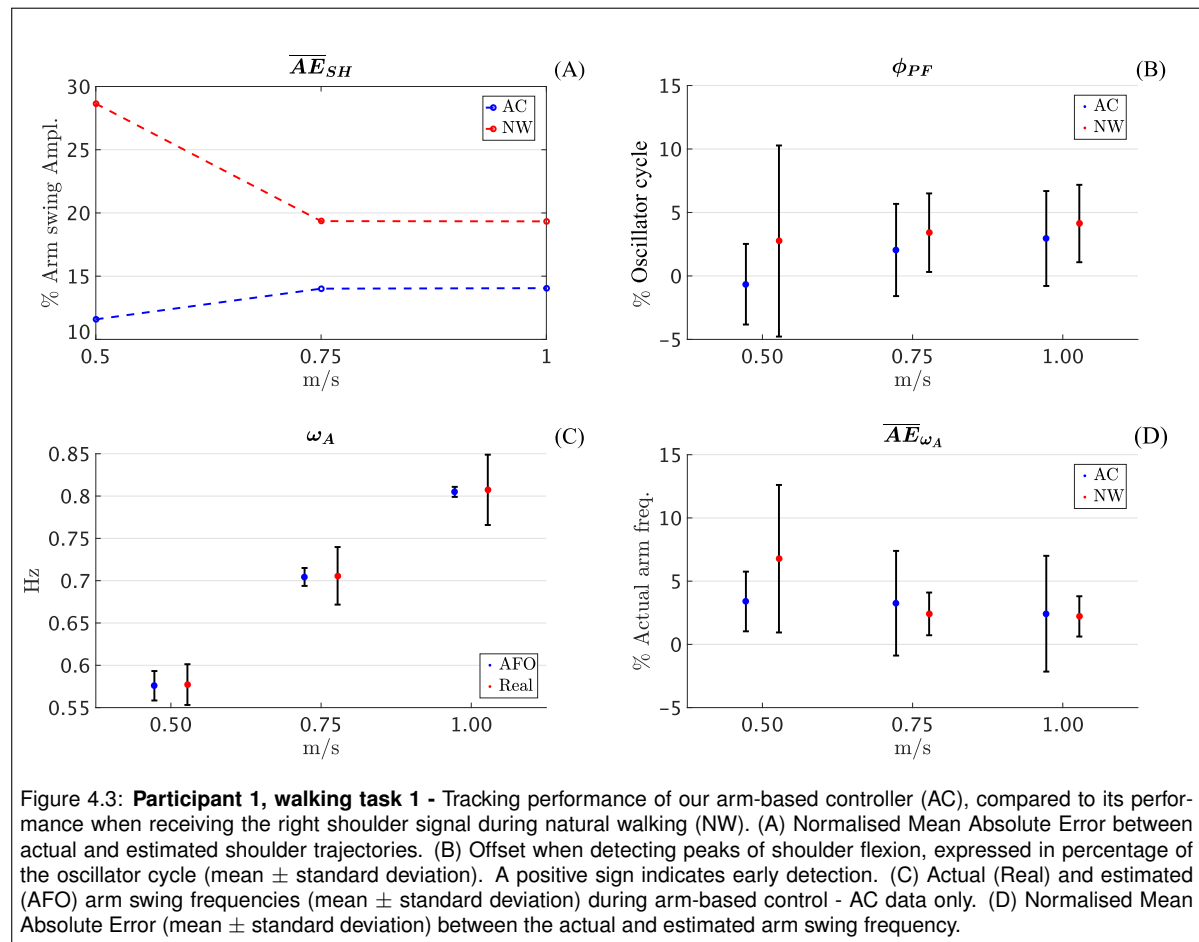


Gait Estimation

The $\omega(t)$ parameters of the left and right adaptive frequency oscillators were excellent estimators of the stride cadence, especially within 0.75-1.25 m/s (figure 4.2, plot A). However, for the majority of the speed conditions, the heel-strike events were predicted with a positive time offset, which means earlier than their actual onsets (figure 4.2, plot B). Once expressed in the percentage of the oscillator cycle, this detection error ranges from a max of about 15% to almost null offset as the walking speed increases (figure 4.2, plot C). Considering that each oscillator properly synchronised to the input angular shoulder position while having a frequency very similar to the stride cadence, the primary reason for the observer error in heel-strike detection is given by the algorithm wrongly assuming such foot contact to occur concomitantly to the peak of flexion of the contralateral shoulder. This conclusion is further supported by plot D of figure 4.2, which shows the existence of a natural speed-dependent offset between these two types of gait events during normal walking of participant 1.

Arm-leg coordination

Participant 1 adopted single swinging within 0.5-1.25 m/s (figure F.2, Appendix F). At 0.25 m/s the average angular profiles resembled double swinging, especially for the left shoulder. The transition between these two coordination modes was likely initiated around 0.5 m/s, as suggested by a small secondary peak in the late part of the stride cycle. Therefore, the above mentioned sporadic occurrence of minor peaks of shoulder flexion was likely associated with the transition in interlimb coordination mode.



4.1.2. Arm-based control: Task 1

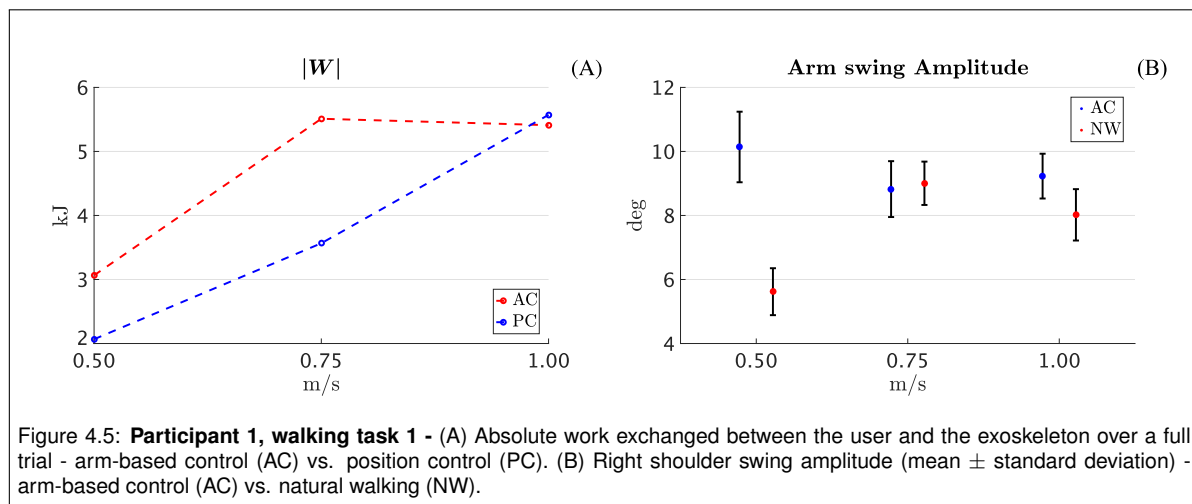
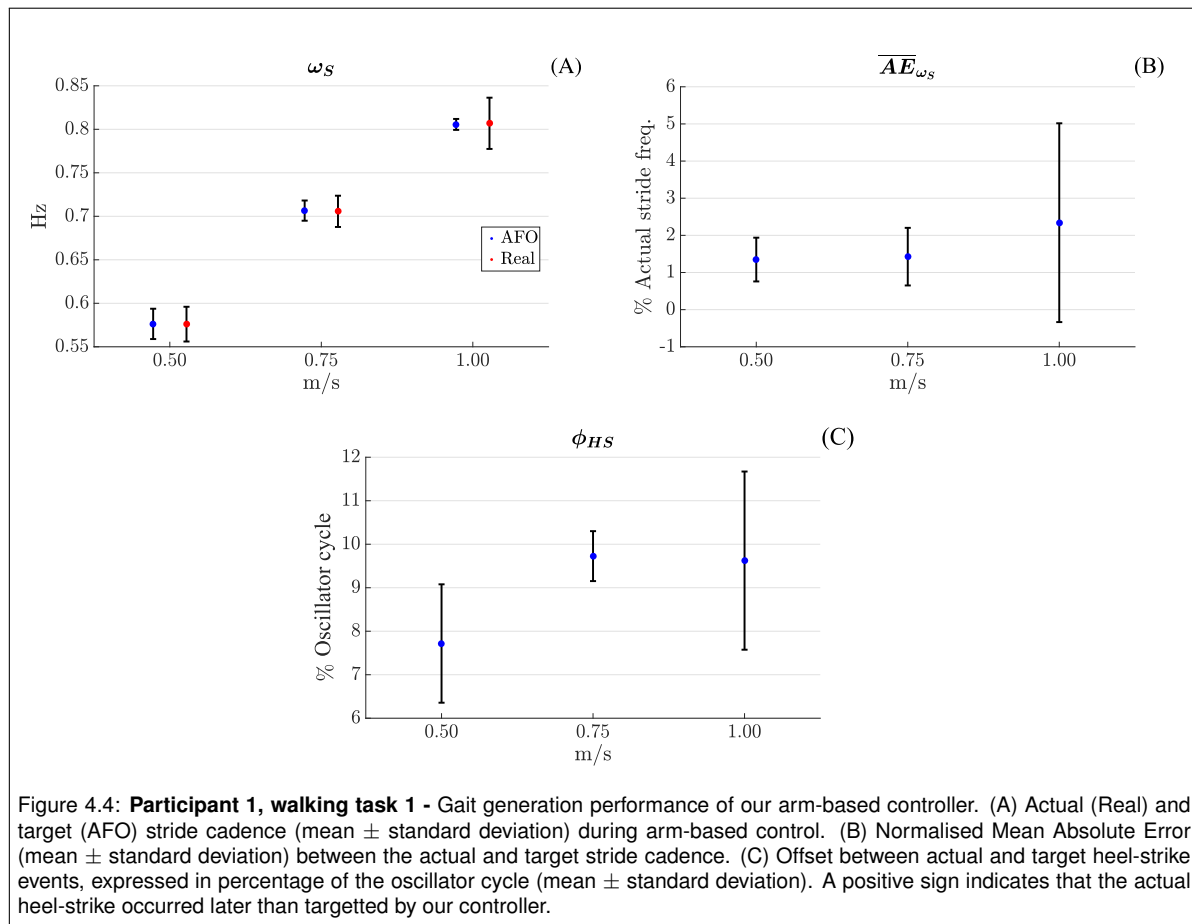
Controllable range

Participant 1 could not complete walking at 0.25 and 1.25 m/s. However, the 1.25 m/s speed condition failed because of hardware malfunctioning in the Lopes II which was unrelated to using our arm-based controller. Participant 1 found too challenging to transit between following steady-speed conditions continuously. Therefore, each trial of task 1 was initiated in position control, and only after a few seconds of adaptation, the control mode was switched to arm-based control.

Tracking performance

During arm-based control in task 1, the adaptive frequency oscillator correctly synchronised to the right shoulder rotation for all the completed trials (figure F.3, Appendix F), with \overline{AE}_{SH} always lower than 15% of the average arm swing amplitude (figure 4.3, plot A). The adaptive frequency oscillator estimated very well the timing of shoulder flexion peaks, as shown by quite small time offsets: -0.012 ± 0.057 , -0.028 ± 0.052 and -0.037 ± 0.048 seconds for 0.5, 0.75 and 1 m/s, respectively. Expressed in percentage of the oscillator cycle, the detection error never exceeded $\pm 5\%$ (figure 4.3, plot B). Correctly, participant 1 increased the arm swing frequency as the walking speed rose (figure 4.3, plot C), and the Arm Observer could track the different cadences closely at all speed conditions (figure 4.3, plot D).

Compared to the results of natural walking, the overall matching between the adaptive frequency oscillator and the input shoulder signal improved during arm-based control (figure 4.3, plot A). A similar result was expected, since when using our algorithm the user actively contributes to the generation of periodic arm oscillations, thus facilitating the synchronisation of the Arm Observer. However, the tracking performance in terms of detection of flexion peaks and estimation of the arm swing frequency did not change noticeably compared to the results of natural walking (figure 4.3, plot B and D). Actually,

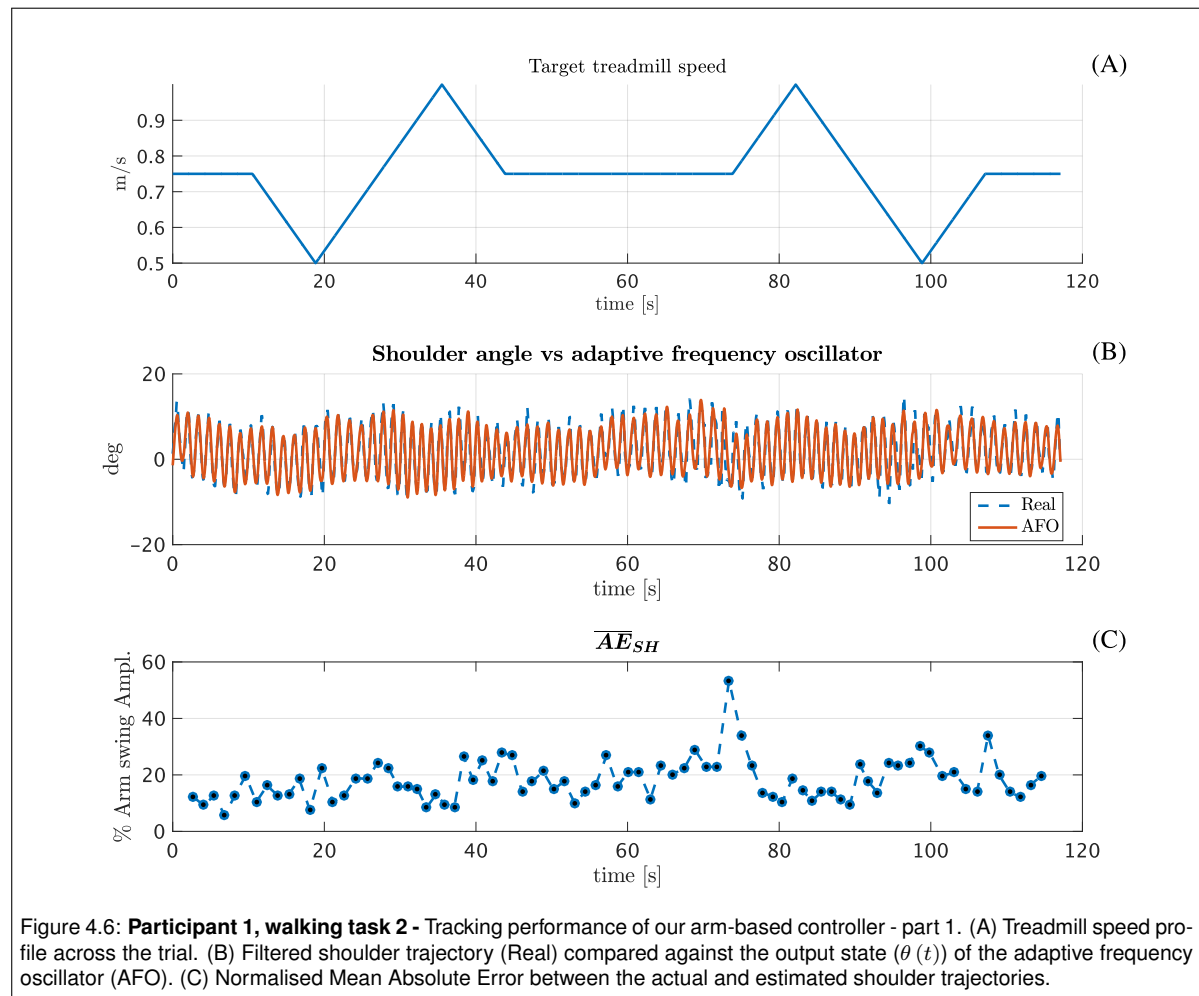


\overline{AE}_{ω_A} was slightly more precise and accurate for the natural walking condition when the speed was within 0.75-1 m/s.

Gait generation

Participant 1 correctly increased the stride cadence during faster walking speeds (figure 4.4, plot A). The closeness, on average, of the parameter $\omega(t)$ of the adaptive frequency oscillator to the measured stride cadence (figure 4.4, plot A), as well as the very small values of \overline{AE}_{ω_s} (figure 4.4, plot B) confirms that our controller actually dictated the stride cadence of the human-machine complex.

There was a consistent offset between the target and actual occurrences of the heel-strike events,



both in terms of time offset (0.14 ± 0.021 , 0.14 ± 0.0085 and 0.12 ± 0.026 seconds for 0.5, 0.75 and 1 m/s, respectively) and percentage of the oscillator cycle offset (figure 4.4, plot C). Contrary to what observed during natural walking, the smallest offset occurred at 0.5 m/s, i.e. the slowest speed condition achieved in task 1 by participant 1.

Absolute work & arm swing amplitude

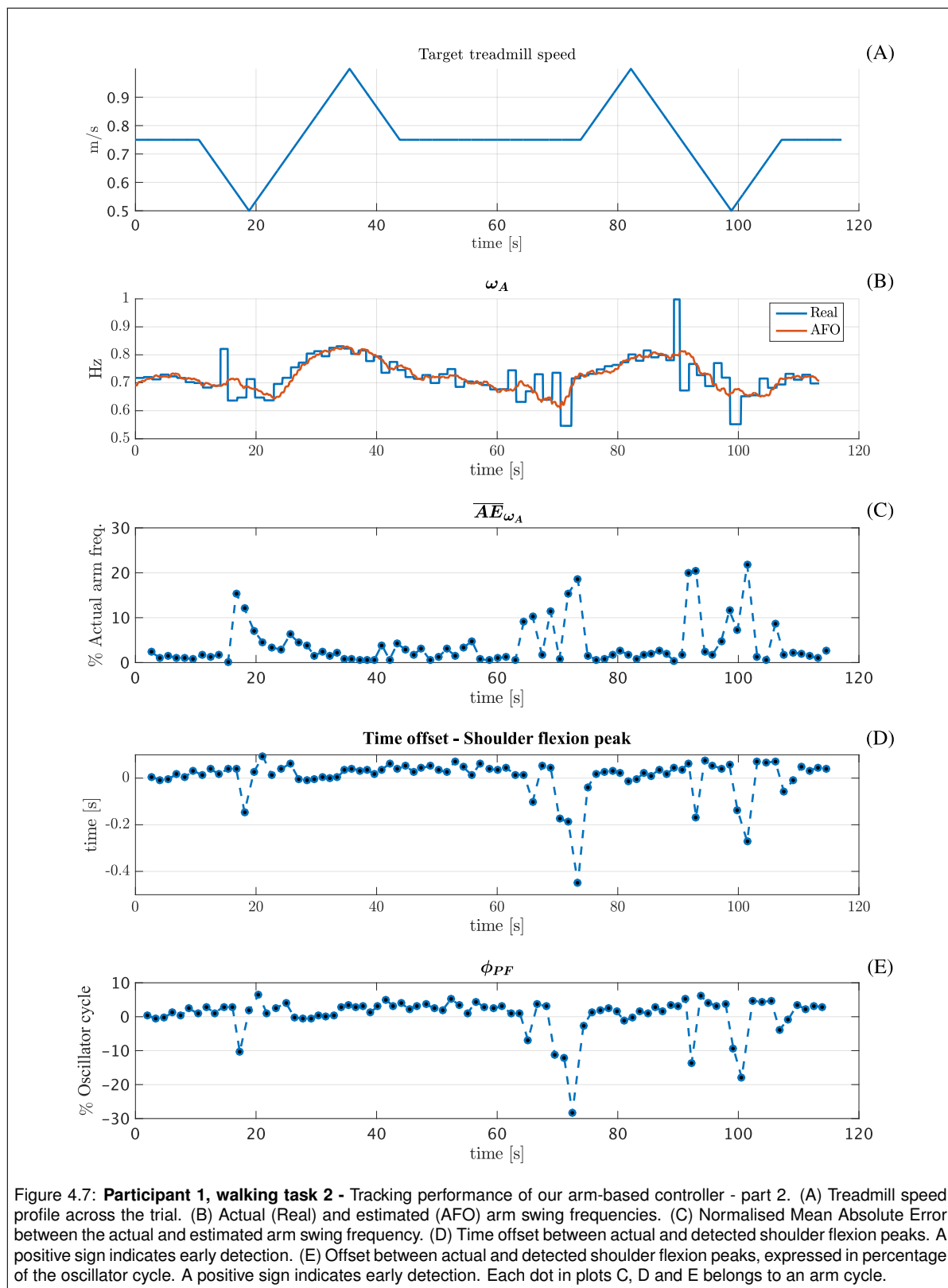
Compared to position control, walking with the arm-based controller comported a lower absolute work, exchanged between participant 1 and the Lopes II, only at the 1 m/s speed condition and with a minimal difference (figure 4.5, plot A). For the remaining two conditions, position control was always less energetically demanding, and thus likely more comfortable for participant 1.

Within 0.75-1 m/s, the user's arm swing amplitude did not change consistently, either within and between natural walking and arm-based control (figure 4.5, plot B). However, walking at 0.5 m/s was characterised by slightly larger shoulder rotations, especially if compared to the corresponding value measured during natural walking. The average shoulder trajectory of participant 1 when walking in position control presented an amplitude generally smaller than what observed during natural walking, especially for the trials at 0.5 and 1 m/s (figure F.4, Appendix F). On the contrary, the average shoulder trajectory adopted during arm-based control was very similar to natural walking data, except for a delay in the occurrence of maximum shoulder extension (the valley in plot) when walking at 0.75 m/s.

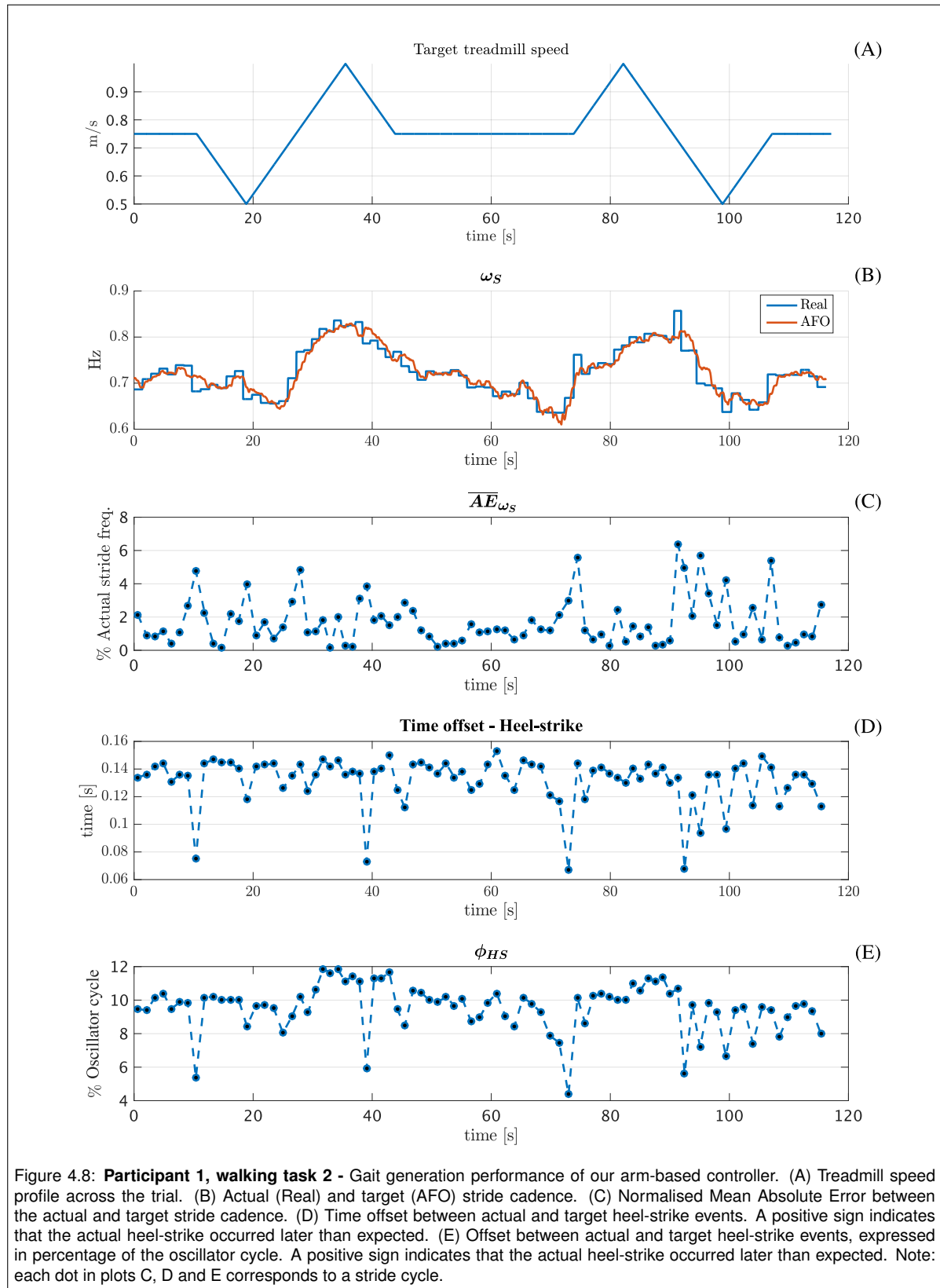
4.1.3. Arm-based control: Task 2

Tracking performance

Throughout task 2, the adaptive frequency oscillator could track the shoulder angular profile of participant 1 well (figure 4.6, plot B). Furthermore, the tracking performance did not change significantly

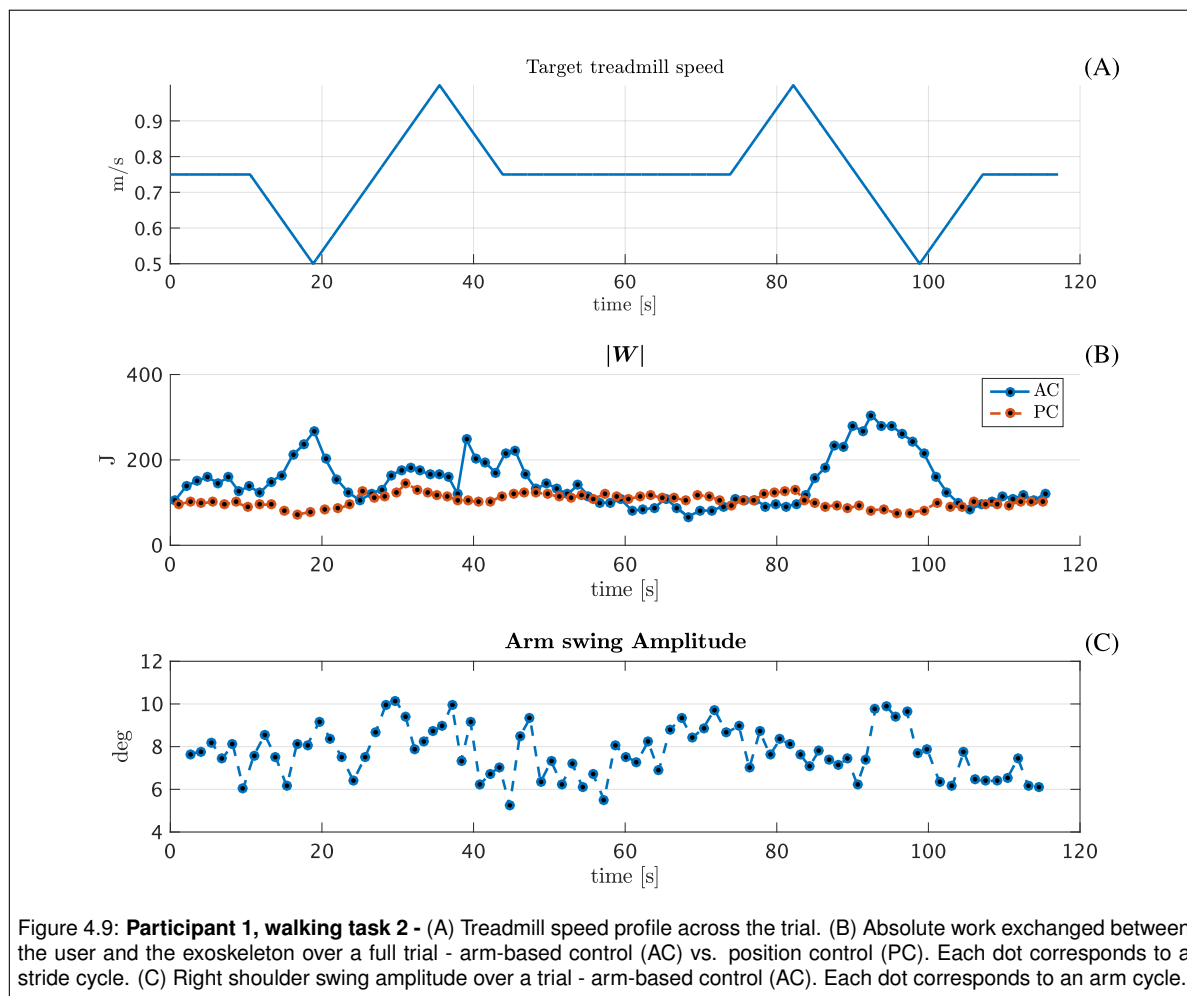


between intervals at constant and variable speeds (figure 4.6, plot C). At about 75 seconds there was a noticeable increment in \overline{AE}_{SH} , joined by similar reduced performance concerning the estimation of the arm swing frequency (figure 4.7, plots B and C) and the detection of peaks of shoulder flexion (figure 4.7, plots D and E). Nevertheless, this reduced tracking performance lasted over only a few arm



cycles, which were all antecedent to the second interval with variable speed.

During the two intervals at variable treadmill velocity, participant 1 changed the arm swing frequency proportionally to the walking speed (figure 4.7, plots B), but around the two instances at min-



imum treadmill speed, the swing cadence became more variable (especially for the second interval with variable velocity). This variability in the shoulder rotation is likely responsible for the concomitant more erroneous estimation of the arm swing frequency (figure 4.7, plots C), and less precise detection of the peaks of shoulder flexion (figure 4.7, plots D and E).

Gait generation

The oscillator parameter $\omega(t)$ was similar to the stride cadence throughout task 2 (figure 4.8, plot B), with \overline{AE}_{ω_s} below 4% of the real stride cadence most of the time (figure 4.8, plot C). Therefore, also under a variable treadmill speed, our algorithm could generate a gait whose stride frequency changed proportionally to the belt velocity, correctly depending on the cadence of the arm swing. However, \overline{AE}_{ω_s} was more variable during the two intervals with changing treadmill velocity, which might be an indicator of reduced synergy between the user and the Lopes II: participant 1 might have perceived the gait promoted by the robot as inappropriate, and thus intentionally countered it.

For the majority of the task, the actual left heel-strike occurred with about 0.12-0.14 seconds delay (about 8-10% of the oscillator cycle) with respect to the timing targeted by the arm-based controller (figure 4.8, plot D and E), a finding consistent with the results of task 1. However, the second interval at variable treadmill speed was characterised by a much more variable heel-strike detection error than during the rest of the trial. Therefore, it is possible that participant 1 had more difficulties in controlling the Lopes II during the second part of task 2.

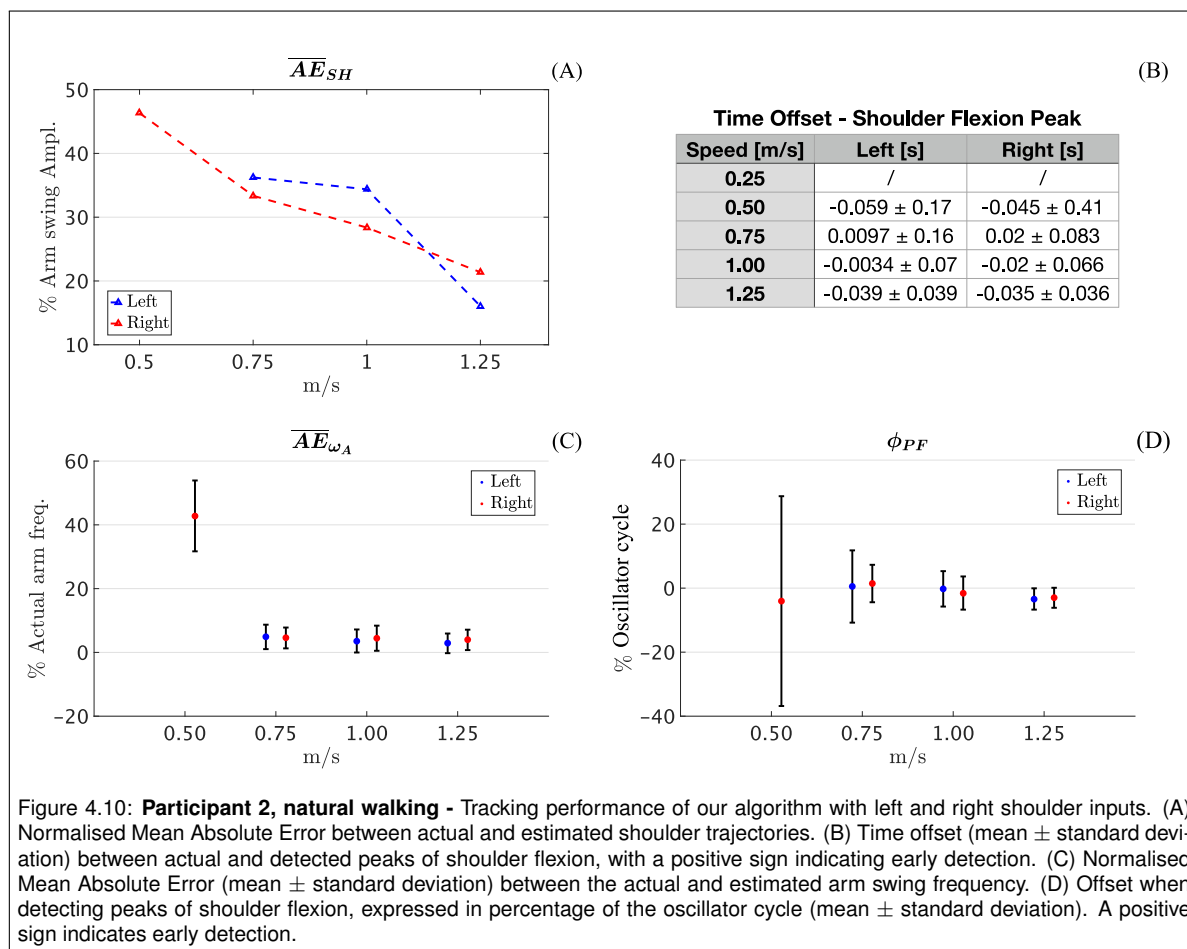
Absolute work & arm swing amplitude

When using the arm-based controller, reducing the treadmill speed comported an incremental exchange of absolute work between the user and the machine (figure 4.9, plot B). This increment reached

its maximum anytime the treadmill speed was close to its minimum value. Considering that participant 1 was unable to use the arm-based controller at 0.25 m/s during task 1, such a finding is reasonable. Furthermore, except when in the neighbourhood of the minimum treadmill velocity, the absolute work during arm-based control was quite similar to that observed during position control.

During task 2, the user's arm swing amplitude changed very little, ranging from 6 to 10 degrees and with fluctuations not clearly related to the treadmill speed (figure 4.9, plot C).

4.2. Participant 2



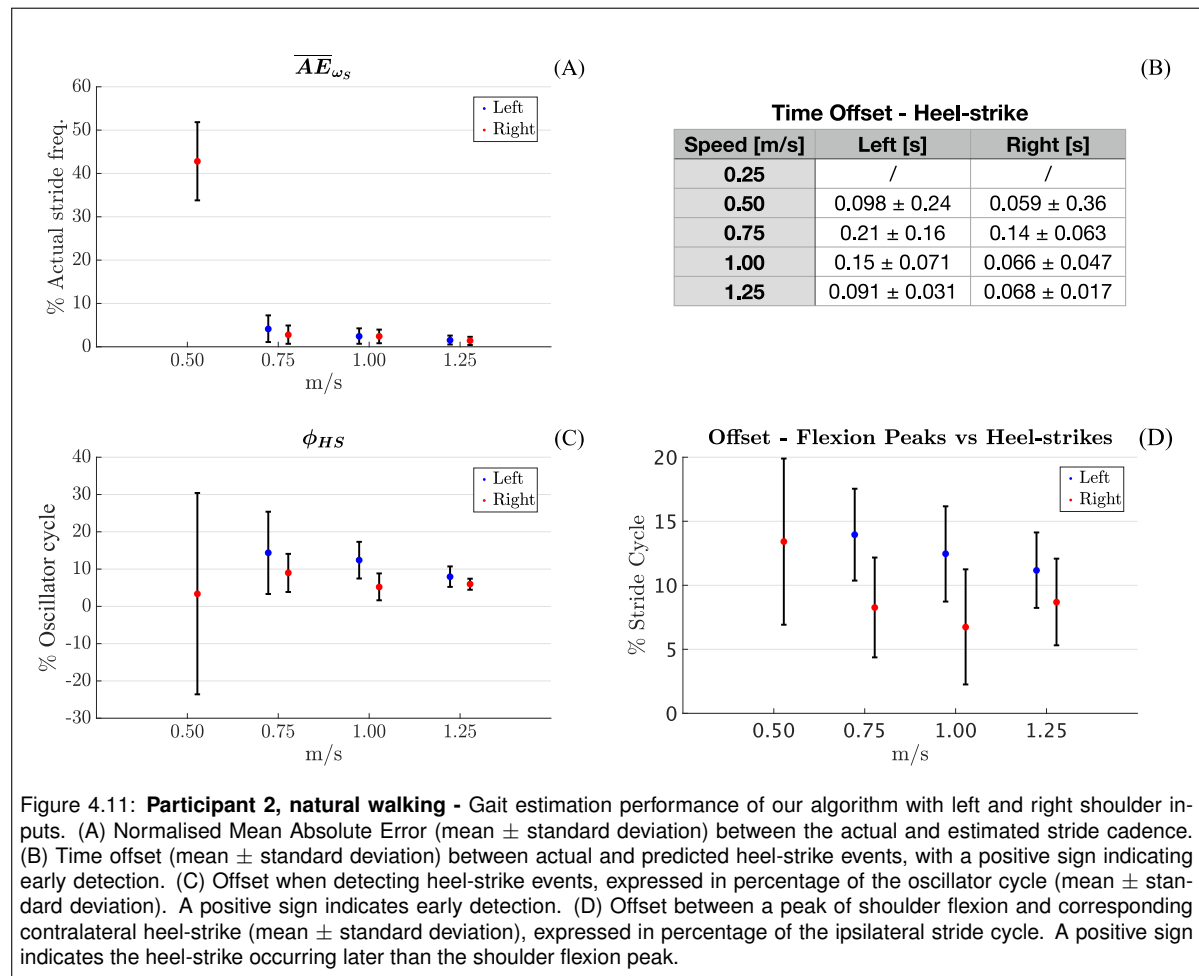
4.2.1. Natural walking

Tracking performance

Increasing the walking speed reduced the error of each adaptive frequency oscillator in tracking its input shoulder trajectory, with an almost inversely proportional trend for the right side (figure 4.10, plot A). Inspection of the time traces (figure F.5, Appendix F) further confirms that within the range of 0.75-1.25 m/s the synchronisation of each Arm Observer to its shoulder signal was excellent. Left and right swing patterns, however, presented a mix of major and minor peaks of shoulder flexion when walking at 0.5 m/s. This feature comported an increased irregularity in the shoulder signal, thus playing a consistent role in reducing the tracking performance of the Arm Observer at this speed condition and similarly to what observed for participant 1. For the right side, it was possible to discriminate an arm cycle as the segment of data between two consecutive major peaks, considering the remaining local maxima as noise due to their much smaller magnitudes. For the left side, on the contrary, the angular shoulder trajectory was more irregular, with major and minor peaks often having comparable heights. This property made a reliable segmentation of the data into arm cycles impossible, and thus an analysis of the behaviour of the left Arm Observer was not carried for the 0.5 m/s trial associated with natural walking.

Each adaptive frequency oscillator produced both excellent estimations of the arm swing frequency and correct detections of the shoulder flexion maxima (4.10, plot C, plot D and table B). At 0.5 m/s performance dropped for both \overline{AE}_{ω_A} and ϕ_{PF} , consistent with the trend of \overline{AE}_{SH} .

Side differences were minimal and mostly limited to the overall tracking behaviour, i.e. \overline{AE}_{SH} , thus not affecting the outputs of the Arm Observer needed by the Gait Generator.



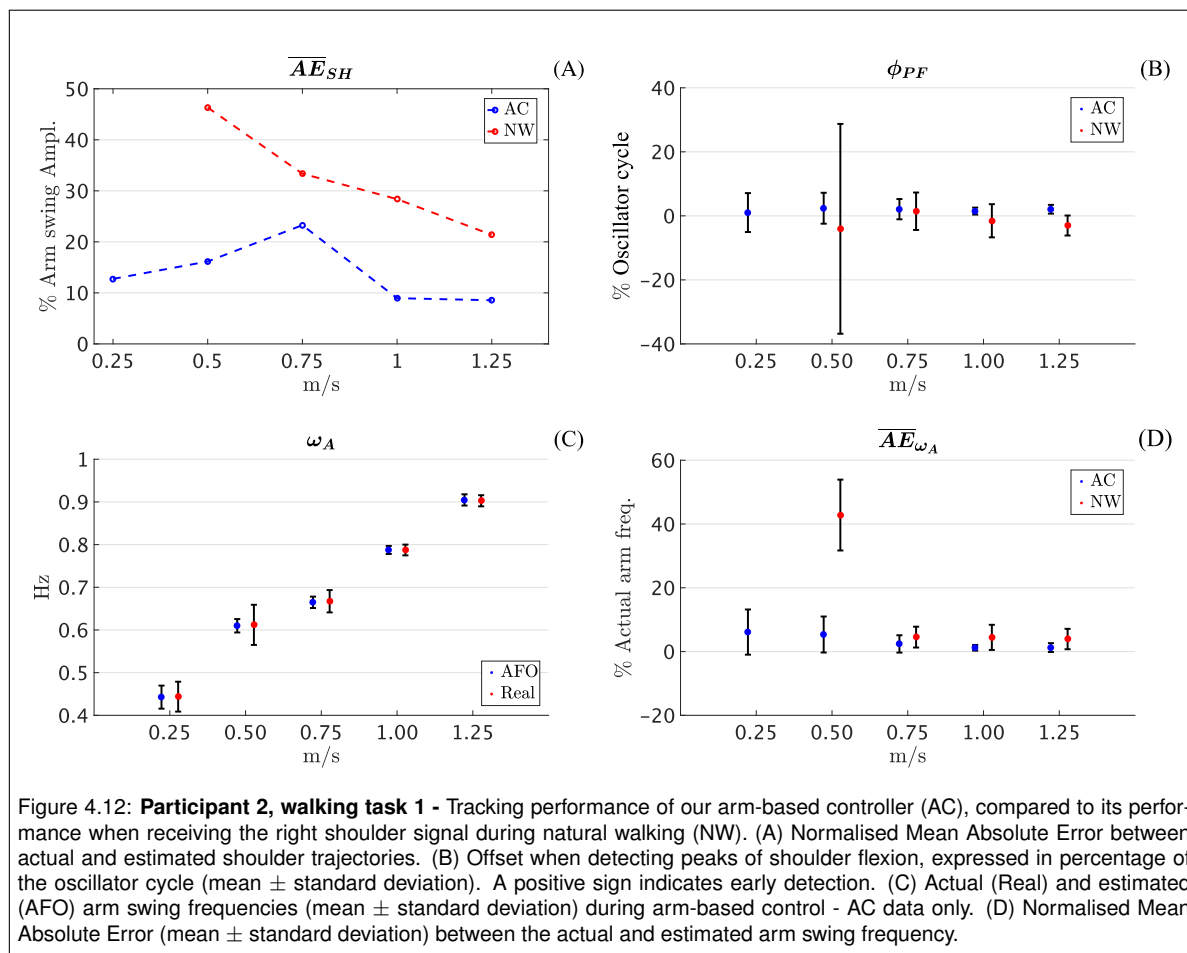
Gait Estimation

The $\omega(t)$ parameter of the adaptive frequency oscillator estimated the contralateral stride cadence very well for walking speeds within the range of 0.75-1.25 m/s, with similar performance between left and right sides (figure 4.11, plot A). \overline{AE}_{ω_s} reduced with increasing walking speed, suggesting better approximations of the stride cadence during faster gaits.

Heel-strike events were consistently predicted with positive time shifts, i.e. in advance respect to their actual occurrences (figure 4.11, table B). Above 0.5 m/s, this time offset reduced with increasing walking speeds. Once expressed in the percentage of the oscillator cycle, the heel-strike detection error was less than 15% for most of the tested conditions (figure 4.11, plot C). Similarly to participant 1, this phase error is primarily associated with a natural offset between a peak of shoulder flexion and the corresponding contralateral heel-strike (figure 4.11, plot D). On average, these two events were more coincident for the right arm-left foot complex, leading the right Arm Observer to more precise heel-strike detections.

Arm-leg coordination

The arm swing of participant 2 resembled single swinging mostly at 1.25 m/s (figure F.6, Appendix F). Already at 1 m/s, the shoulder trajectories show the occurrence of a secondary peak (valley) for the left (right) angular profile. At 0.5 m/s, double swinging is prominent for both shoulders, and at 0.25 m/s it is not possible anymore to distinguish between major and minor peaks of shoulder flexion.



4.2.2. Arm-based control: Task 1

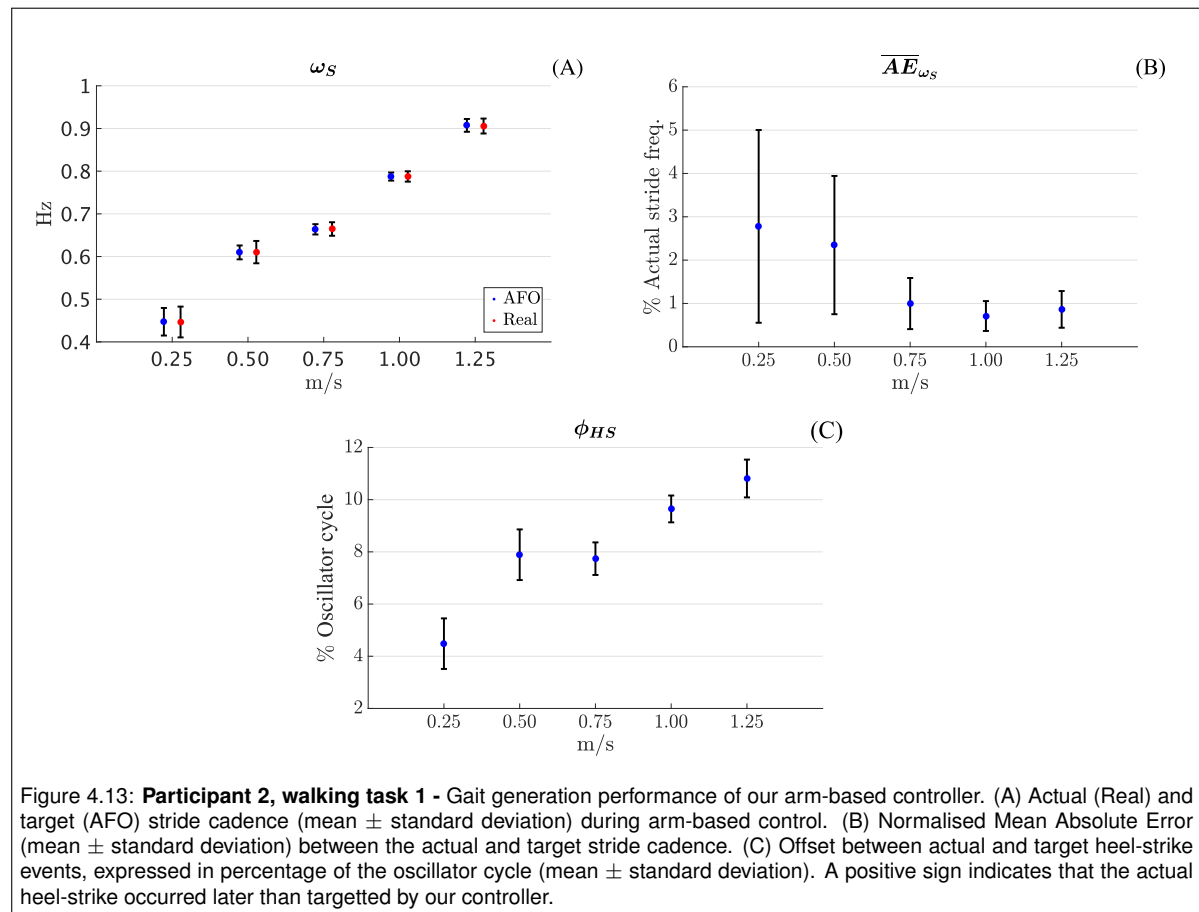
Controllable range

Participant 2 could complete all speed conditions and transit from one treadmill velocity to the following one while maintaining the arm-based controller active, i.e. without starting each trial in position control. Accordingly, during arm-based control, participant 2 could conform to treadmill accelerations equals to 0.1 m/s/s, and decelerations of 0.5 m/s/s (transition rate limits in-built into the Lopes II). Despite completing the trial of task 1 at 0.25 m/s, participant 2 mentioned finding challenging using the arm-based controller at such a speed condition. Precisely, he stated to find unintuitive swinging the arm slow enough to match the treadmill velocity.

Tracking performance

The adaptive frequency oscillator synchronised well to the shoulder rotation during all the trials of task 1 (figure F.7, Appendix F). The detection of peaks of shoulder flexion was excellent, whether the offset error was expressed in time (0.023 ± 0.13 , 0.038 ± 0.078 , 0.031 ± 0.048 , 0.018 ± 0.014 and 0.022 ± 0.015 seconds for 0.25, 0.5, 0.75, 1 and 1.25 m/s, respectively) or percentage of the oscillator cycle (figure 4.12, plot B). As for participant 1, participant 2 correctly conformed to increasing walking speeds by increasing the arm swing frequency (figure 4.12, plot C), and this latter parameter was tracked with high precision by the Arm Observer across all conditions involving arm-based control (figure 4.12, plot D). Furthermore, \overline{AE}_{ω_A} (on average) reduced with faster gaits.

Comparison with the results from natural walking shows that the tracking performance improved during arm-based control, despite \overline{AE}_{SH} increased proportionally to the walking speed within the range of 0.25-0.75 m/s (figure 4.12, plot A). On the contrary, the performance in estimating the arm swing frequency and detecting the peaks of shoulder flexion did not change conspicuously between natural walking and arm-based control (figure 4.12, plot B and D).



Gait generation

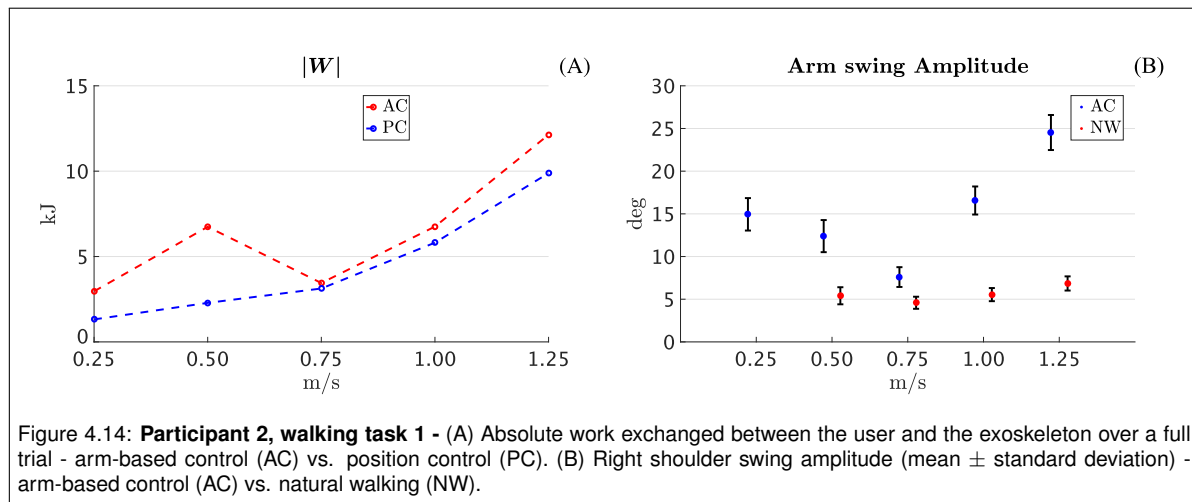
The stride cadence of participant 2 correctly increased with the walking speed during task 1, and, on average, the $\omega(t)$ parameter of the adaptive frequency oscillator was similar to the real stride cadence (figure 4.13, plot A). Small \overline{AE}_{ω_s} values further confirm this finding (figure 4.13, plot B), suggesting a correct transmission of the oscillator frequency, and thus of the arm swing cadence, to the stride frequency.

The actual heel-strikes occurred later than when targeted by the arm-based controller, with a time offset equal to: 0.098 ± 0.016 , 0.13 ± 0.015 , 0.12 ± 0.0084 , 0.12 ± 0.0058 and 0.12 ± 0.0071 seconds for 0.25, 0.5, 0.75, 1 and 1.25 m/s. In the percentage of the stride cycle, the offset ranged within 4-11%, and contrary to what observed during natural walking, it increased (almost proportionally) with faster treadmill velocities (figure 4.13, plot C).

Absolute work & arm swing amplitude

Compared to position control, participant 2 always exchanged more work with the Lopes II when walking with the arm-based controller (figure 4.14, plot A). However, the difference in $|W|$ between the two control modes was large when walking at 0.5 m/s, but it was noticeably more contained for the other conditions. Therefore, it seems that participant 2 did not find using the arm-based controller much more challenging than walking in position control, especially when walking at 0.75 and 1 m/s.

During arm-based control, participant 2 changed the amplitude of the arm swing according to the walking velocity, but with an ambiguous trend: a proportional relationship within 0.75-1.25 m/s (as one would expect in a healthy gait), and an almost inversely proportional relation within 0.25-0.75 m/s. During natural walking, such a V-shaped trend was also faintly present, and thus this unusual behaviour might be a peculiar gait characteristic of participant 2 rather than an adaptation to the arm-based controller. During arm-based control, the amplitude of the arm swing was always larger than what observed during natural walking, with about 20 degrees of max discrepancy occurring at 1.25 m/s. The average shoulder trajectory measured during normal walking was better replicated by the position



controller rather than our arm-based algorithm (figure F.8, Appendix F). This was mostly because during natural walking single swinging was the dominant coordination mode of participant 2 only at 1.25 m/s. Reducing the velocity to 1 m/s already comported hints of double swinging, which became the dominant interlimb synchronisation pattern already at 0.5 m/s.

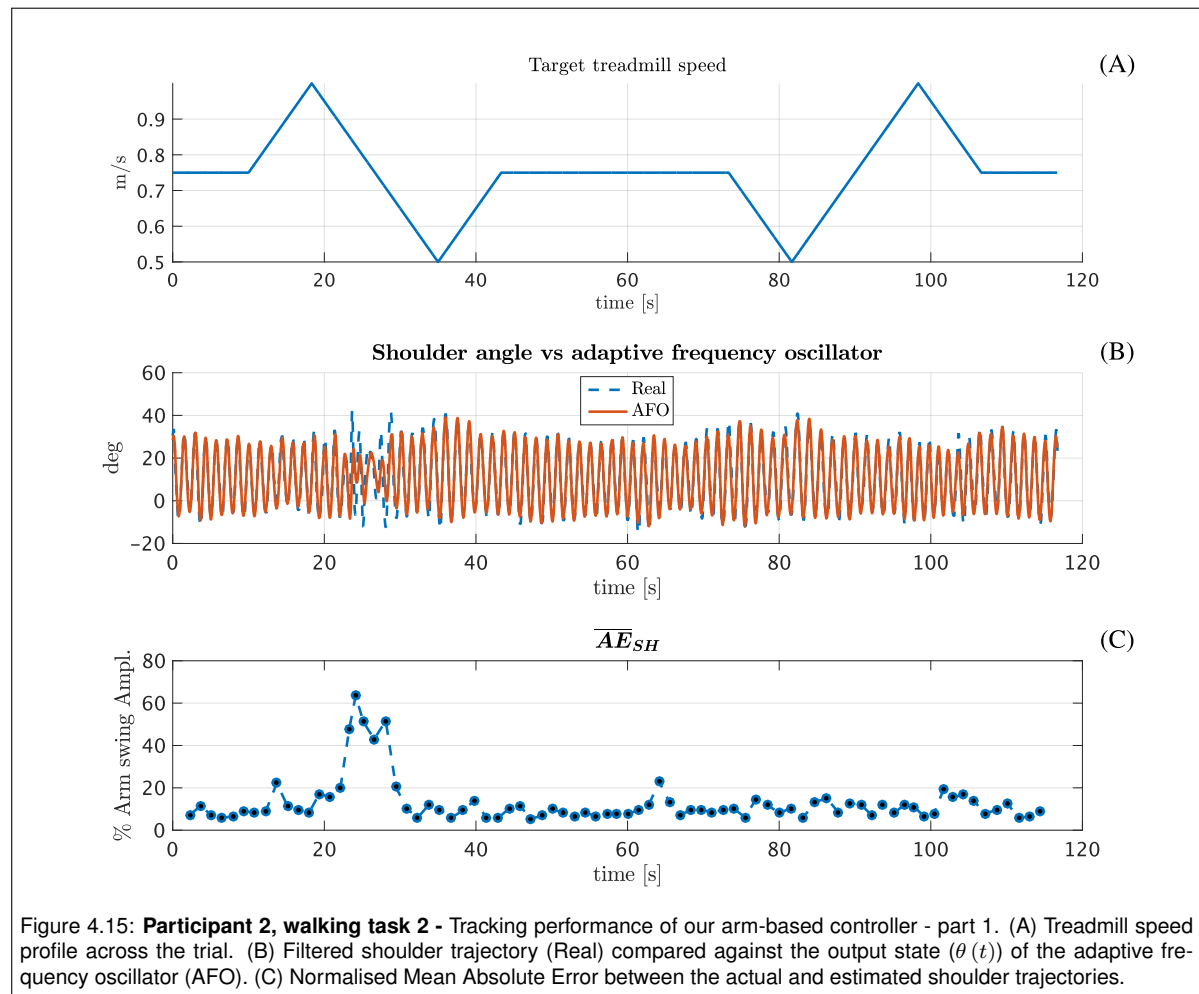


Figure 4.15: **Participant 2, walking task 2** - Tracking performance of our arm-based controller - part 1. (A) Treadmill speed profile across the trial. (B) Filtered shoulder trajectory (Real) compared against the output state ($\theta(t)$) of the adaptive frequency oscillator (AFO). (C) Normalised Mean Absolute Error between the actual and estimated shoulder trajectories.

4.2.3. Arm-based control: Task 2

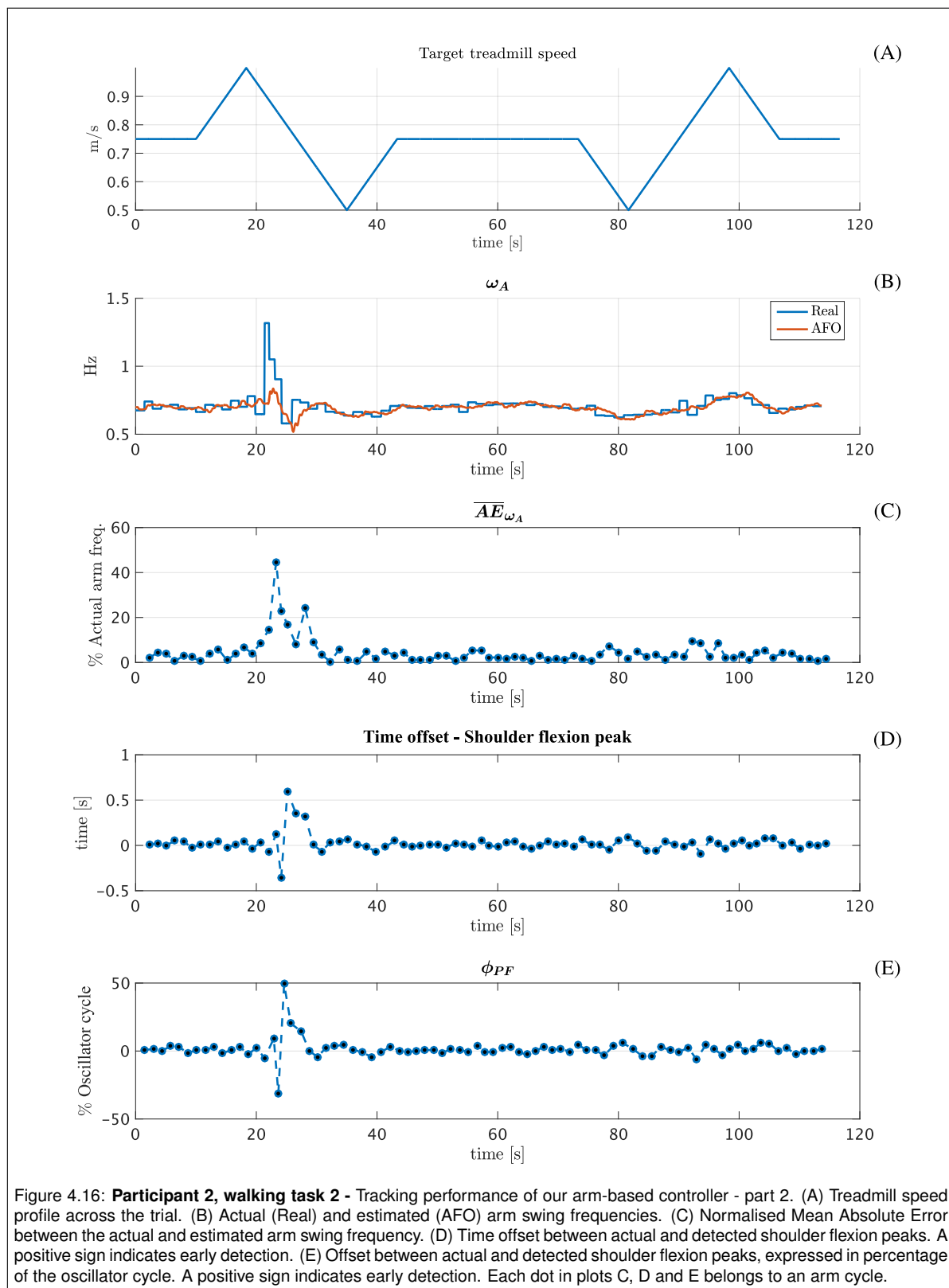
Tracking performance

During task 2, the matching between actual and estimated shoulder trajectories was high (figure 4.15, plot B), with \overline{AE}_{SH} under 20% of the average arm swing amplitude most of the time. At about 25 seconds user's stumbling perturbed the shoulder rotation, causing a large drop in the tracking performance. However, participant 2 could withstand this gait discontinuity by quickly regaining a controlled swing of the right arm. Because of time constraints, it was not possible to repeat the task. Nevertheless, reporting this trial is interesting since it shows that the arm-based controller can face a sudden perturbation of the arm swing without necessarily impairing the gait. Also, the intermediate phase at a constant walking speed acted as a wash-over period for the second part of task 2, making the data associated with the second interval at variable walking velocity likely independent of the stumbling. The plots in figure 4.16 tend to confirm this by showing that during this second interval: participant 2 changed the arm swing frequency proportionally to the belt velocity (plot B); the adaptive oscillator correctly estimated the arm swing cadence (plot C); the detection of the peaks of shoulder flexion was good, in terms of both time (plot D) and percentage of the oscillator cycle (plot E).

Gait generation

Except when the stumbling occurred, the $\omega(t)$ parameter of the adaptive oscillator closely matched the stride cadence, with \overline{AE}_{ω_S} almost always below 5% of the actual stride frequency (figure 4.17, plot C). Therefore, the oscillator frequency, and thus the cadence of the arm swing, was correctly transmitted to the Lopes II also throughout task 2.

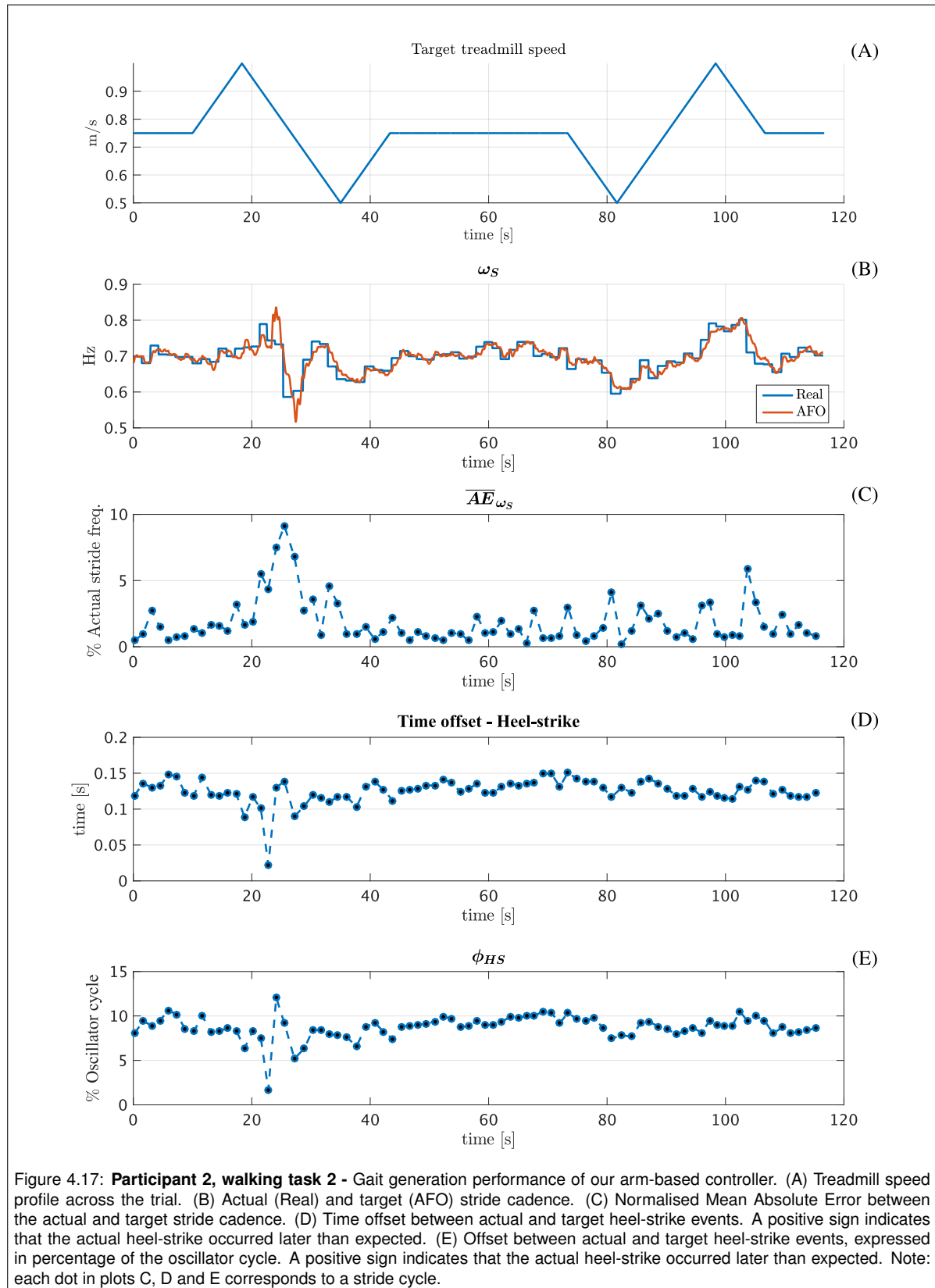
Consistently with task 1 results, during task 2 the heel-strikes occurred later than when targeted by the arm-based controller, with a time offset within the range of 0.1-0.15 seconds (figure 4.17, plot



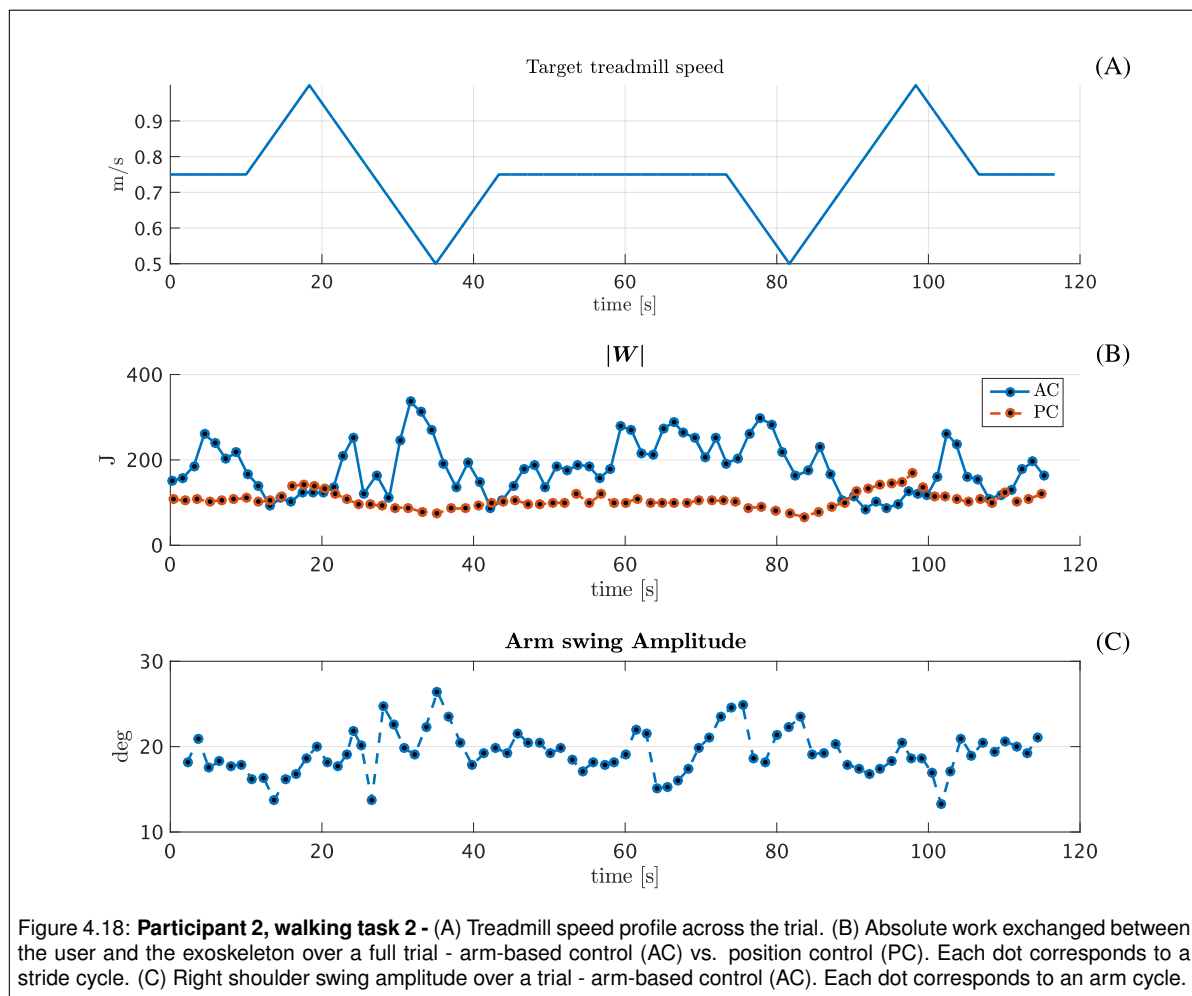
D), corresponding to about 9% of the oscillator cycle (figure 4.17, plot E).

Absolute work & arm swing amplitude

Compared to position control, arm-based control required a greater exchange of absolute work be-



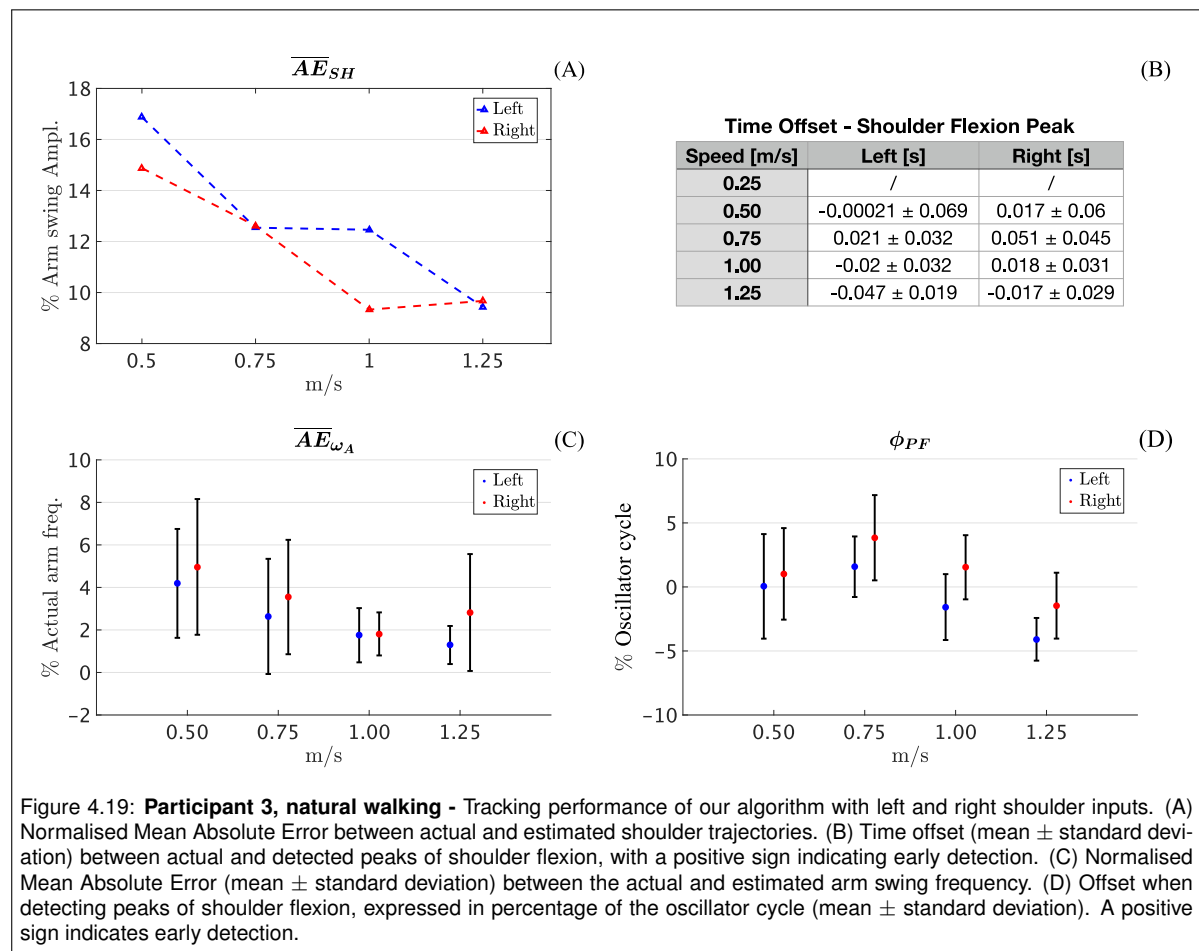
tween participant 2 and the robot (figure 4.18, plot B), suggesting that the user countered the Lopes II trajectories more when using the arm-based controller. In particular, this divergence seems to en-



large during treadmill decelerations, suggesting the arm-based controller to cause more discomfort especially when breaking the walking speed. This consideration, however, is partly contradicted by a similar trend in the dissimilarity of $|W|$ values during the second half of the interval at constant 0.75 m/s.

Participant 2 changed the amplitude of the arm swing during task 2, within a range of 15-25 degrees (figure 4.18, plot C). However, the variation was not clearly related to the ongoing treadmill velocity.

4.3. Participant 3



4.3.1. Natural walking

Tracking performance

The overall synchronisation between each adaptive frequency oscillator and the associated shoulder signal increased with faster gaits, as indicated by the inversely proportional relation between \overline{AE}_{SH} and the walking speed (figure 4.19, plot A). The time traces further confirms that the matching between actual and estimated shoulder trajectories was very high for the walking speeds above 0.25 m/s (figure F.9, Appendix F). In general, the right adaptive frequency oscillator performed slightly better concerning the overall tracking performance.

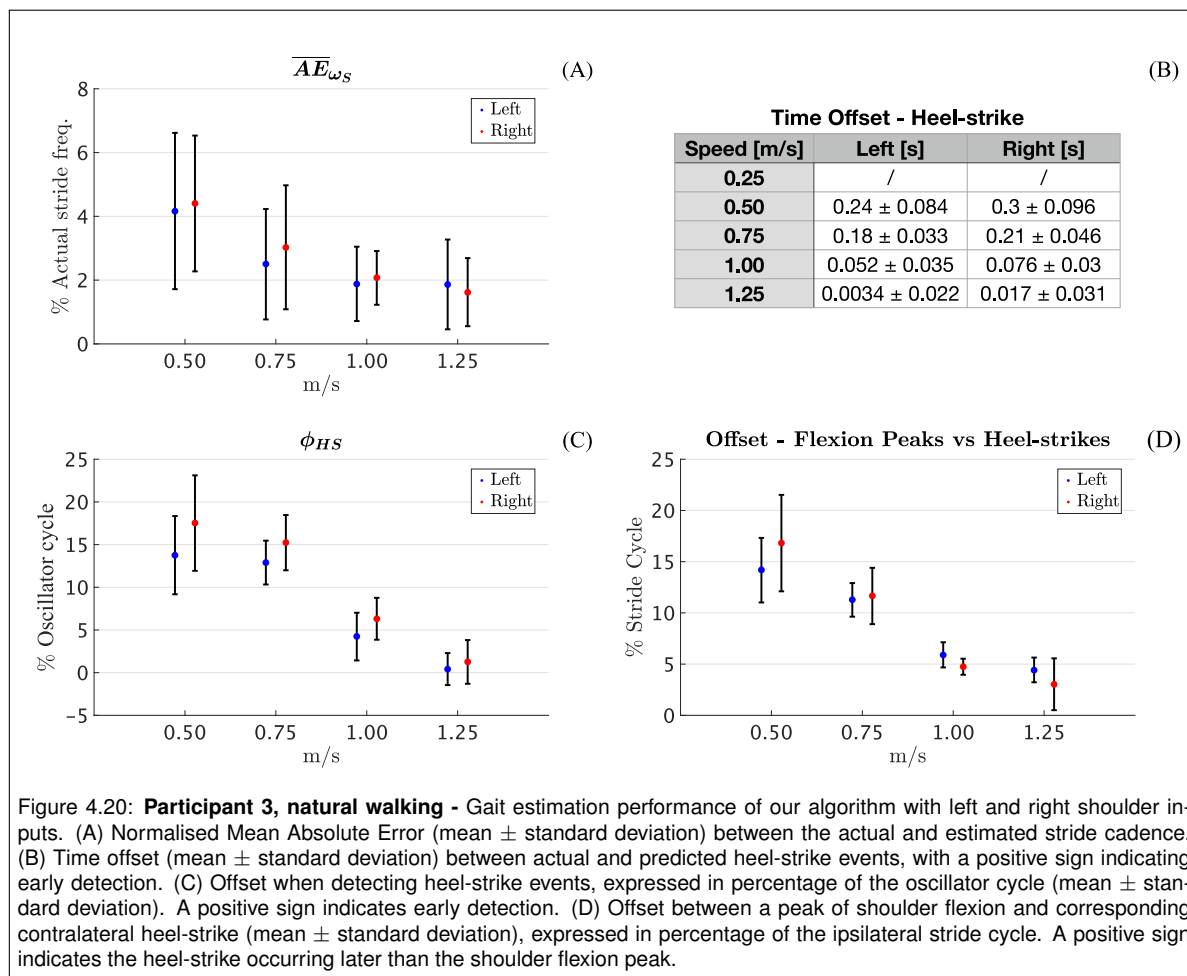
Estimation of the arm swing frequency was excellent for all trials, with \overline{AE}_{ω_A} (on average) reducing with faster gaits and almost no side differences (figure 4.19, plot C).

Detections of shoulder flexion peaks were characterised by small time offsets (figure 4.19, table B), which converted in the percentage of the oscillator cycle, stayed within the range of about $\pm 5\%$ (figure 4.19, plot D). However, the variability in the data does not permit to discriminate clear changes of ϕ_{PF} with either the body side or the treadmill speed.

Gait Estimation

The parameter $\omega(t)$ of the adaptive frequency oscillator could approximate the stride cadence well, with similar performance between the left and right sides (figure 4.20, plot A). Increasing the speed produced slightly better approximations, although the improvements were too small compared to the data variability to assess with certainty a dependence on the walking velocity.

On the contrary, across all speed conditions there was a consistent, positive offset in the heel-strike



detection, meaning too early detection of this gait event (figure 4.20, Table B and plot D). Such an offset was inversely proportional to the walking speed and converged to almost exact predictions when moving towards the 1.25 m/s condition. Like the other participants, this feature was predominantly caused by the natural arm-leg coordination of participant 3 rather than by an inappropriate synchronisation of the adaptive frequency oscillator, as shown by a very similar speed dependent timing between the actual onset of a peak of shoulder flexion and the corresponding contralateral heel-strike (figure 4.20, plot D).

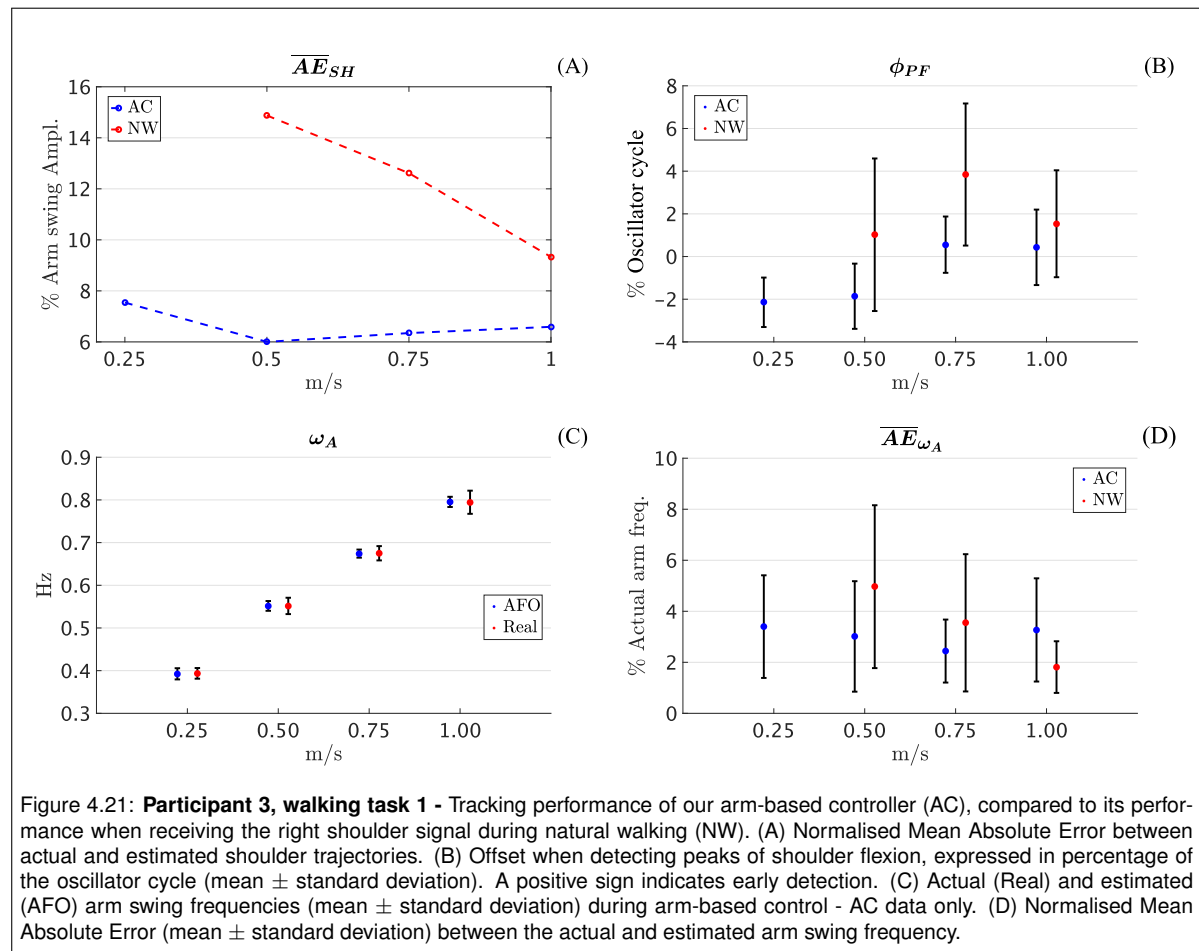
Arm-leg coordination

Participant 3 adopted single swinging within 0.5-1.25 m/s (figure F.10, Appendix F). Only at 0.25 m/s, double swinging occurred, but more visibly for the left shoulder. Notice that compared to other participants, there are no hints of mode transition for participant 3: none of the speed-conditions above 0.25 m/s present signs for the development of a secondary peak. Therefore, the interlimb mode transition for participant 3 occurred much more abruptly than for the other participants.

4.3.2. Arm-based control: Task 1

Controllable range

When using the arm-based controller, participant 3 could complete all trials except walking at 1.25 m/s. Failing to fulfil this condition, however, was caused by hardware malfunctioning in the Lopes II, and thus it was unrelated to the controlling mode. Also, participant 3 could successfully transit between two consecutive speed-conditions with the arm-based controller turned on, i.e. without the need of starting each trial in position control. Participant 3 stated to prefer arm-based control over position control when walking at 0.25 m/s during task 1.



Tracking performance

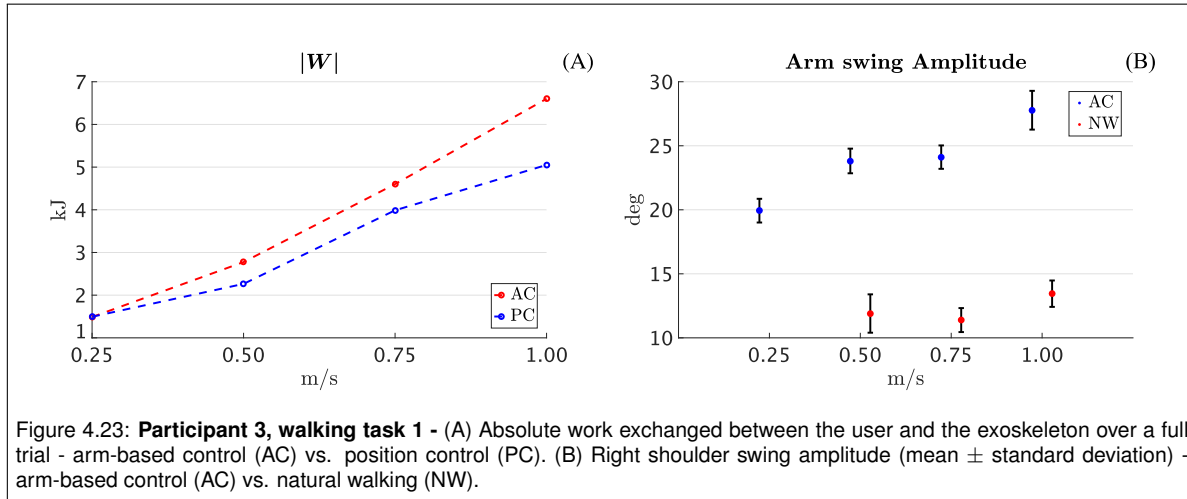
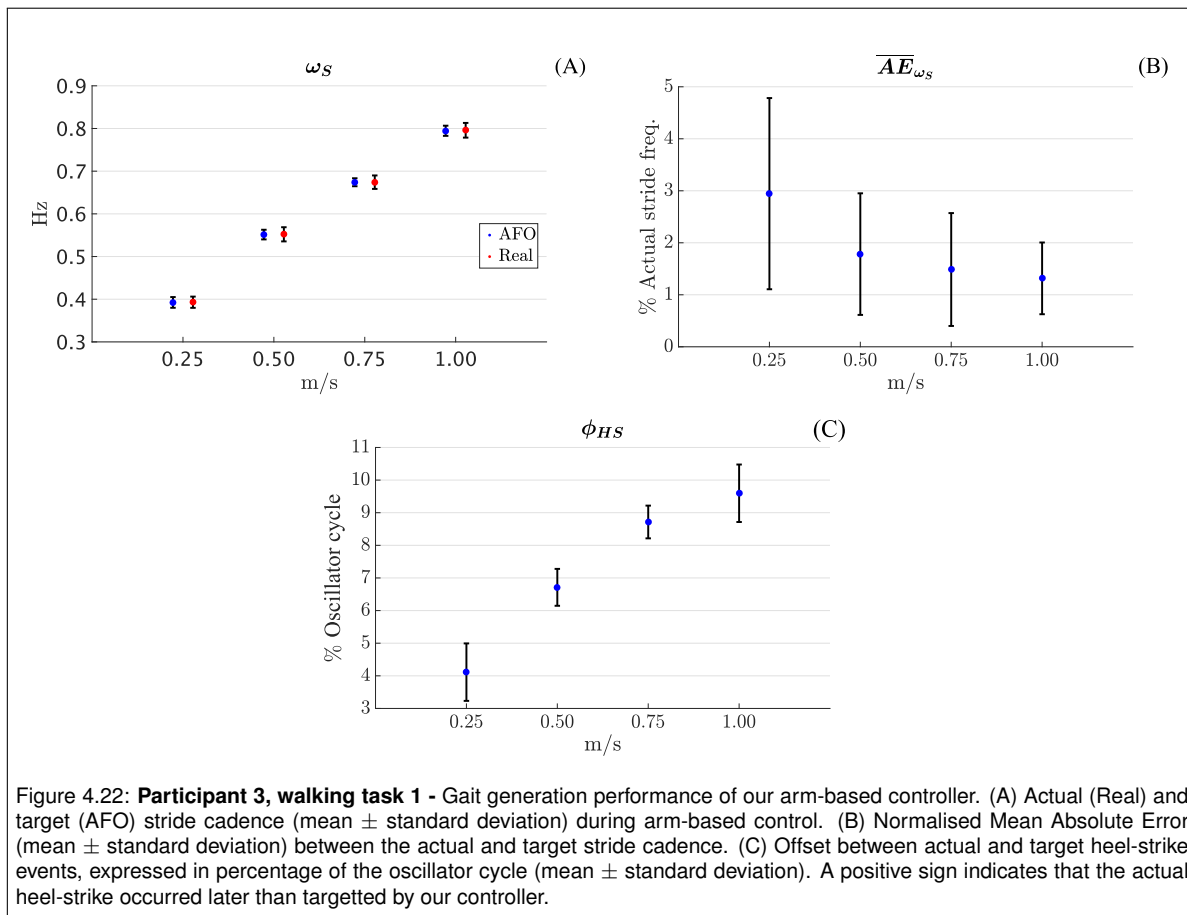
The adaptive frequency oscillator could track the actual right shoulder profile well (figure F.11, Appendix F), with \overline{AE}_{SH} always smaller than 8% of the average arm swing amplitude (figure 4.21, plot A). Participant 3 correctly changed the arm swing frequency proportionally to the walking speed (figure 4.21, plot C). The cadence of the shoulder rotation was estimated very precisely by the Arm Observer, as indicated by \overline{AE}_{ω_A} values always contained, on average, within 2-4% of the actual arm swing frequency value (figure 4.21, plot D). Detection of the peaks of shoulder flexion was also excellent, both in terms of time offset (-0.055 ± 0.03 , -0.034 ± 0.028 , 0.0079 ± 0.02 , and 0.005 ± 0.022 seconds for 0.25, 0.5, 0.75, and 1 m/s, respectively) and percentage of the oscillator cycle (figure 4.21, plot B).

Compared to natural walking, during arm-based control the overall tracking performance was superior (figure 4.21, plot A), which is expected due to the user's active contribution in generating repetitive shoulder rotations. Even the estimation of the arm swing frequency and the detection of shoulder flexion maxima had greater accuracy and precision when using the arm-based controller (figure 4.21, plot D and B).

Gait generation

The stride cadence of participant 3 was proportional to the walking speed, as expected in a healthy gait (figure 4.22, plot A). The $\omega(t)$ parameter of the adaptive oscillator was very close to the measured stride cadence at all speed conditions, with minimal values of \overline{AE}_{ω_S} (figure 4.22, plot B). Therefore, the arm-based controller correctly converted its estimate of the arm swing frequency into the stride frequency during task 1.

The actual heel-strike events occurred consistently later than when targetted by the arm-based controller, with time offset equal to: 0.1 ± 0.021 , 0.12 ± 0.01 , 0.13 ± 0.0075 , and 0.12 ± 0.0095 seconds for 0.25, 0.5, 0.75, and 1 m/s, respectively. This delay was proportional to the walking speed, and once expressed in the percentage of the oscillator cycle, it went from about 4% at 0.25 m/s up to



about 10% at 1 m/s (figure 4.22, plot C).

Absolute work & arm swing amplitude

The absolute work exchanged between participant 3 and the Lopes II was higher during arm-based control than during position control, even though the two trends were quite similar (figure 4.23, plot A). In fact, for both control conditions, $|W|$ was proportional to the walking speed, with about the same value at 0.25 m/s and a slightly steeper slope for the arm-based controller data. Therefore, increasing the speed during arm-based control made the user opposing to the robot trajectories incrementally more than during position control.

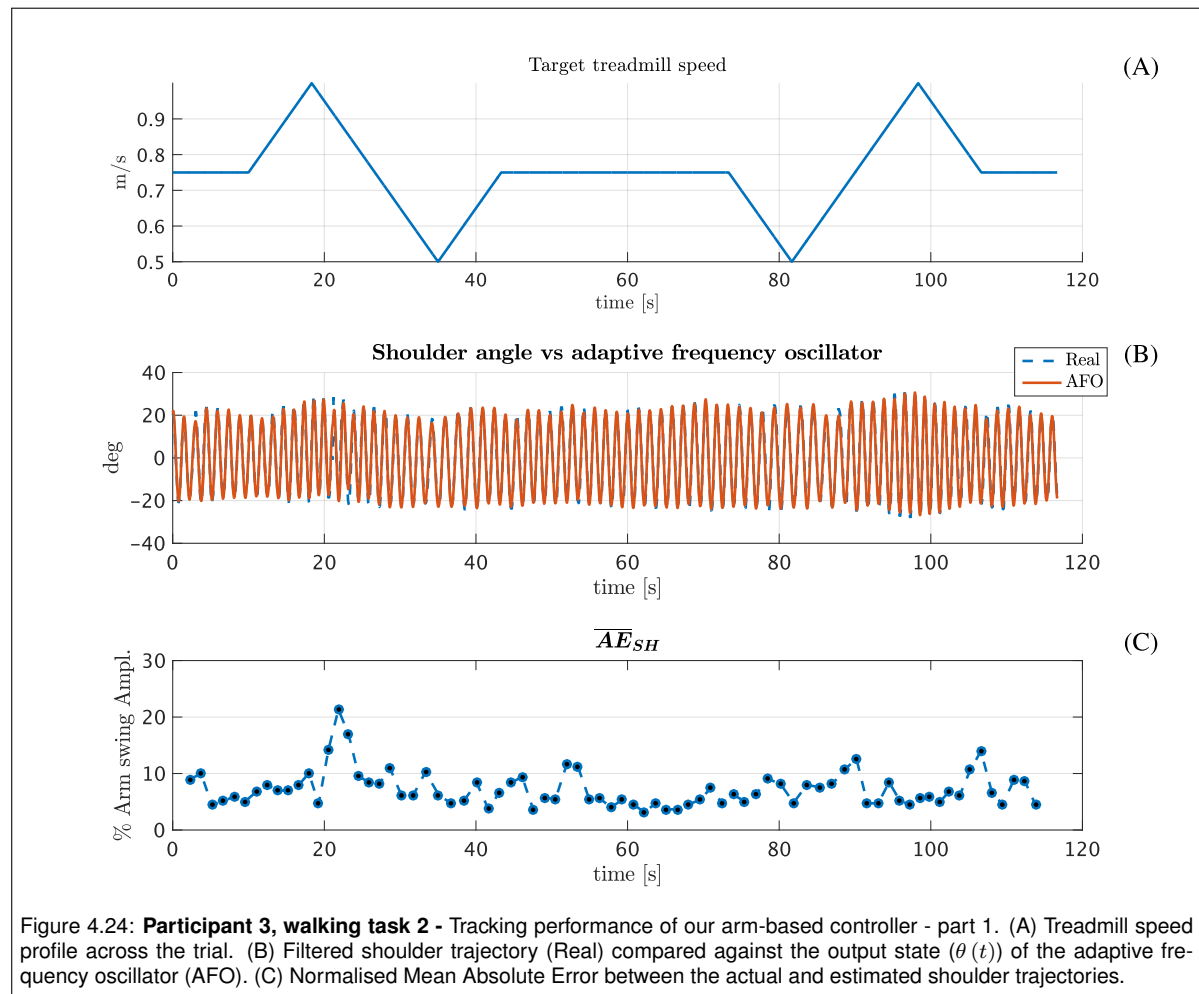


Figure 4.24: **Participant 3, walking task 2** - Tracking performance of our arm-based controller - part 1. (A) Treadmill speed profile across the trial. (B) Filtered shoulder trajectory (Real) compared against the output state ($\theta(t)$) of the adaptive frequency oscillator (AFO). (C) Normalised Mean Absolute Error between the actual and estimated shoulder trajectories.

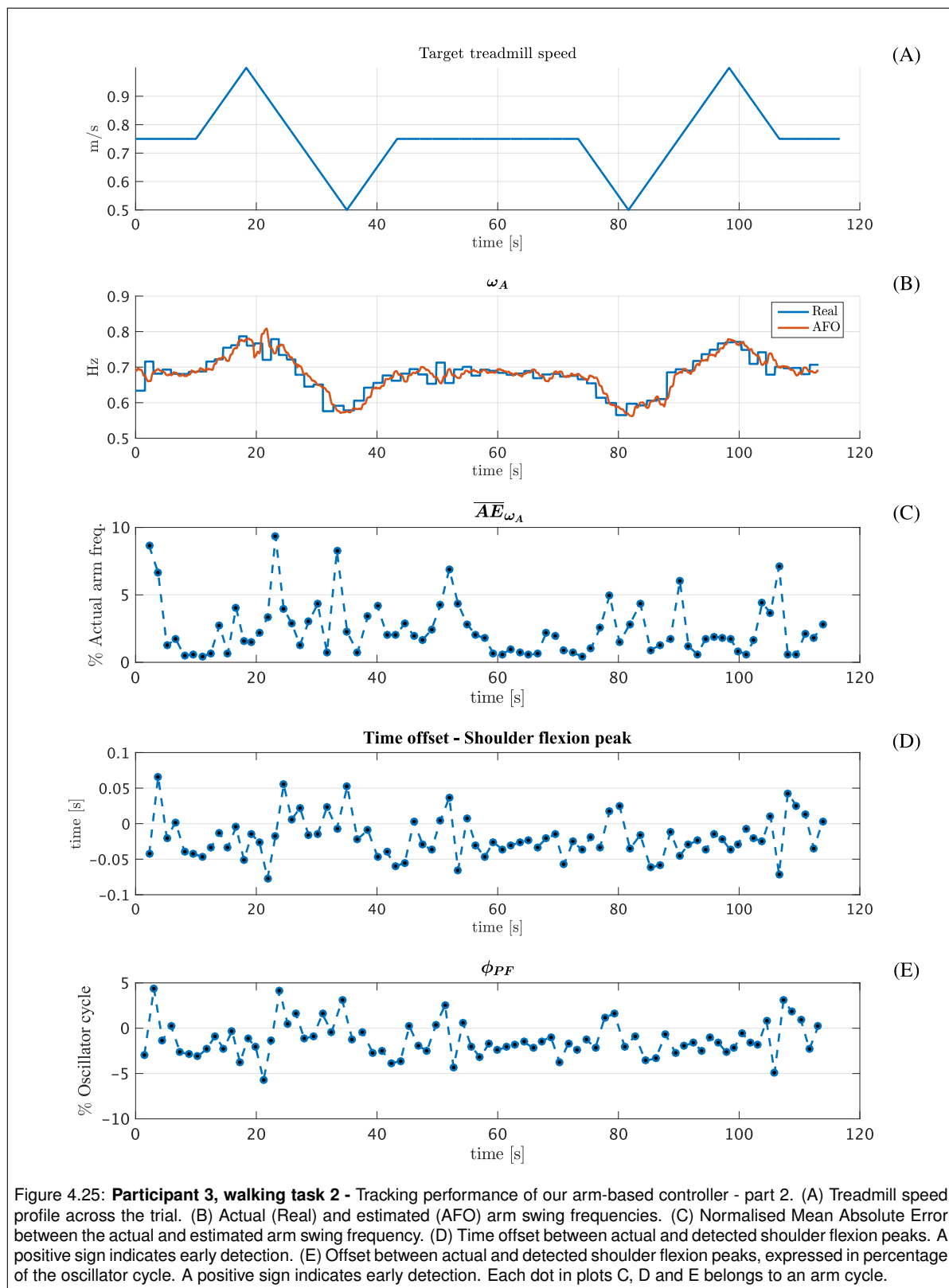
Participant 3 adopted arm swing amplitudes which were proportional to the walking speed during task 1, but change of only a few degrees between consecutive trials (figure 4.23, plot B). The magnitude of the arm amplitude was always about 15 degrees larger than the corresponding value observed during natural walking. Except at 0.25 m/s, the shape of the average shoulder trajectory measured during normal walking was better replicated by our arm-based controller rather than the position (figure F.12, Appendix F). Instead, position control comported an almost absent arm swing during all the trials.

4.3.3. Arm-based control: Task 2

Tracking performance

The similarity between the actual shoulder profiles and the trajectories estimated by the adaptive frequency oscillator was high throughout task 2 (figure 4.24, plot B and C). However, during the first interval of variable velocity, a distinct peak of \overline{AE}_{SH} occurred just after the treadmill reached its maximum speed. Post-hoc inspection of the raw signal associated with the angular position of the right shoulder revealed that, at the time in which this peak occurred, the Xsens suit failed to transmit data to the Lopes II xPC correctly: for few seconds the signal froze to a constant value. Therefore, the reduction in tracking performance is an artefact linked to the sensor malfunctioning. Similarly to the stumbling event of participant 2, such a finding shows that, thanks to the filtering action of the adaptive frequency oscillator, the arm-based controller could face sudden (but temporary) discontinuities in the input signal without destabilising the gait.

Participant 3 correctly adapted the arm swing frequency to the ongoing treadmill velocity, and the Arm Observer consistently tracked these changes (figure 4.25, plot B and C). \overline{AE}_{ω_A} was more variable during the two intervals at changing treadmill velocity, and these variations did not have a definite relation to the ongoing speed. Still, \overline{AE}_{ω_A} was limited to small values (below 5% of the real arm swing



frequency) for most of task 2.

The detection of shoulder flexion peaks was good, with time offsets confined within the range of ± 0.05 seconds ($\pm 5\%$ in the percentage of the oscillator cycle) most of the time and without distinct differences between intervals at variable and constant treadmill speed (figure 4.25, plots D and E).

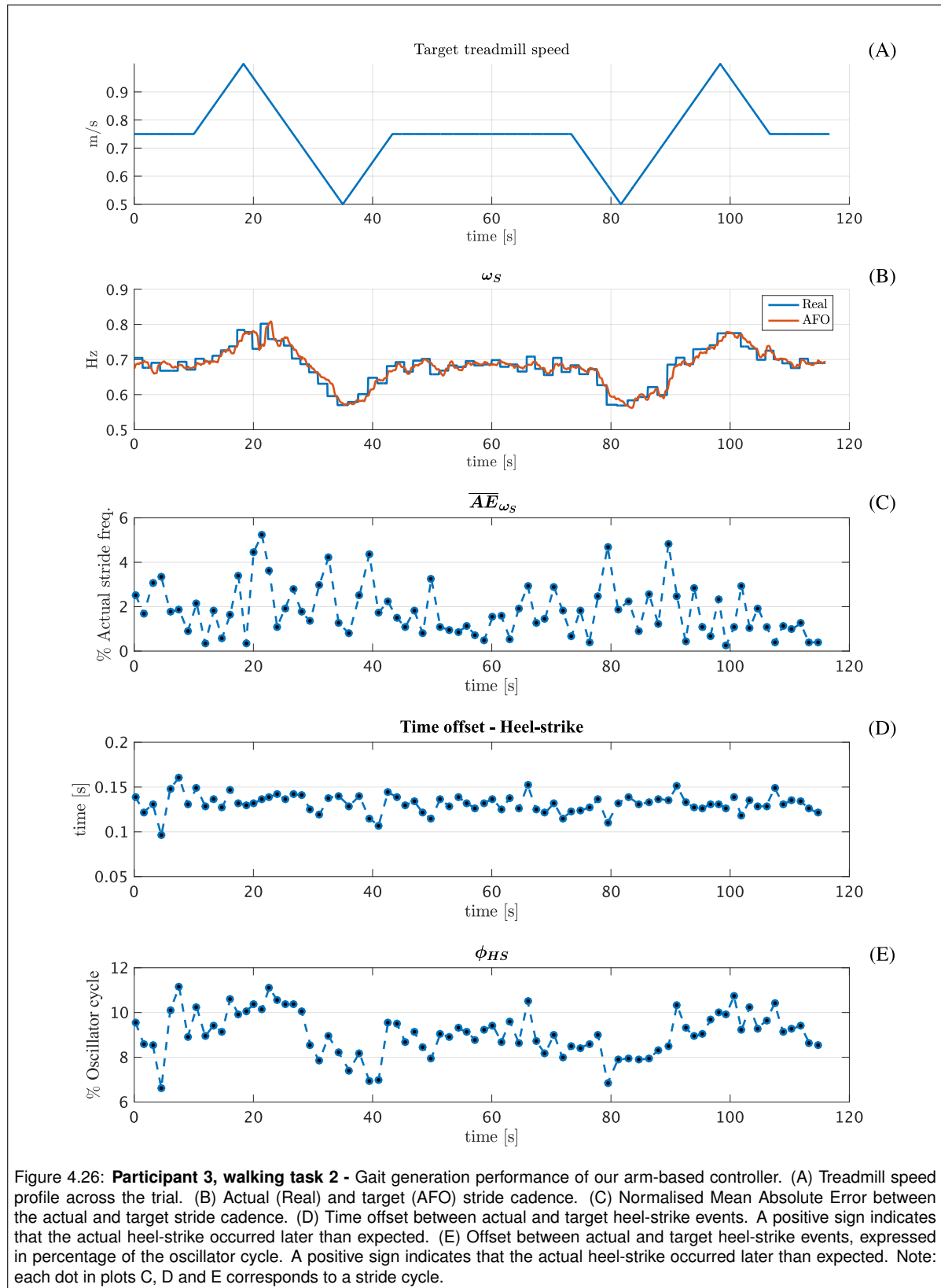
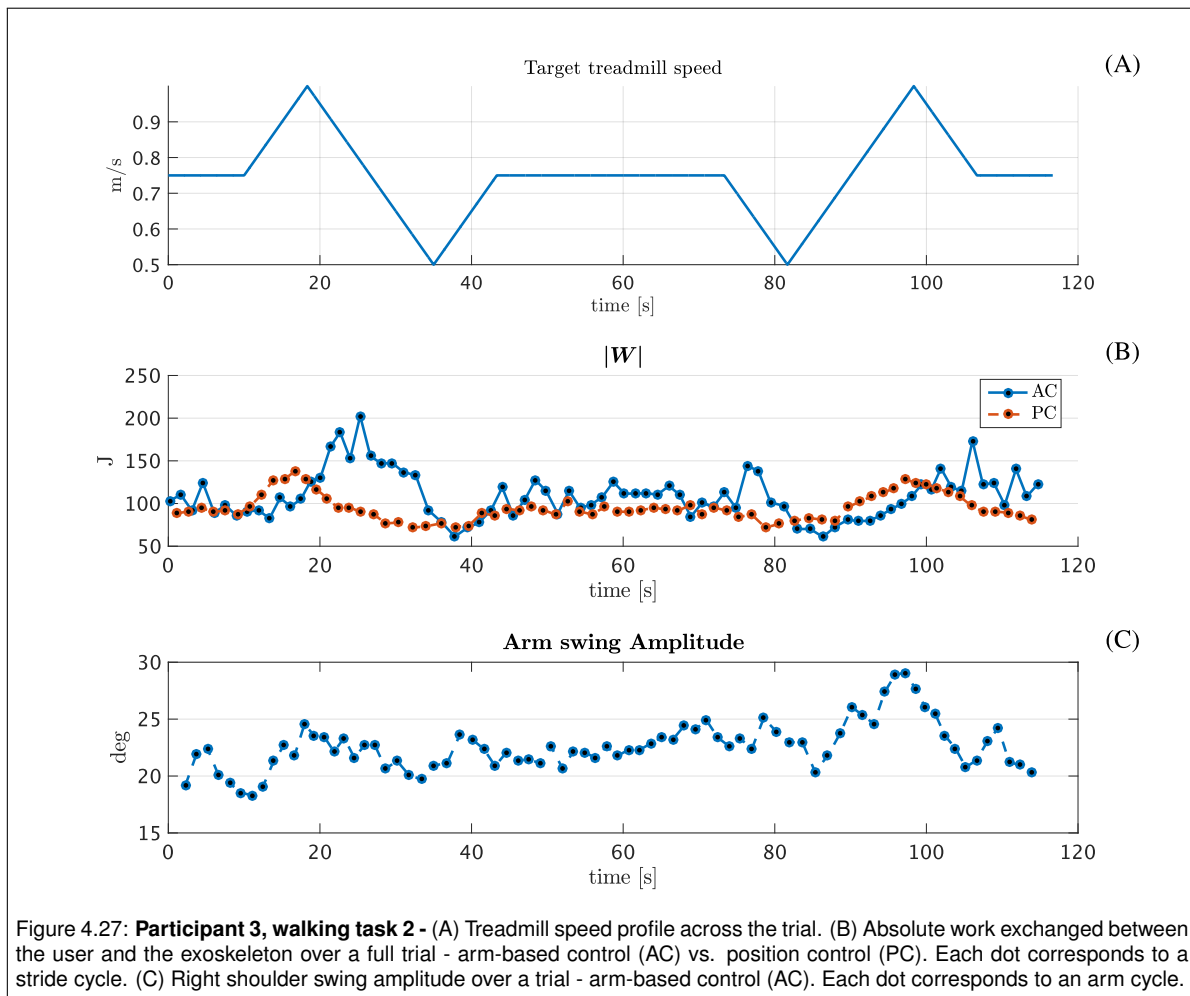


Figure 4.26: **Participant 3, walking task 2** - Gait generation performance of our arm-based controller. (A) Treadmill speed profile across the trial. (B) Actual (Real) and target (AFO) stride cadence. (C) Normalised Mean Absolute Error between the actual and target stride cadence. (D) Time offset between actual and target heel-strike events. A positive sign indicates that the actual heel-strike occurred later than expected. (E) Offset between actual and target heel-strike events, expressed in percentage of the oscillator cycle. A positive sign indicates that the actual heel-strike occurred later than expected. Note: each dot in plots C, D and E corresponds to a stride cycle.



Gait generation

The stride cadence changed proportionally to the ongoing walking speed and accordingly to the $\omega(t)$ parameter of the adaptive frequency oscillator (figure 4.26, plot B), as also indicated by \overline{AE}_{ω_S} being lower than 4% of the real stride cadence value for most of task 2 (figure 4.26, plot C). Therefore, even during task 2, the algorithm correctly transmitted the arm swing frequency to the gait dynamics. However, the two intervals at variable speed were characterised by larger and more intense variations of \overline{AE}_{ω_S} than the part at constant treadmill velocity. Such fluctuations might indicate a reduced synergy between the user and the Lopes II, with participant 3 opposing more to the gait that was promoted by the robot.

The trend of the heel-strike detection error was similar to that observed during task 1, i.e. foot drops occurred with a time delay that ranged between 0.1-0.15 seconds (figure 4.26, plot D). In percentage of the oscillator cycle, this offset was confined within about 6-11%, highlighting a trend faintly proportional to the treadmill speed (figure 4.26, plot E).

Absolute work & arm swing amplitude

The absolute error exchanged between participant 3 and the Lopes II had a similar trend when walking with the two control modes (figure 4.27, plot B). During position control, $|W|$ reached its major peaks close to the two instances of maximum treadmill speed. During arm-based control, the local maxima of $|W|$ were higher in magnitude than those of position control and occurred within the decelerating tracks of the speed profile. This finding indicates that during arm-based control participant 3 had more difficulties in breaking the gait of the Lopes II rather than accelerating it, while during position control the opposite was true.

Participant 3 changed the arm swing amplitude almost proportionally to the walking speed during

the two intervals at variable treadmill velocity (figure 4.27, plot C). During the intermediate interval at constant 0.75 m/s, the arm swing amplitude increased steadily over time, but still the overall gain was small (about 5 degrees).

5

Discussion

5.1. Analysis of natural walking

We chose natural walking as the experimental framework for validating the reliability of our control architecture in extrapolating relevant features of the arm-leg coordination. We based such validation on proving two points:

1. Tracking performance: how well the adaptive oscillator could synchronise to its target shoulder signal;
2. Gait estimation: the suitability of the adaptive oscillator parameters for estimating pace properties, assuming successful synchronisation with the shoulder signal has occurred.

Natural walking offered the perfect condition to test these aspects. This task not only allows us to validate our controller with healthy interlimb data, but also to assess lateral asymmetries, i.e. whether the data of one of the two shoulders results in superior performance our algorithm. Addressing this last issue was important because our algorithm requires only the signal from one upper limb to work, and the literature suggests side asymmetries in the arm swing.

5.1.1. Tracking performance

For all the participants, the results confirm that at walking speeds within 0.75-1.25 m/s the synchronisation between each adaptive frequency oscillator and its input shoulder signal was excellent, with the oscillator parameters $\omega(t)$ and $\phi(t)$ precisely estimating the arm swing frequency and timing of shoulder flexion peaks, respectively. Reducing the walking speed below such a range compromised the matching between actual and estimated shoulder trajectories, and as a consequence, the reliability of $\omega(t)$ and $\phi(t)$ as estimators of the arm swing properties reduced as well. At 0.5 m/s, this diminished tracking performance seems caused by the gradual transition from single to double swinging. This change in coordination mode made minor peaks of shoulder flexion to emerge sporadically within an arm cycle, resulting in a more ambiguous duration of the arm oscillation. The transition was strongly subject-specific and side-dependent, and so its effect on the tracking performance. However, the analysis attests that our algorithm failed to work at 0.25 m/s. At this walking speed, the amplitude of the arm swing decreases consistently, a fact that combined with the height variability in the peaks of shoulder flexion, made the signal too irregular to be tracked by our Arm Observer.

5.1.2. Gait estimation

The $\omega(t)$ parameter of the adaptive frequency oscillator was an excellent estimator of the stride cadence when the walking speed was over 0.5 m/s, thanks to the dominance of single swinging as interlimb coordination mode. However, heel-strike detection was less precise. The results indicate that this gait event was estimated consistently in advance to its actual occurrence, with a magnitude of the offset that was inversely proportional to the walking speed. The error, however, does not seem caused by a malfunctioning of our control algorithm, but rather by the design approximation that we made by assuming the coincidence between the peaks of shoulder flexions and contralateral heel-strikes.

Accordingly, $\phi(t) = 0$ was very representative of peaks of shoulder flexion, but less of contralateral heel-strikes. Increasing the speed comported the participants spontaneously adopting more coincident occurrences of shoulder flexion peaks with heel-strike events, a fact that improved the heel-strike detection carried by our algorithm. Our finding of a speed-dependent timing in the arm-leg relative motion is coherent with the work of Carpinella et al. [3] (see figure 4, pag. 78), which even points out the dependence of such an offset on the experimental set-up (treadmill vs. overground walking).

5.1.3. Side-differences

A part of our result analysis investigates whether the performance of our arm-based controller is affected by lateral differences in the arm swing, a topic which is not well addressed by the literature (see Chapter 1). Our experimental analysis does not provide solid reasons to prefer one side of the body as a source of inputs to our controller, which displayed similar performance when feed by either left or right shoulder trajectories.

5.2. Analysis of task 1 and 2

The second half of the experiments consisted of testing our arm-based controller on a real-time implementation. For this objective, we asked three participants to control, through our algorithm, the Lopes II, a treadmill-based lower limb exoskeleton (see Chapter 4). In particular, we studied the functionality of the algorithm while performing two tasks: walking with constant (task 1) and variable (task 2) treadmill speeds. In this way, our experimental protocol was similar to that used by La Scaleia et al. [21], permitting a partial comparison of our algorithm with their proposed arm-based controller. However, the range of walking speed that we tested was different from this previous study: our speed interval was more appropriate for gait rehabilitation and assistance (0.25-1.25 m/s). In our experimental analysis, we also investigated the shoulder trajectory promoted by our arm-based controller, with a particular focus on the arm swing amplitude and its adaptation to the walking speed. We centred this part of the investigation on evaluating whether our algorithm could overcome one of the limitations in [21]: exaggerated arm swing amplitude - potentially forced to be fixed across walking speeds. Eventually, we also compared our controller against position control, a default control mode for the Lopes II. This was a minor part of our analysis, which we predominantly centred on comparing the differences in the user's control effort.

5.2.1. Task 1: constant treadmill speed

The results from task 1 suggest that our arm-based controller allows to drive a lower limb exoskeleton with walking speeds in the range of 0.5-1 m/s. People could even control the Lopes II at 1.25 m/s, but hardware malfunctioning impeded two of the participants to complete this testing condition. Walking at 0.25 m/s was not possible for participant 1, and participant 2 mentioned to find unintuitive swinging the arm slowly enough to meet this treadmill velocity. On the contrary, participant 3 stated to prefer arm-based control over position control when testing such a slow gait speed. The functionality of the arm-based controller did not change consistently to justify the difficulties associated with participants 1 and 2. The fact that our algorithm does not support a transition to double swinging does not provide a full explanation either: all the participants walked with double swinging at 0.25 m/s, including participant 3. Therefore, these contradicting results might be associated with subject-specific preferences, or with aspects of the human-machine interaction that we did not include in the analysis.

Heel-strike events occurred consistently later than when targeted by the arm-based controller. Considering the results from natural walking, we were expecting inaccuracies in the interlimb timing promoted by our controller. However, while during natural walking increasing the gait speed made shoulder flexion peaks and heel-strike events more coincident, the opposite happened with our controller. It is likely that wearing an exoskeleton comported a reorganisation of the spontaneous interlimb timing, and that this aspect was not adequately represented in our algorithm. A change in the natural interlimb coordination due to wearing the Lopes II is also suggested by data recorded during position control. When using this latter controller, people were reluctant in swinging their arms, as shown by the average shoulder trajectories in figures F.4, F.8 and F.12 of Appendix F. This finding is surprising since part of the literature suggests the arm swing to improve the gait balance [24]. As such, one would expect people to emphasise their arm rotations to counter the gait perturbation introduced by the Lopes II. Our finding advocates for a more in-depth investigation on the effects of wearable robotics

on the user's arm-leg coupling, an experimental framework which might be useful also for validating models of human interlimb coordination.

Our arm-based controller allowed the participants to change the stride cadence by varying the arm swing frequency, and, as desired, people changed the cadence of the arm oscillation proportionally to the walking speed. Also, our algorithm did not force the user to maintain a fixed arm swing amplitude across the tested conditions. Still, speed-dependent variations of the arm swing amplitude were very small in magnitude, and for only one user (participant 3) they were proportional to the walking speed. In particular, when walking below 0.75 m/s, the remaining two participants had unnatural inversely proportional relations of their arm swing amplitude to the treadmill velocity. This abnormal trend might be another sign of the perceived control difficulty by participants 1 and 2 during the slowest conditions. For instance, it is possible that these users found unintuitive to reduce their shoulder angular velocity below a certain threshold. As a compensatory strategy, they might have increased the arm rotation to reduce the arm swing frequency further.

Compared to the data recorded during natural walking, people adopted emphasised shoulder rotation when using our arm-based controller. However, these larger amplitudes were not necessary for the correct functionality of our algorithm: the overall tracking performance improved during arm-based control, but \overline{AE}_{ω_A} and ϕ_{PF} preserved similar characteristics to those observed during natural walking. The emphasised arm swing amplitude during arm-based control does not seem caused by wearing the exoskeleton, considering that during position control the participants' arm swing amplitude was almost null. It is possible that asking people to consciously swing their arms comported the emphasised rotations, considering the pieces of evidence suggesting a dependence of the arm swing amplitude on the cognitive task [14]. Still, our analysis did not include any metrics to validate such a consideration, which we leave as a hypothesis for future studies

Compared to position control, our controller can promote shoulder trajectories that are closer to the natural ones, especially for walking speeds within 0.75-1.25 m/s. Still, the fitness of our algorithm was subject-specific since position control produced more natural arm swing patterns if a person had a more dominant double swinging coordination.

Given a specific speed condition, $|W|$ was usually higher during arm-based control than during position control, suggesting more demanding control effort with our controller. The speed-dependent trend of this energetic difference changed remarkably across the participants. This fact, together with the limited number of participants involved in our study, did not allow us to distinguish a certain aspect of our algorithm associated with this surplus of control effort.

5.2.2. Task 2: variable treadmill speed

All the participants could complete task 2, proving that our arm-based controller allows online adaptation of the walking speed - at least within the tested range (0.5-1 m/s). Throughout the task, each user correctly changed the arm swing frequency proportionally to the treadmill velocity. However, the amplitude of the shoulder rotation changed of only a few degrees, with data variability that does not allow to detect a clear dependence on the walking speed. Part of the data fluctuations, however, might have been provoked by our experimental protocol since the participants might have perceived changes in the treadmill dynamics with some delay.

Regarding tracking performance and gait generation, the functionality of our arm-based controller was similar among the intervals at variable and constant treadmill speeds. However, analysis of the differences in $|W|$ suggests that the user had more difficulties in decelerating the exoskeleton when using our controller. Considering that two participants out of three found walking at the slowest speed condition more problematic during task 1, a similar conclusion seems reasonable.

The results of task 2 also show that our arm-based controller can withstand perturbations to the input shoulder signal. This robustness is due to the filtering properties of the adaptive frequency oscillator, which permitted to minimise discontinuities in the input data that were caused by two accidental scenarios: user's stumbling and sensor malfunctioning. A systematic quantification of the robustness of our algorithm was not part of our analysis, and we leave this objective for later studies. However, our results raise the question of whether it is worth considering sensory fusion as an improvement for subsequent design versions of our controller. Due to the in-built filtering properties of the adaptive oscillator, the overall gain in signal-to-noise ratio when combining the signals from both shoulders might be unworthy compared to the increased algorithm complexity. Moreover, minimising the set of input signals to one limb data might have significant practical advantages: for instance, a new exoskeleton

user, or a person with severe lower leg impairments, can use the free arm for extra support, such as grabbing a hand bar or using a crutch.

5.3. Comparison to other techniques

Our control algorithm could address some of the limitations associated with the arm-based controller described in [21]. By making their algorithm dependent on the deltoid EMGs, La Scaleia et al. [21] had to implement extensive signal processing techniques to deal with the weak activity of the arm swing muscles. By relying on shoulder kinematic data, our implementation requires just a small set of equations (see Chapter 2) to extrapolate characterising details of the interlimb coordination. Moreover, our algorithm already embeds filtering properties, resulting in robustness against (temporary) input discontinuities. Our algorithm was also successfully tested within a range of walking speeds more representative of robotic gait rehabilitation and assistance - despite its diminished functionality at 0.25 m/s.

In Chapter 1, we observed that the controller proposed by La Scaleia et al. [21] requires shoulder rotations larger than normal and potentially impedes a proportional relation of the arm swing amplitude with the walking speed. Our experimental analysis, however, shows that speed-dependent adaptations of the arm swing amplitude are small in magnitude when walking normally. For this reason, limiting the adaptability of the shoulder rotation amplitude might not be as detrimental as we argued in Chapter 1. Nevertheless, our control algorithm still transcends the work of La Scaleia et al. [21] by granting to the user the ability of self-regulating his/her arm swing amplitude, i.e. it does not impose any restriction a priori.

Because of people also adopting emphasised arm swing amplitudes when using our arm-based controller, we can not argue that our method was better than the previous implementation in this regard. Still, La Scaleia et al. [21] do not report a quantification of the extra amplitude needed by their algorithm. As such, it is still possible that our proposed approach requires less surplus of shoulder rotation.

In general, we expect that other arm-based controllers would have similar issues to the method of La Scaleia et al. [21] when using shoulder muscle EMGs as inputs. As such, it is likely that our algorithm can outperform even online extensions of the regression approach proposed by Chéron et al. [5]: they trained a dynamic recurrent neuronal network over shoulder EMG data to produce (offline) gait trajectories. Nevertheless, a question that remains open is whether an arm-based controller that uses regression techniques on interlimb kinematic data would outperform the achievements of this thesis project. A reasonable candidate to make such a comparison would be extending Complementary Limb Motion Estimation (CLME) to upper limb data. By exploiting the synergetic properties of human gait, CLME uses Principal Component Analysis (PCA) to infer the motion of an impaired extremity from data recorded at a sound limb [39–41].

We expect our controller to still have some advantages over similar approaches. For instance, CLME was tested using a sound leg data. Because arm-leg coupling is much weaker than the leg-leg one [48], it is possible that PCA, or any other regression approach dependent on the strength of the limb coupling, would fail in extracting the interlimb synergy. Moreover, human arm-leg coordination has subject-specific and task-dependent properties (see Chapter 1) which might be difficult to represent in a training dataset. Another interesting feature of our controller, which is likely absent in a strict regression-based mapping of the arm-leg trajectories, is its modularity: the Arm Observer can be coupled with gait generator algorithms that are different from the one we used, potentially adapting our control structure to exoskeletons requiring other types of command inputs [37]. This flexibility is a significant asset when considering the current absence of a mobile exoskeleton suitable for arm-based control, and thus the need for compatibility with potential new generations of low-level controllers.

5.4. Limitations

Despite the mentioned benefits of our controller over other approaches, our work has limitations as well. To begin with, our arm-based controller can not start the gait. In our exoskeleton implementation, gait initiation was carried by position control. This was a technical solution, which works well for a treadmill-based exoskeleton, such as the Lopes II. In fact, the user is given time to reach a stable arm-leg coordination and feel comfortable with the device on, while the adaptive frequency oscillator can converge to the shoulder signal in the meantime. A similar gait initiation strategy, however, is prob-

lematic for mobile applications. In particular, when walking overground, the available straight walking distance is limited by the walking environment. Therefore, the extension of our proposed algorithm to a mobile exoskeleton requires to design a strategy for initialising the system and the gait within a minimum number of steps. Furthermore, our arm-controller would also require additional navigation functions, such as steering left and right.

Another limiting factor for extending our controller to mobile applications is that the implementation of the just described functions requires knowledge about the exoskeleton specifics. However, a mobile exoskeleton suitable for arm-based control is not available yet: the current technologies force motor impaired users to carry assisting walking aids. The literature also shows that the requirements for a control architecture can change consistently among different devices [37]. Therefore, despite we advocated for the benefit of our modular design, we can not ensure that our controller would be transferable to new exoskeleton generations without major modifications.

An important problem in our study concerns the transferability of our results. To the best of our knowledge, the influence of an exoskeleton on human interlimb coordination has never been studied. This fact and the current lack of a proper understanding of the arm swing make challenging the generalisation of our study. In other words, the performance reached by our controller might be specific of our experimental set-up, i.e. the Lopes II. Different exoskeletons, and more in general testing conditions, might comport a different user's response to our control strategy. For instance, we expect a different, but hopefully improved, control performance whether the treadmill speed could promptly adapt to the user's gait velocity, that is an antithetical scenario to task 2.

The generalisability of our results is also diminished by the exiguous number of participants that we could test. Unfortunately, experience with the Lopes II was an essential requirement to take part in our experimentation (see Chapter 3), and only few of trained users were available at the time of our study. Due to this restricted sample, we could not apply inferential statistics to our results. Such a more sophisticated analysis would have been beneficial, for instance, to unveil whether implementing a transition to double swinging can enhance our algorithm controllability. Repeating our experiments with a larger sample of participants might also extend the analysis to topics that we could not cover, such as the influence of hand-dominance on our controller performance.

Another limitation of our experimental protocol is the lack of training sessions with our controller. As such, the comparison of our controller performance with that achieved during position control was partly biased, since participants were expert users only of this latter condition. Despite we gave people a few minute of practice with our algorithm, this does not ensure that participants reached the same dexterity and level of confidence in using our controller. This fact might have caused the observed discrepancies in controllability at 0.25 m/s. A long term study can unveil the full potential of our method. For instance, it can confirm whether becoming more comfortable with our algorithm results in arm swing amplitudes closer to those observed during natural walking (or whether participants can be trained to adopt more natural shoulder trajectories).

Comparison to position control was also limited by our use of $|W|$ as metric for evaluating the perceived control effort. In the literature, there are no studies validating such an approach, and despite $|W|$ trend was consistent with other metrics, such as the delayed heel-strikes, other measurements would have been more rigorous: for instance, the measurements of the user's metabolic cost by oxygen intake. However, recording metabolic data would have also overcomplicated the experiment, extending excessively its duration due to the many associated challenges (such as lengthy and complex calibration processes and management of cumbersome equipment).

6

Conclusions

In this thesis, we designed a control algorithm to drive online a lower limb exoskeleton through the user's arm swing. A control strategy that exploits human interlimb coordination may be beneficial to robotic gait rehabilitation and assistance. In particular, it offers a valid alternative when the user's motor impairment makes data from the lower limbs unpractical to measure. A previous attempt of a similar design is found in [21]. In their study, La Scaleia et al. [21] proposed an algorithm that extracts the duration of a forthcoming step from the gait-related rhythmic activity of deltoid muscles and then stretches some predefined gait trajectories accordingly. In chapter 2, however, we observed that relying on such a weak muscular activity is limiting, and potentially impedes the applicability of the controller to real gait rehabilitation and assistance.

The most significant contribution of this thesis is to propose an arm-based controller that depends only on shoulder kinematic data, virtually not imposing explicit constraints on the amplitude of the arm swing. We based our novel approach on mimicking single swinging, an interlimb coordination pattern that occurs during normal walking and that consists of each arm moving in-phase with the contralateral leg. In order to reproduce single swinging, we implemented a control structure combining the adaptive frequency oscillator discussed in [34] with the regression model for the generation of lower limb trajectories described in [16]. In particular, we proposed the use of the adaptive oscillator to extract the arm swing frequency and phase of the arm rotation from online measurements of the angular shoulder rotation in the sagittal plane. From these estimations, our algorithm determines the desired walking speed and the current phase of the stride cycle, and consequently the target trajectories for the exoskeleton joints.

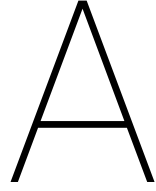
Another contribution of this thesis is the validation of our proposed control algorithm by a human-subject study. The first objective of our experimental investigation was to verify the suitability of an adaptive frequency oscillator for extrapolating information about natural arm-leg coordination. Experimental data recorded during treadmill walking at different speed conditions show that our approach was legit when walking faster than 0.5 m/s. Precisely, our algorithm produces excellent estimations of the arm swing frequency, stride cadence and timing of shoulder flexion peaks, but more inaccurate heel-strike detections. When walking slower than 0.5 m/s, the participants' shoulder rotation was too irregular for the system to track.

The second objective of our human-subject study was to validate our arm-based controller once implemented on a physical device. Especially, we aimed to demonstrate that our algorithm permits to walk over a range of walking speeds more representative of gait rehabilitation and assistance than that chosen in [21]. We carried this experimental study by implementing our code on the Lopes II, a treadmill-based lower limb exoskeleton developed at the University of Twente.

Our experiments show that our expectations were met for the most. Participants could drive the robot within 0.5-1 m/s, whether the treadmill speed stayed constant at a specific value or varied according to predefined patterns. Walking at 1.25 m/s was possible as well, but hardware malfunctioning limited the data available for the analysis. On the contrary, walking at 0.25 m/s was problematic for two of the participants. According to the results, it also seems that people had more troubles in decelerating with our arm-based controller than accelerating. However, this asymmetric controllability does not seem associated with the lack, in our proposed algorithm, of a mechanism to change interlimb

coordination under a certain threshold speed.

We also investigated whether our arm-based controller allows people to change their arm swing amplitude according to the walking speed, a feature that was not possible with the algorithm of La Scaleia et al. [21]. The results show that our controller allows to regulate the arm swing amplitude, but participants changed their shoulder rotations of only a few degrees across the tested conditions. Furthermore, people self-selected arm rotations generally larger than those observed during normal walking at the same treadmill conditions. Such emphasised shoulder amplitudes were not necessary for the correct functionality of our algorithm and might be associated with the conscious control of the arm swing imposed by arm-based control.



Mapping Function: Theoretical derivation

In Chapter 2, we introduced equation 2.4, which correlates the walking speed $v(t)$, expressed in m/s, to the stride cadence $\omega_S(t)$, expressed in Hz. We derived this formulation as follows - for readability, we drop the indication of time dependence. First, we considered the definition of step ratio given in [16]:

$$\text{step ratio} = \frac{1}{4} \frac{l_S}{\omega_S} \quad (\text{A.1})$$

where l_S is the stride length. Considering that $v = l_S \cdot \omega_S$, equation A.1 can be rewritten as:

$$\text{step ratio} = \frac{1}{4} \frac{v}{\omega_S^2} \quad (\text{A.2})$$

In [16], the step ratio was also related to the walking speed v through the following regression model:

$$\text{step ratio} = \beta_0 + \beta_1 \cdot v + \beta_2 \cdot h \quad (\text{A.3})$$

where: h is the patient height, while β_0 , β_1 and β_2 are regression coefficients empirically derived in [16] and equals to -0.532 , 0.020 and 0.47 , respectively.

By replacing equation A.3 into equation A.2 and expressing everything in terms of the walking speed v , we eventually computed the relation described in Chapter 2:

$$v = 4 \omega_S^2 \cdot \frac{\beta_0 + \beta_2 \cdot h}{1 - 4\beta_1 \cdot \omega_S^2} \quad (\text{A.4})$$

B

Simulink Implementation

This Appendix describes the Simulink implementation of our arm-based controller that we use for testing with the Lopes II. In addition to the components already presented in Chapter 2, three additional modules were necessary for conducting our experiments: the Position Controller, the Controller Switch and the Gait Termination. Some of the control blocks presented below are part of the Lopes II developmental library. Their description is here omitted since already available in the manual associated with this library, a documentation that can be retrieved by contacting: g.vanoort@utwente.nl

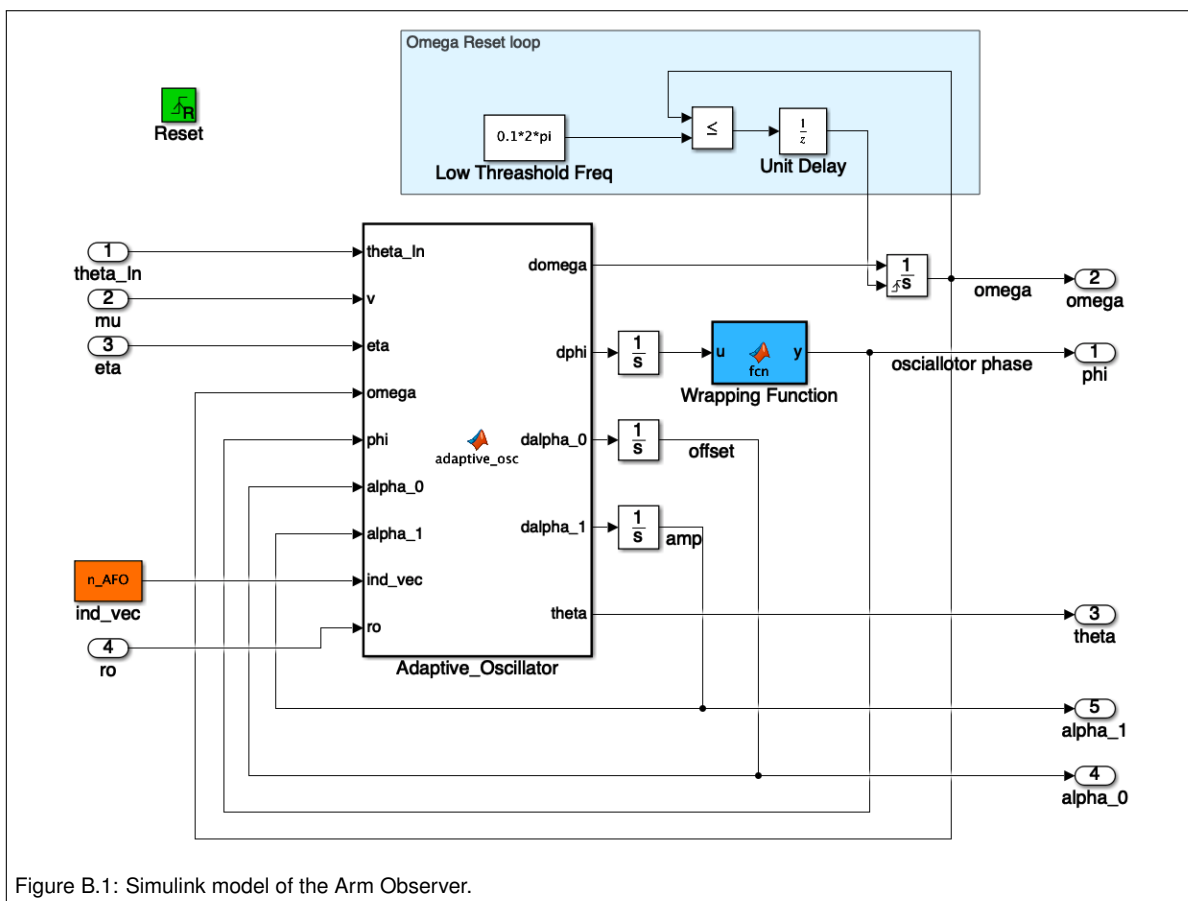


Figure B.1: Simulink model of the Arm Observer.

Table B.1: Input-output to the Simulink model of the Arm Observer. Given a specific variable, the left column indicates the nomenclature used within the Simulink blocks, while the right column indicates that adopted when describing the algorithm in Chapter 2.

INPUTS		
Simulink Model	Description	Symbol Chapter 3
theta_IN	Shoulder angular position	$\theta_{IN}(t)$
mu	Learning coefficient for $\omega(t)$ dynamics	ν
eta	Learning coefficient for $\alpha_0(t)$ dynamics	η
ro	Learning coefficient for $\alpha_1(t)$ dynamics	ρ
n_AFO	Number of adaptive oscillators to include	N/A

OUTPUTS		
Simulink Model	Description	Symbol Chapter 3
phi	Phase of the adaptive oscillator	$\phi(t)$
omega	Dynamic frequency parameter of the adaptive oscillator	$\omega(t)$
theta	Output state of the adaptive oscillator	$\theta(t)$
alpha_0	Offset of the adaptive oscillator	$\alpha_0(t)$
alpha_1	Amplitude of the adaptive oscillator	$\alpha_1(t)$

B.1. Arm Observer

The Simulink system which models the Arm Observer (figure B.1) includes the following components:

- the white block named “Adaptive_Oscillator” contains the set of equations characterising the adaptive frequency oscillator, as described in Chapter 2;
- the blue block named “Wrapping Function” wraps the phase of the oscillator, that is $\phi(t) \in [0, 2\pi]$;
- the blocks inside the light blue area are part of a loop mechanism to reset $\omega(t)$ if it drops below 10% of 2π . This control loop and threshold value were also implemented in [34], and they guarantee that the frequency of the adaptive oscillator does not become zero, a problem which can occur if the input signal is not null on average [30]. Because of this loop mechanism, our arm-based controller can not work with arm swing frequencies smaller than 0.1 Hz. The results in chapter 4 show that this threshold was appropriate since each participant’s arm swing frequency was always above 0.3 Hz across the tested speed conditions.
- the green block enables the experimenter to reset the Arm Observer to its initial conditions. To avoid dangerous discontinuities in the gait trajectories, this function was only available during position control. As such, it mostly served to facilitate the initialisation of our arm-based controller by speeding up the synchronisation of the adaptive frequency oscillator to the shoulder signal.

Table B.1 illustrates the outputs and inputs to the Simulink model of the Arm Observer, and when appropriate, the symbol that we used in Chapter 2 to describe the same quantity. The “n_AFO” parameter indicates how many adaptive frequency oscillators to include in the Arm Observer, based on the technique described in [5, 27]. When using a pool, each adaptive oscillator synchronises to one of the frequency components of the driving input, extending the Arm Observer functionality to signals less similar to sinusoids. When testing our algorithm by some pilot experiments, we did not find consistent benefits in choosing a pool of oscillators over a single unit. In fact, using multiple oscillators comported undesired complications of the algorithm: for instance, the need of unambiguously detecting which oscillator converged to the dominant frequency of the input signal. Therefore, we set $n_{AFO} = 1$ in this thesis project.

B.2. Gait Generator

Fig.B.2 shows the Simulink implementations of the Gait Generator. The Mapping Function submodule consists of the blocks within the two coloured areas. The section in the green one converts the $\omega(t)$ of the adaptive frequency parameter into the target walking speed, $v(t)$, for the Trajectory Generator, with the orange block containing the equation 2.4 from Chapter 2. The input “SpeedEstimatorOnOff” is a binary switch button:

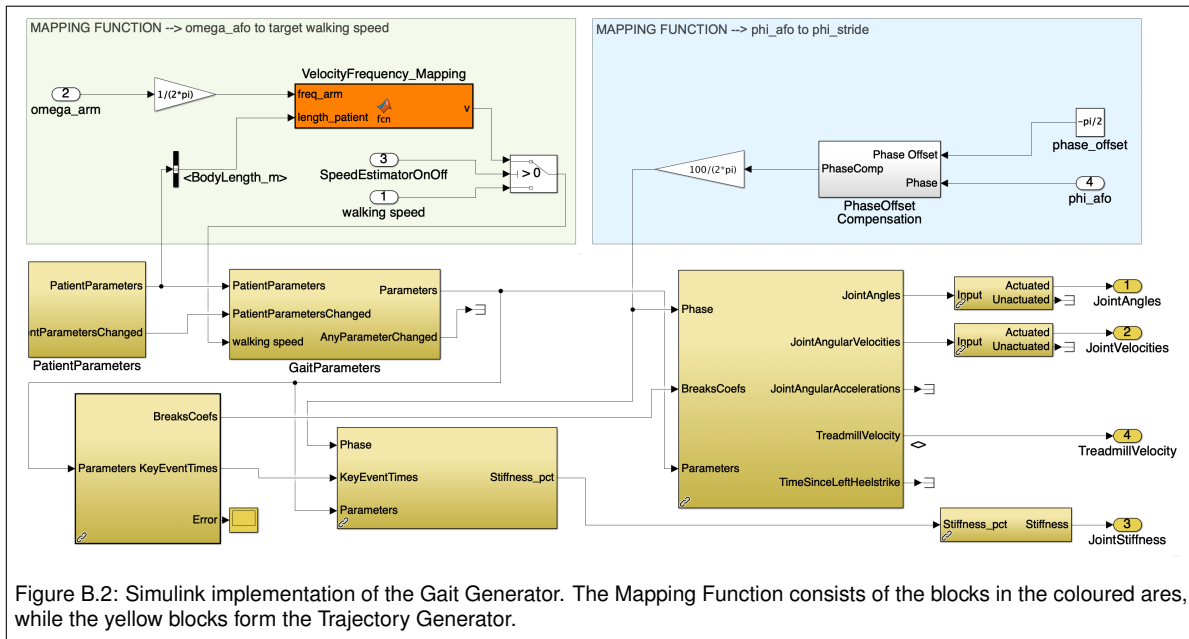


Figure B.2: Simulink implementation of the Gait Generator. The Mapping Function consists of the blocks in the coloured areas, while the yellow blocks form the Trajectory Generator.

- “SpeedEstimatorOnOff” = 1: $v(t)$ is computed from $\omega(t)$;
- “SpeedEstimatorOnOff” = 0: $v(t)$ is arbitrarily assigned by the experimenter, through the hard-coded input variable “walking speed”;

During our experiments, “SpeedEstimatorOnOff” was always set to 1. The blocks in the light blue area convert the phase of the oscillator, $\phi(t)$, into the estimation of the percentage of the stride cycle, $\phi_S(t)$, according to equation 2.5 described in Chapter 2.

The Trajectory Generator consists of the yellow blocks in fig.B.2. This system of blocks was already part of the LOPES II developmental library. The Simulink implementation of the Trajectory Generator diverges from our description in Chapter 2 for three main aspects:

- the key-events that are used by these blocks to produce joint trajectories are slightly different from those selected in [16], and were chosen specifically for usage with the Lopes II;
- it allows a larger selection of user’s anatomical parameters to customise the gait: mass and height, leg upper and lower lengths, foot length and height, pelvis width and height;
- it produces a vector including stiffness coefficients for the exoskeleton joints. It also compute a target velocity for the treadmill, but we never used this signal in our control structure.

These discrepancies, however, are minor adjustments of what we outlined in Chapter 2 and their description is extensively addressed in the technical documentation of the Lopes II developmental library. This manual also carefully describes each of the yellow blocks in figure B.2. We do not repeat such a description here. This is because the only modification that we brought to the original block organisation was to replace the parts concerning the computation of the stride phase and target speed by the blocks composing the Mapping Function.

B.3. Safety Mechanism & Gait Termination modules

The Safety Mechanism, as we implemented it in Simulink (figure B.3), receives as input the phase of the adaptive frequency oscillator (“RShPhaseComp” and “LShPhaseComp” for the right and left shoulder signals, respectively), subtracts it to the phase value at the previous algorithm iteration and sets a binary variable (“BreakAFO”) to 1 if the result is within the range $(0, \pi]$. If BreakAFO becomes 1, the Gait Termination is activated. To avoid gait termination during the Arm Observer initialisation, the Safety Mechanism works only when the arm-based controller is in use: under this condition, the variable “ArmOn” becomes equal to 1.

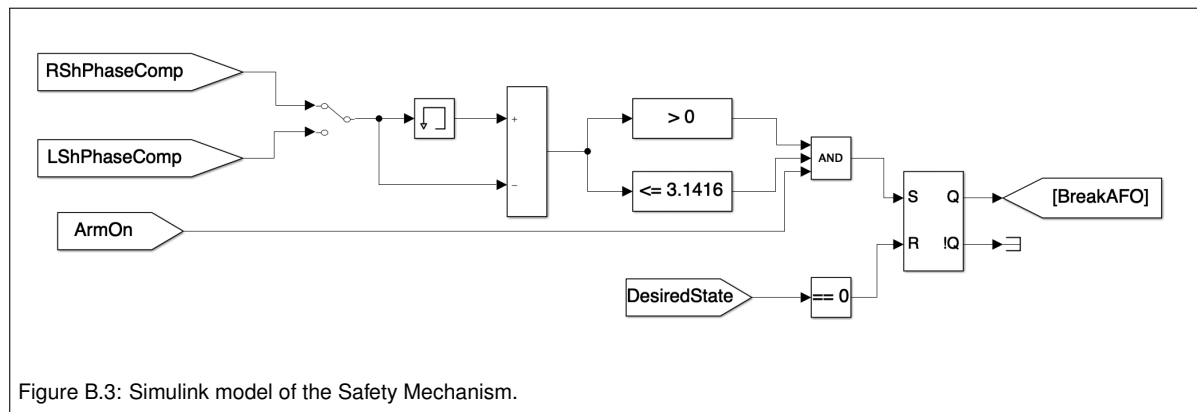


Figure B.3: Simulink model of the Safety Mechanism.

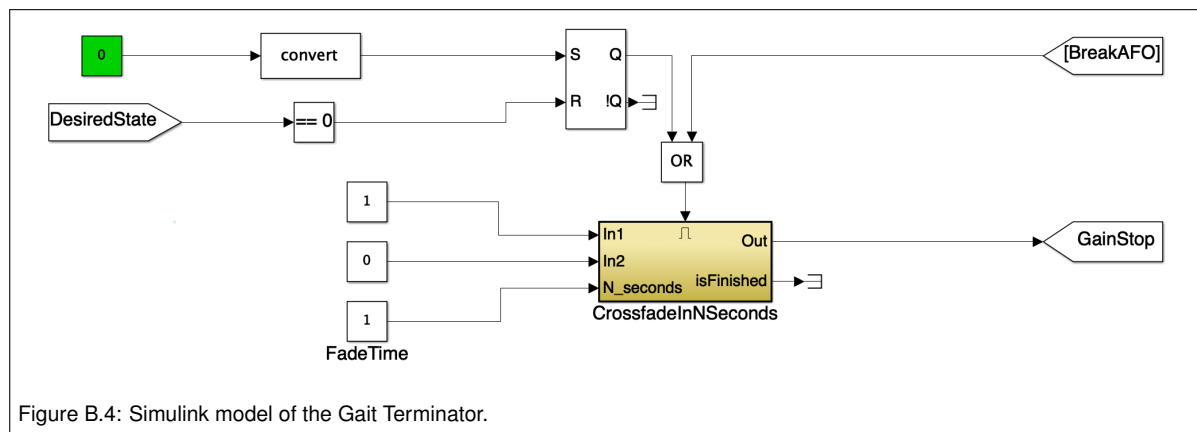


Figure B.4: Simulink model of the Gait Terminator.

The Simulink implementation of the Gait Terminator is illustrated in figure B.4. Once activated, this module crossfades a variable named “GainStop” from 1 to 0 within one second. GainStop premultiplies the vectors of stiffness coefficients sent by the Gait Generator to the Lopes II LLC and also the signal associated with the target velocity for the treadmill. Therefore, fading GainStop to zero makes the robot fading into Zero Impedance mode (see Chapter 3) and the treadmill decelerating to zero velocity. However, the Lopes II low-level architecture always limits the treadmill deceleration to max 0.5 m/s/s, regardless of the crossfade timing of GainStop. The Gait Termination can also be triggered at any moment by the experimenter by a GUI switch-button that we connected to the green block in figure B.4. In case of gait stop, the Safety Mechanism and Gait Terminator modules reset by setting the Lopes II state to “off”. The experimenter could perform this action by a GUI button, which allowed to set the variable “DesiredState” equal to zero.

B.4. Position Controller

Position Control was a default control mode of the Lopes II, during which the joint trajectories only depends on the treadmill velocity. This is achieved in Simulink by using the Trajectory Generator available in the Lopes II developmental library, the module named “Position_Control_Gait_Generator” in figure B.5. Basically, it consists of the same blocks shown in figure B.2, except for those belonging to the Mapping Function. These latter components are replaced as follows:

- the stride phase is estimated from a phase oscillator whose frequency is proportional to the treadmill velocity;
- the target walking speed is fixed by the experimenter through the variable “TreadmillVelocity” (we connected this parameter to a GUI).

A more in-depth description of the original Trajectory Generator module is given in the documentation associated with the Lopes II developmental library.

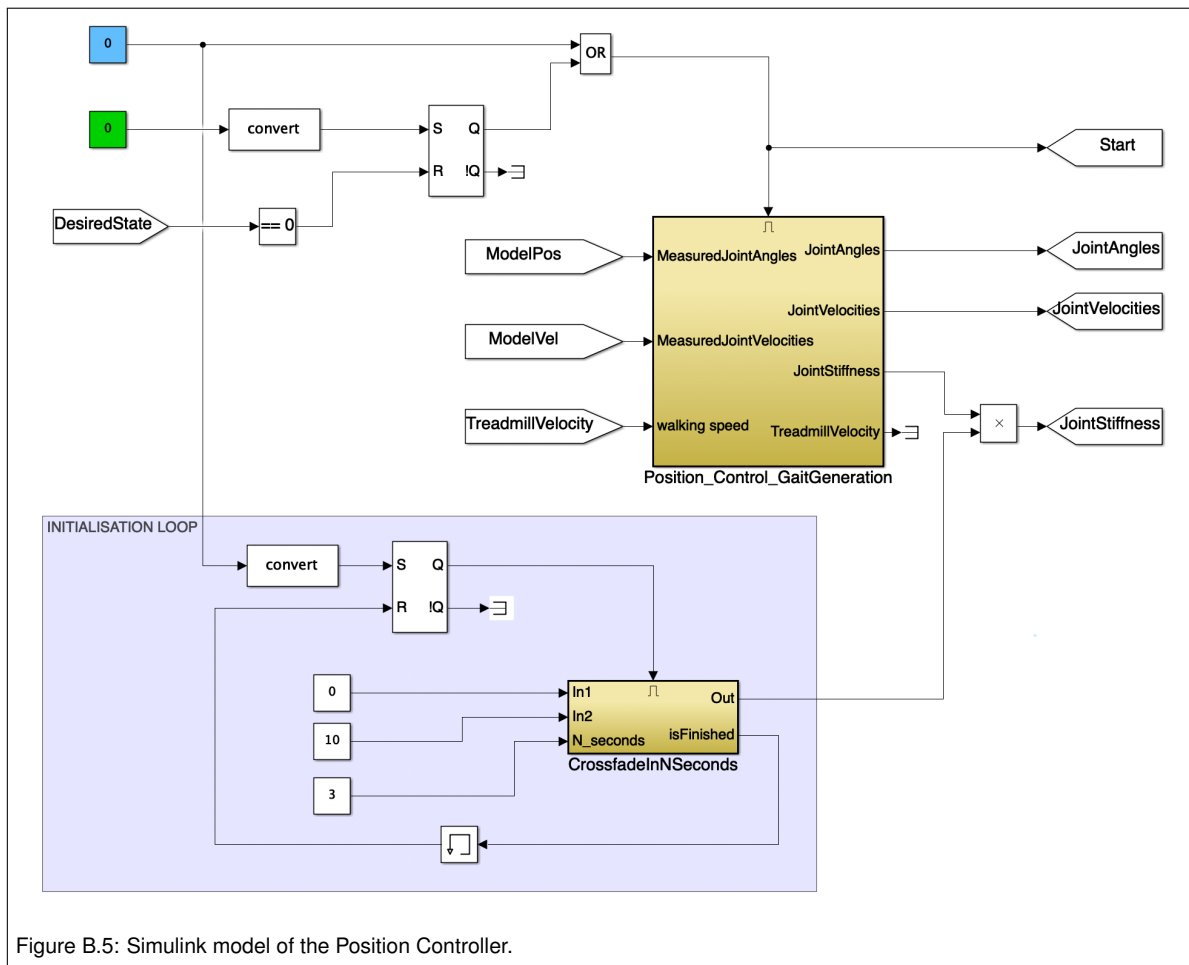


Figure B.5: Simulink model of the Position Controller.

In our implementation of the position controller, we added an external control loop that helps the user to assume the initial leg configuration at gait start. The algorithm works as follows:

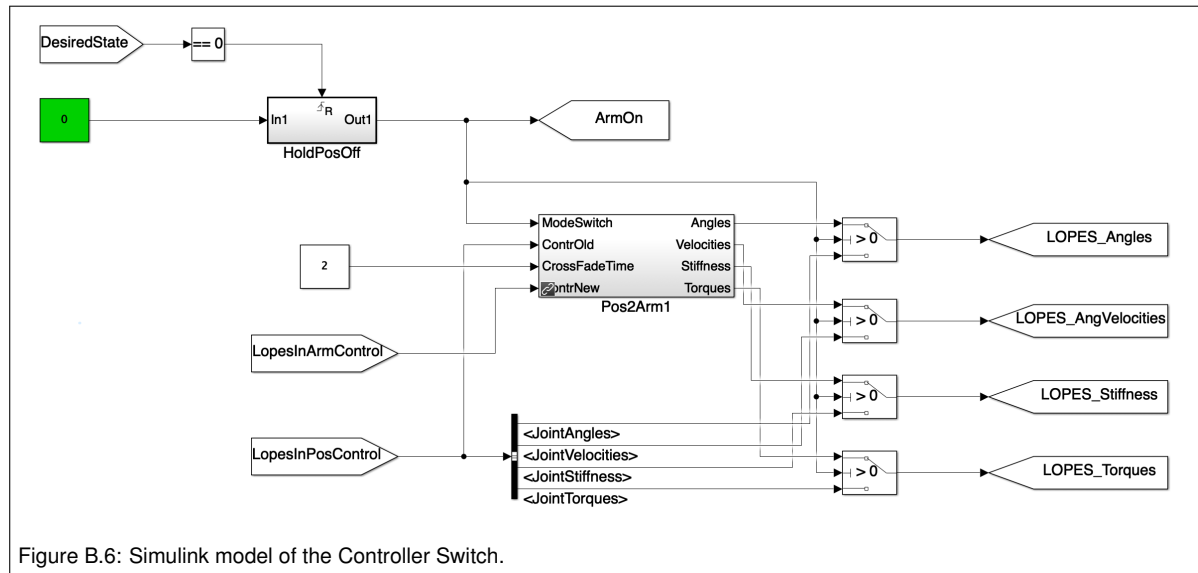
1. the experimenter presses a GUI button linked to the blue block, and this value switches to 1 for just one Simulink iteration;
2. This one-iteration switch activates the Position_Control_GaitGeneration module, freezing this system outputs to the values associated with the 0% of the stride cycle;
3. Meantime, the loop in the coloured area is also activated by the one-iteration switch. This system of block crossfades a constant from 0 to 10 within 3 seconds.
4. this crossfading variable multiplies the vector of joint stiffness coefficient sent to the Lopes II. As such, the robot joints gradually stiffen around their initial configuration, “gently” pushing the user legs with them.

The green block in figure B.5 is a binary variable, linked to a switch button in the experimenter’s GUI and used to activate position control. Restarting position control, and the associated leg-initialisation loop, was possible by setting the Lopes II state to “off”. The experimenter could perform this action by a GUI button, which allowed to set the variable “DesiredState” equal to zero.

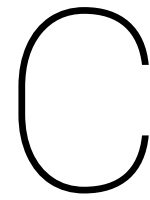
B.5. Controller Switch

The Controller Switch permits to change the Lopes II control mode from position to arm-based control. It performs this function by crossfading the outputs of the Gait Generator and Position Control modules, as in:

$$O = \tau \cdot O_{AC} + (1 - \tau) \cdot O_{PC}$$



where: O_i is any of the signal sent by the i -th controller to the Lopes II LLC, with $i = AC$ for arm-based control and $i = PC$ for position control; τ is a binary coefficient that linearly changes from 0 to 1 in 2 seconds. In the Simulink implementation of the Controller Switch, the crossfading action is carried by the block named “Pos2Arm1” (see figure B.6). Resetting the Controller Switch was possible by setting the Lopes II state to “off”. The experimenter could perform this action by a GUI button, which allowed to set the variable “DesiredState” equal to zero.



Consent Form

It is displayed below the Consent form given to the participant during the experiment. Notice that, visual feedback was not given during the actual experimentation, since it was found distracting for the participant. Instead, it was verbally asked to keep a central position, and auditory feedback (experimenter correction) were given if the participant was moving away from such a position.

Topic

Information for participant in the test "Robot assisted walking with arm-based controller"

Introduction

Dear Sir / Madam,

You have been contacted to participate in the research mentioned above. You must be able to base your permission or refusal on comprehensive information on our part. That is why you receive this written information, which you can read quietly and discuss with us any moment.

Goal and background of the research

At the University of Twente, a robot has been developed in recent years, which is used for the treatment of patients with walking problems. This so-called walking robot is attached to the legs of a patient and therefore provides support during walking. By using the walking robot, the walking function of patients could be trained better and more intensively than manual physiotherapy, while the burden on therapists is reduced. Furthermore, the walking robot can be used to map the progress of a therapeutic protocol better. The use of the walking robot has been tested in healthy subjects and a dozen CVA (stroke) patients. An essential aspect of robot-rehabilitation is to give to the exoskeleton an estimation of the user's intentions, such as the desired walking speed. Many pieces of research suggest that actively engaging the patient in the generation of the gait could benefit the rehabilitation outcomes.

The purpose of this study is to test the use of an algorithm that adapts the robotic gait to the motion of the user's arms, so to reproduce the natural arm-leg coordination during walking. Primarily, we want to test the ability of a human-participant in adopting and maintaining for few minutes different walking speeds by changing his/her arm swing accordingly. While walking in the robot, we want to measure characteristics of the walking pattern, such as shoulder rotations, feet ground-contacts, and displacements of the pelvis, with which we could, for example, later determine the performance of our control approach and optimise future designs. Also, we will compare such a controller against position control. During position control, the robot lower limbs will move according to the same set of joint trajectories used by the arm controller, but the corresponding walking speed will be selected by the experimenter. For this study, people with healthy gait are sought. With the data from this study, the current version of our arm-based controller will be analysed and possibly further improved, with the final aim of eventually testing it with specific patient groups. Other devices that are expected to benefit from our arm-based controller are mobile exoskeletons. Still, important hardware limitations do not allow motor-impaired users to currently use these devices without crutches or extra walking aids. Therefore, we expected to deploy our controller into mobile exoskeleton as a long term objective. In fact, we expect that once people will be able to use mobile exoskeletons without committing their arms to extra supporting systems, our control method would provide an intuitive method for piloting such devices.



Fig.1: Participant walking in the LOPES III

When are you eligible for the research?

You are eligible to participate in this study if you are between the ages of 18 and 70, can participate independently in the study and do not have impairments of the gait.

What does the research mean for you?

You will be asked to walk at different walking speeds while using the two above mentioned control modalities (one at time). If time allowed, we will consider to record an extra session, similar to the previous two in terms of tasks to be completed, but requiring to walk without wearing the LOPES III. For more details about each session, please refer to the Appendix. Notice that the motion of your arms will be measured by a special suit which has multiple sensors recording the anatomical motion of the wearer. Some of your anatomical metrics, such as height, weight, feet length, etc. will be measured to calibrate the suit software to your body anatomy. You will be

asked to wear this suit during the whole experimentation. Additionally, your gait behaviour will be measured by position and force sensors in the LOPES III, but also video and audio recorded. Overall, the estimated duration of the test is about 1.5 - 2 hours, at the end of which you are free to ask as many questions as you like about our research. The measurements with the walking robot will take place in the LOPES III room of the Department of Biomedical Mechanical Engineering at the University of Twente (de Horst room Z131).

Possible side effects / risks

Walking in the walking robot is safe, thanks to multiple safety systems in-built in the device. Besides, the researcher carrying out the research will check the participant's perceived comfort and level of challenge continuously. Two emergency buttons are at a reachable distance of the user: pressing any of these two buttons slows down immediately both the robot and treadmill.

Walking with the LOPES III requires some extra effort than normal walking: it may feel like using a training machine of a gym and thus it may cause some muscle fatigue, for example. This will be prevented as much as possible by adjusting any task intensity to your condition and the severity you experience. You can also indicate at any time that you want to terminate a certain task. There may be some skin irritation due to the straps with which the LOPES III is attached to your legs. This will also be prevented as much as possible.

Possible benefits

You will not directly benefit from participating in this study, except for experiencing first-hand what means to train your gait with an high-tech rehabilitation robot. You will contribute to the development of a new controller for walking robots, an algorithm that we expect it will be used in the short term to improve gait training, and in the long term to drive mobile exoskeleton.

Confidentiality

The information collected about you during the investigation will be treated confidentially according to (inter)national rules and laws, including the Personal Data Protection Act. The data will be coded in such a way that they can not be traced back to you. The coding is therefore not based on, for example, birth date, initials and gender. Audio recordings will be destroyed after signal processing, and any video will be recorded in a way that conceals your face.

If you decide to participate in this study, you consent to the following:

- Employees in this study and supervisors can view your data. They are obliged to keep these details secret.
- If you decide to discontinue your participation in the study, your data collected before this decision may still be processed together with other data collected as part of the medical research.
- Data collected during this research may be published in a scientific journal, conference and similar.

Voluntary participation

You are free to allow or deny participation in this study. Even if you give permission, you can withdraw it at any time without giving any reason. Whatever you decide, it will not bring about any consequences. This study does not include any form of monetary compensation.

For further information

If you have any questions, you can submit them to the responsible researcher.

Sincerely,

Fabio Izzì, M.Sc. student in Biomechanical Design at TUDelft, currently visiting researcher in the Biomechanics Department at UTwente, +31629219311.

PERMISSION STATEMENT

Title of the research:

“Robot assisted walking with arm-based controller”

Study characteristic:

I confirm that I have read the information letter for the test subject and I understand the information. I have had enough time to think about my participation and have had the opportunity to ask questions. These questions have been answered satisfactorily.

I give permission for participation in the aforementioned medical-scientific research.

I know that my participation is entirely voluntary and that I can withdraw my consent at any time without having to give a reason for it.

I give permission for authorized persons from the University of Twente and competent authorities to have access to my research data.

I authorize the processing of the data for the purposes and in the manner described in this information letter and attached Appendix.

Name of the person:

Signature:

Date:

Researcher's name:

Signature:

Date:

Topic

Appendix I, Specific information study: " Robot-assisted walking with an arm-based controller."

What does the research mean for you?

In this study, two different ways of controlling the walking robot will be tested. With the arm-based controller, you will be asked to control the motion of the robotic legs by varying the oscillations of your arms. The code is designed to synchronize a back-n-forward rotation of your arm to a full stride of the robot (a stride is a complete gait cycle). You will be further instructed on the arm-leg coordination to use before the experiment. With the position control, the robotic legs will move according to predefined trajectories. You will be not in control of the walking speed and your arm motion will not influence the behaviour of the robot. Still, you will be asked to walk with the robot without using the handrails, trying to adopt an arm-leg coordination that you perceive comfortable. As optional sessions, we might consider to test a condition when you will be asked to walk as natural as possible on the treadmill without wearing the LOPES III.

Preparation

Before the study, you will be asked to wear the Xsens suit, a motion capture system that will track your gait (<https://www.xsens.com/products/xsens-mvn-animate/>). You will be allowed to change in complete privacy, thanks to an area of the LOPES lab adhibited to changing cabinet. After, we will measure some of your biometrics, such as height, leg length, shoulder distance and so on. These measurements are necessary to calibrate the suit software. Also, you will be asked to walk back and forwards with the suit (about 5 steps in each direction) to finalize the calibration procedure. Later, you will be helped to wear the LOPES III, which will be adjusted to your body anatomy.

Protocol

Per each controller, you will perform two sessions. During Session 1 you will be asked to walk for 2 minutes at 5 different walking speeds. Within these 2 minutes, you will be asked to maintain your position on the treadmill (a visual feedback of your pelvis will be provided). Before transitioning to the next speed, we will always ask you whether you feel comfortable in doing so: we don't want to push you walking at speed levels that you might perceive as excessively challenging. Before Session 1, we will also give you some minutes of practice to get used to the selected controller modality. During Session 2, you will have to control your pelvis position according to a provided visual reference while the treadmill speed will be continuously varied according to two predefined patterns. Between the two patterns, you will walk for 30 seconds at a constant speed. Notice that the speed of the treadmill will not be increased(reduced) above(below) your max(min) speed as reached during Session 1. Also, you will have feedback on both your pelvis position and current speed of the treadmill. Session 2 will be performed twice, with two different rates of speed variations. Notice that between Session 1 and 2 you will be asked whether you need a few minutes of break. If so, the LOPES and treadmill will be stopped for a couple of minutes.

You will always start with Session 1, and then you will perform Sessions 2. After you have completed all the two sessions with a controller, you will have some minutes of rest. After, the procedure will be repeated for the remaining controller. Each session 1 should take about 15 minutes, while each session 2 should take about 5 minutes. Also, notice that you are free to express your intention of terminating the experiment, or a part of it, any time during the two sessions.

Name of the person:

Signature:

Date:

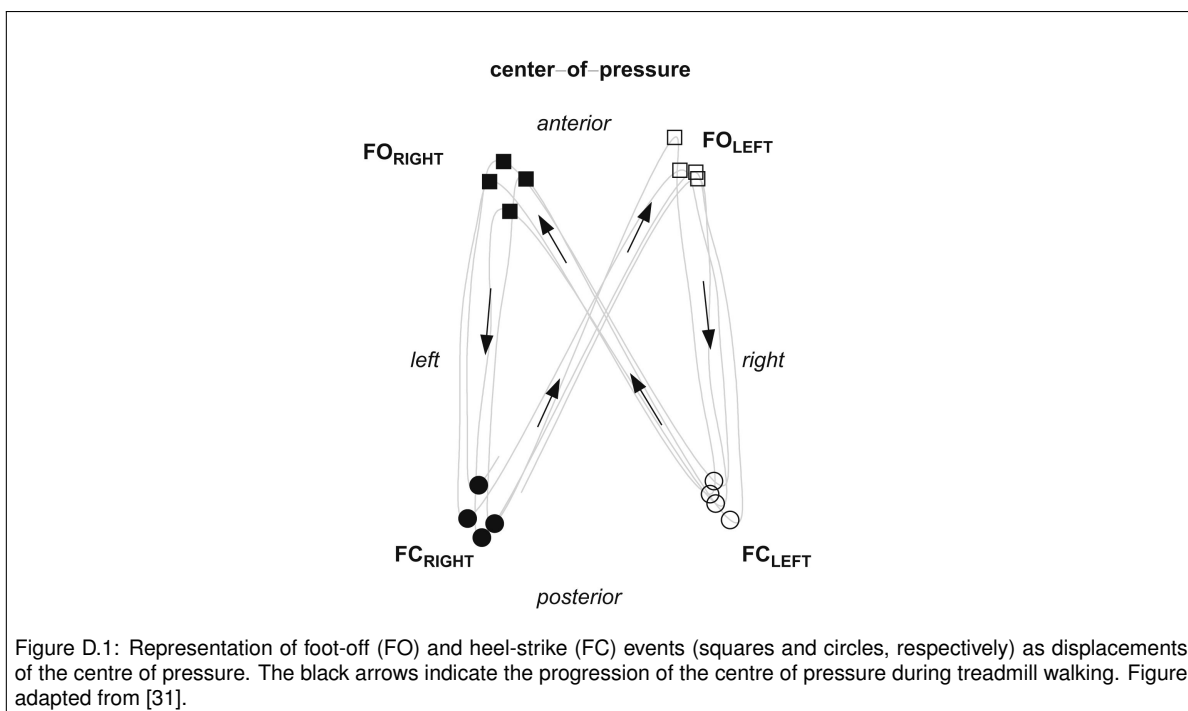
Researcher's name:

Signature:

Date:

D

Heel-strike detection: algorithm



During data analysis, the algorithm for heel-strike detection differed according to whether or not the trial concerned natural walking. By using the information from the exoskeleton position sensors, an in-built block of the Lopes II developmental library estimated the current phase of the stride, producing a signal which could have four possible values:

- 1, during double stance with the left leg in front;
- 2, during right leg swing;
- 3, during double stance with right leg in front;
- 4, during left leg swing.

Therefore, we defined a left heel-strike every time this signal changed from 4 to 1, and a right heel-strike every time it changed from 2 to 3.

During natural walking the participant was not wearing the exoskeleton, and thus it was not possible to use the just mentioned approach. For this experimental condition, we used an algorithm for

Table D.1: Heel-strike detection with natural walking data: Filtering parameters (n = filter order; fc = cutting frequency in Hz) and threshold values used per participant dataset. We converged to these sets of values after some trial-and-error iterations, validated by visual comparison of the resulting heel-strike selection with the associated profile of recorded ground reaction forces.

Participant 1

Speed [m/s]:	0.25	0.50	0.75	1.00	1.25
n	6	6	5	5	5
fc	1.3	2	3	3	3
ϵ_x	0.0001	0.00045	0.00095	0.0011	0.0016
ϵ_z	0.000175	0.00033	0.00032	0.0003	0.00032

Participant 2

Speed [m/s]:	0.25	0.50	0.75	1.00	1.25
n	6	6	5	5	5
fc	1.3	2	3	3	3
ϵ_x	0.00012	0.00038	0.00096	0.00137	0.00164
ϵ_z	0.00011	0.00016	0.00003	0.00011	0.000025

Participant 3

Speed [m/s]:	0.25	0.50	0.75	1.00	1.25
n	6	6	5	5	5
fc	1.3	2	3	3	3
ϵ_x	0.00016	0.0004	0.00095	0.00133	0.0018
ϵ_z	0.00014	0.00033	0.00035	0.00045	0.0005

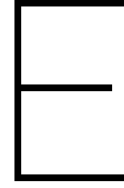
heel-strike detection which exploits the signals recorded by the treadmill force plates. Precisely, our approach was based on the method proposed in [31]: assuming \dot{x}_{CoP} and \dot{z}_{CoP} to be the sagittal and transversal speed components of the centre of pressure (CoP) respectively, and assuming \dot{x}_{CoP} to be positive along the anterior direction, an heel-strike occurs when \dot{x}_{CoP} suddenly increases, with the sign of \dot{z}_{CoP} defining which foot had the impact with the ground (see fig. D.1). Therefore, we implemented the following algorithm per each sequence of data associated to natural walking:

1. we filtered the time traces of the x_{CoP} and z_{CoP} (Butterworth filter, forward and backwards in time) with filtering order and cut-off frequencies as shown in table D.1.
2. from these filtered signals, we numerically derived \dot{x}_{CoP} and \dot{z}_{CoP} by the “gradient.m” Matlab function;
3. we set two thresholds, ϵ_x and ϵ_z , one per each velocity component, as listed in table D.1;
4. we defined a right heel-strike as the time instance in which $\dot{x}_{CoP} > \epsilon_x \wedge \dot{z}_{CoP} > \epsilon_z$, while a left heel-strike when $\dot{x}_{CoP} > \epsilon_x \wedge \dot{z}_{CoP} < -\epsilon_z$, according to the Lopes II sign convention for the frontal plane data.

We further validated the selected heel-strike events by (visually) comparing their timing to the occurrences of peaks in the ground reaction forces (GRF). This comparison allows us to tune the different parameters (filter properties, ϵ_x and ϵ_z) until the selection was found appropriate. Notice that we could have selected the heel-strike events based on the GRF data only, with each of this latter signal peak indicating an instance of foot-contact. However, we preferred our approach for two main reasons:

- For some trials, the GRF signal was too noisy to distinguish peaks associated to foot-contact clearly;
- Analysis of the vertical ground reaction forces does not provide information on the side at which the heel-strike occurs, for which the inspection of the CoP displacements is still necessary;

Our heel-strike detection approach is also more comprehensive in the analysis of the force plates data, i.e. it considers both CoP displacements and GRF information. This aspect, combined with the possibility of tuning multiple parameters (filter properties, ϵ_x and ϵ_z), makes our method quite robust against noisy measurements (especially compared to an algorithm that only relies on detecting GRF peaks).



Data analysis: metrics formulation

This section contains the mathematical formulation of the metrics that we use for the data analysis. If not explicitly presented, name and definition per each of the quantities listed here was given in Chapter 3. According to the same categorisation which we used for the description in Chapter 3, the formulations are sorted into three classes of variables:

- **Stride-cycle metrics:** quantities computed using the segment of data that defines an stride-cycle, i.e. the interval between two consecutive ipsilateral heel-strikes;
- **Arm-cycle metrics:** quantities computed using the segment of data that defines an arm-cycle, i.e. the interval between two consecutive ipsilateral peaks of shoulder flexion;
- **Full-trial metrics:** quantities computed using the segment of data that defines a complete trial.

Since the definitions of ϕ_{PF} and ϕ_{HS} given in Chapter 3 unambiguously characterise these two variables, we omit their mathematical formulations, which would be just tedious to read and will not provide any further understanding.

E.1. Stride-cycle metrics

$$\omega_S = (t_{n_S} - t_1)^{-1}$$
$$\overline{AE}_{\omega_S} = \left(\frac{\sum_{t=t_1}^{t_{n_S}} |\omega_S - \omega(t)|}{n_S} \right) \cdot \frac{100}{\omega_S}$$

where: $t \in [t_1, t_2, \dots, t_{n_S}]$ is the discretised time variable, with t_1 and t_{n_S} being the instances of the two consecutive heel-strike defining the stride and n_S the number of samples recorded within such an interval.

E.1.1. Arm-cycle metrics

$$\begin{aligned}\theta_{max} &= \frac{\theta_{IN}(t_1) + \theta_{IN}(t_{n_A})}{2} \\ \theta_{min} &= \min_t \theta_{IN}(t) \\ \theta_{Amp} &= \frac{\theta_{max} - \theta_{min}}{2} \\ \omega_A &= (t_{n_A} - t_1)^{-1} \\ \overline{AE}_{\omega_A} &= \left(\frac{\sum_{t=t_1}^{t_{n_A}} |\omega_A - \omega(t)|}{n_A} \right) \cdot \frac{100}{\omega_A}\end{aligned}$$

where: $t \in [t_1, t_2, \dots, t_{n_A}]$ is the discretised time variable, with t_1 and t_{n_A} being the instances of the two consecutive ipsilater shoulder flexion peaks and n_A the number of samples recorded within such an interval; θ_{max} estimates the maximum of the angular shoulder position within a shoulder rotation, while θ_{min} its minimum, based on the convention used (positive θ_{IN} for shoulder flexion and negative for shoulder extension).

E.1.2. Full-trial metrics

$$\begin{aligned}\overline{AE}_{SH} &= \left(\frac{\sum_{t=t_1}^{t_{n_T}} |\theta_{IN}(t) - \theta(t)|}{n_T} \right) \cdot \frac{100}{\sum_{k=1}^{19} (\theta_{Amp})_k} \\ |W| &= \sum_j f \left(\left| \vec{T}_j(t) \cdot \vec{\theta}_j(t) \right| \right)\end{aligned}$$

where:

- $t \in [t_1, t_2, \dots, t_{n_T}]$ is the discretised time variable, with t_1 and t_{n_T} being, respectively, the first and last samples of the data segment associated to the trial (n.b: only last 60 seconds for trials of task 1) and n_T the number of samples recorded within such an interval;
- the subscript j indicates the j -th measured joint degrees of freedom and \sum_j the summation over all these elements;
- $f(X(t))$ is the numerical integration of the variable $X(t)$ over the discretised time interval $[t_1, t_2, \dots, t_{n_T}]$ and based on the trapezoid rule.

F

Results: Additional figures

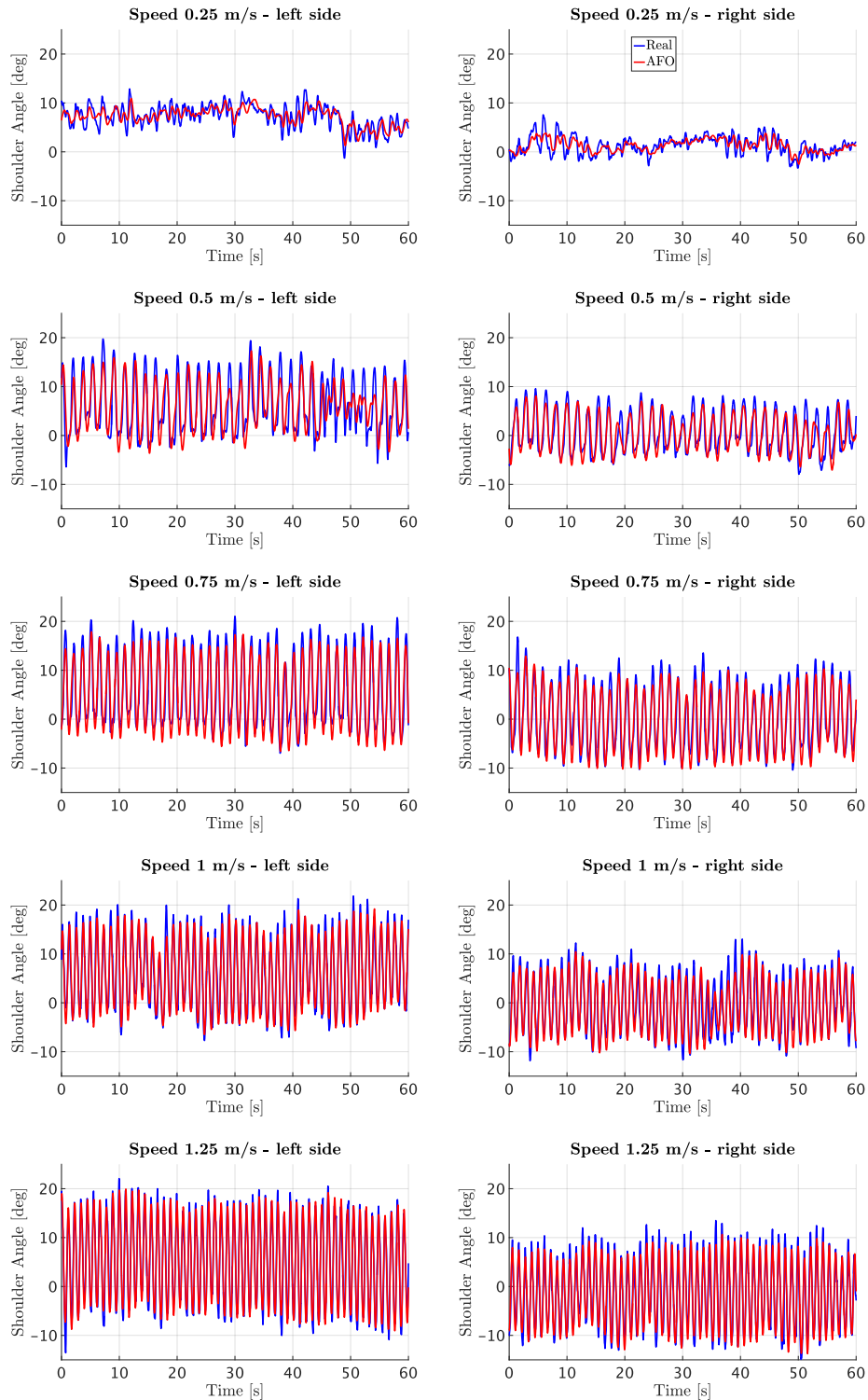


Figure F.1: **Participant 1, natural walking** - The filtered trajectories of each shoulder (Real) are compared against the output states, $\theta(t)$, of the associated adaptive frequency oscillator (AFO).

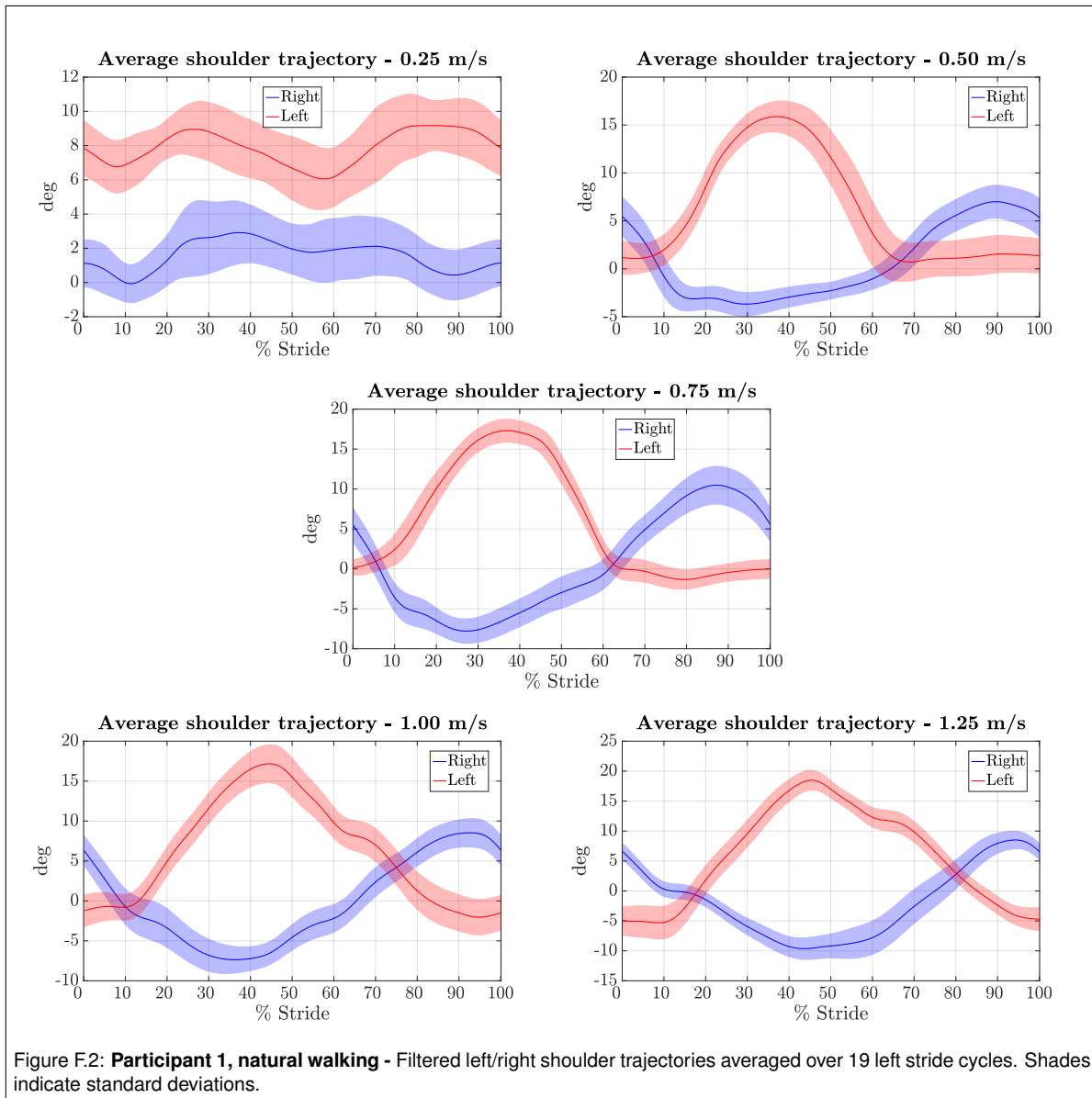
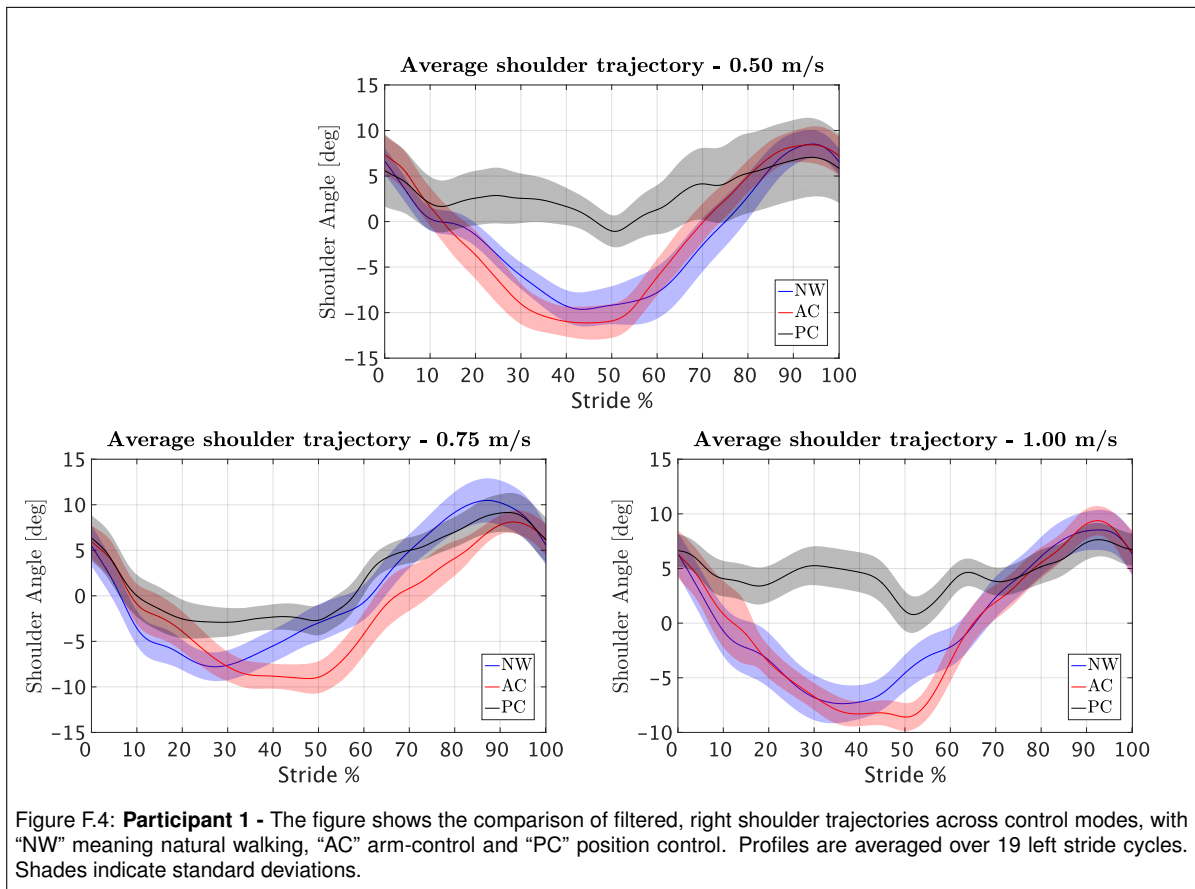
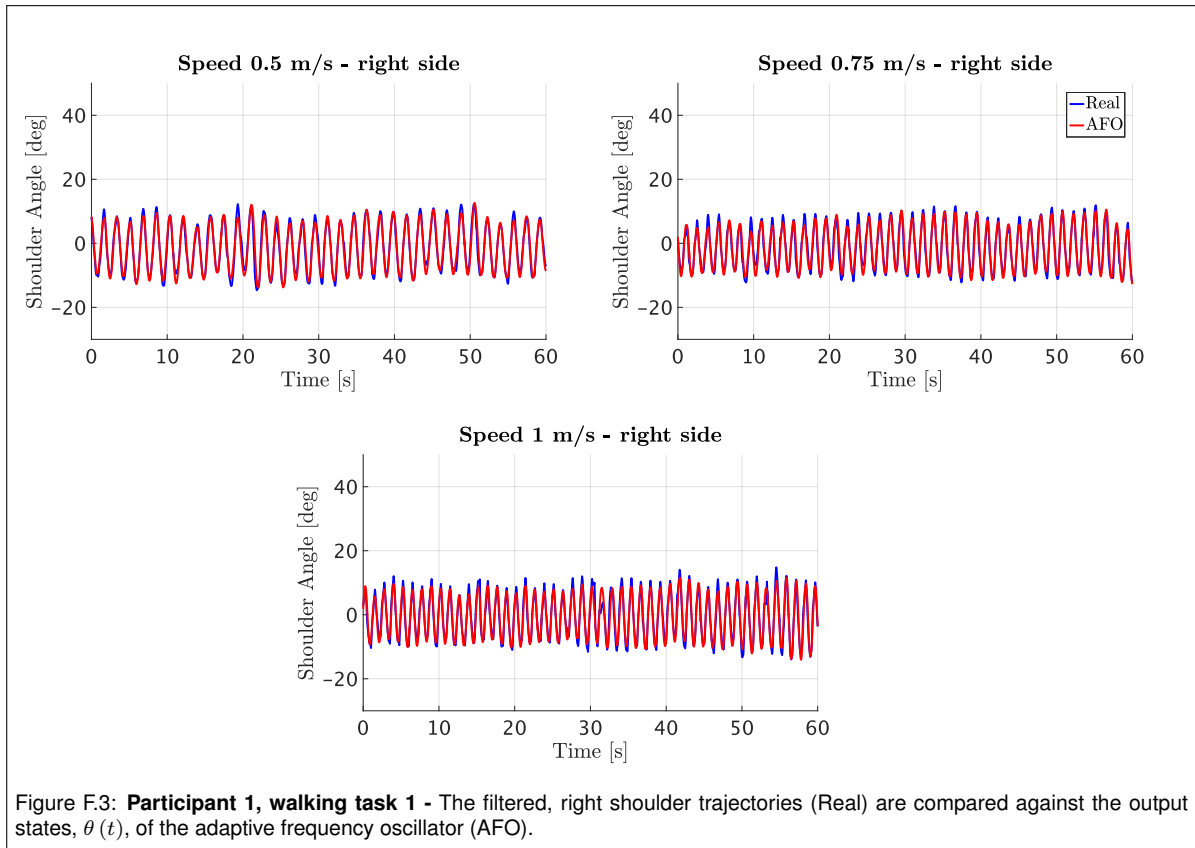


Figure F.2: **Participant 1, natural walking** - Filtered left/right shoulder trajectories averaged over 19 left stride cycles. Shades indicate standard deviations.



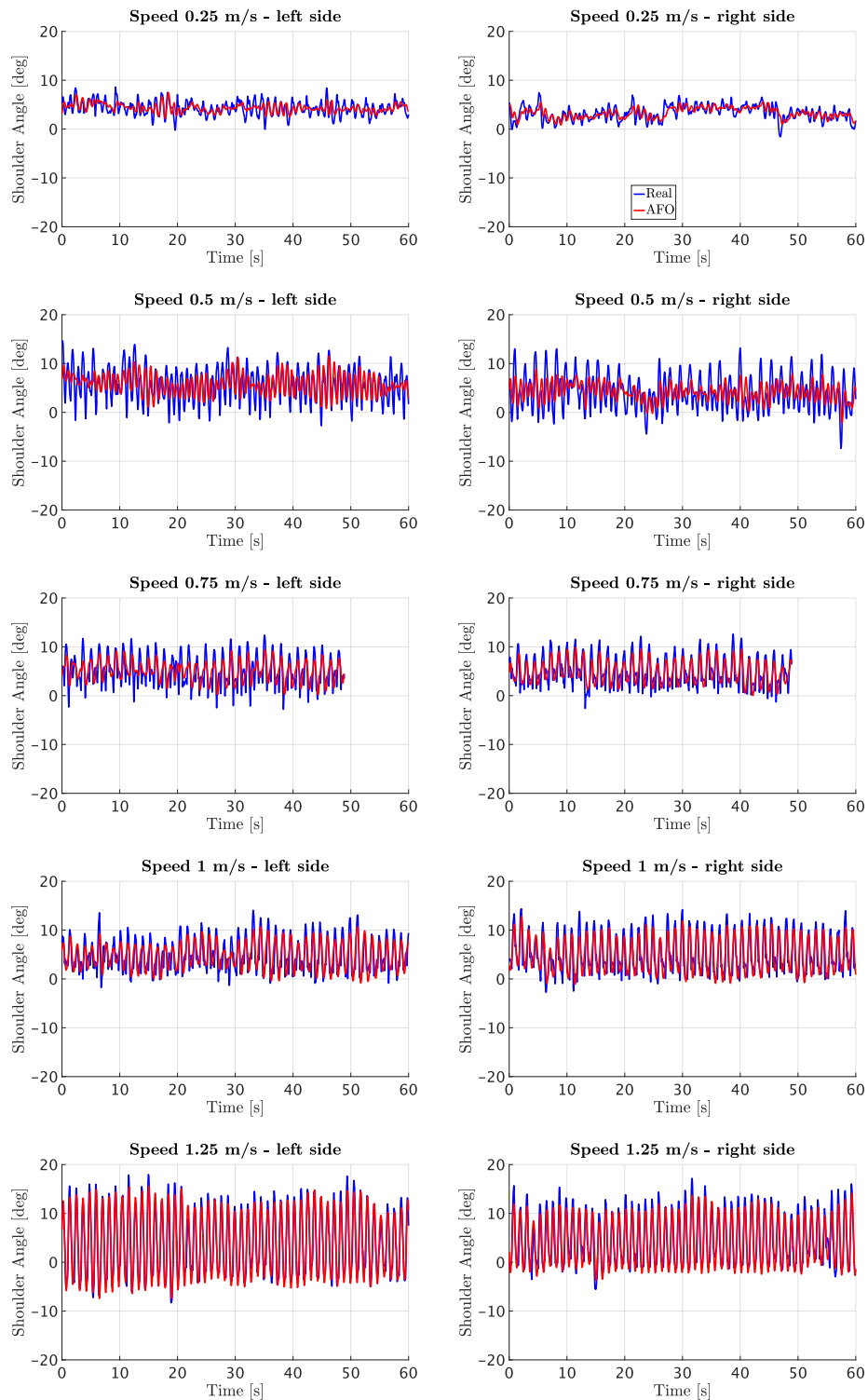
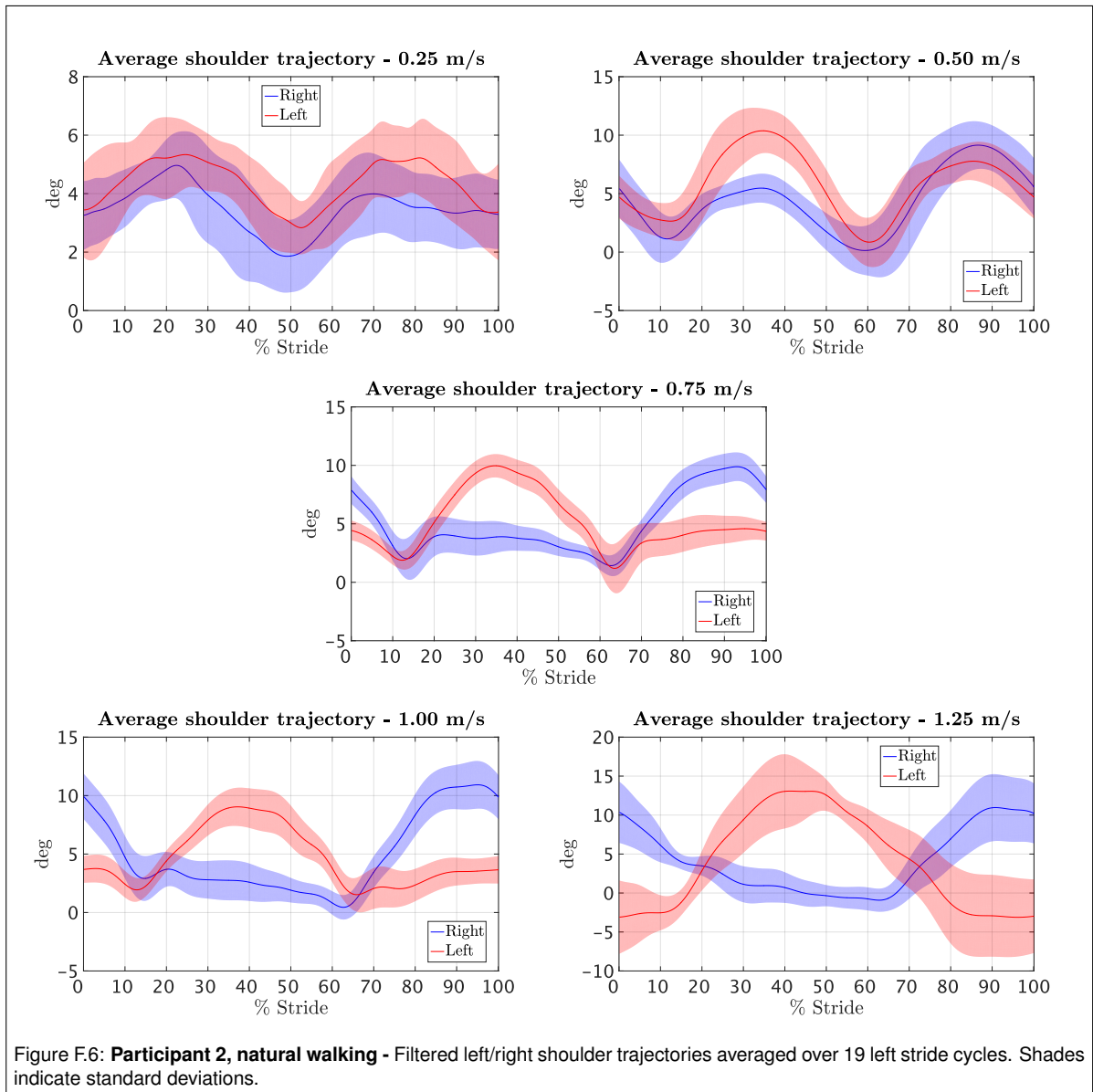
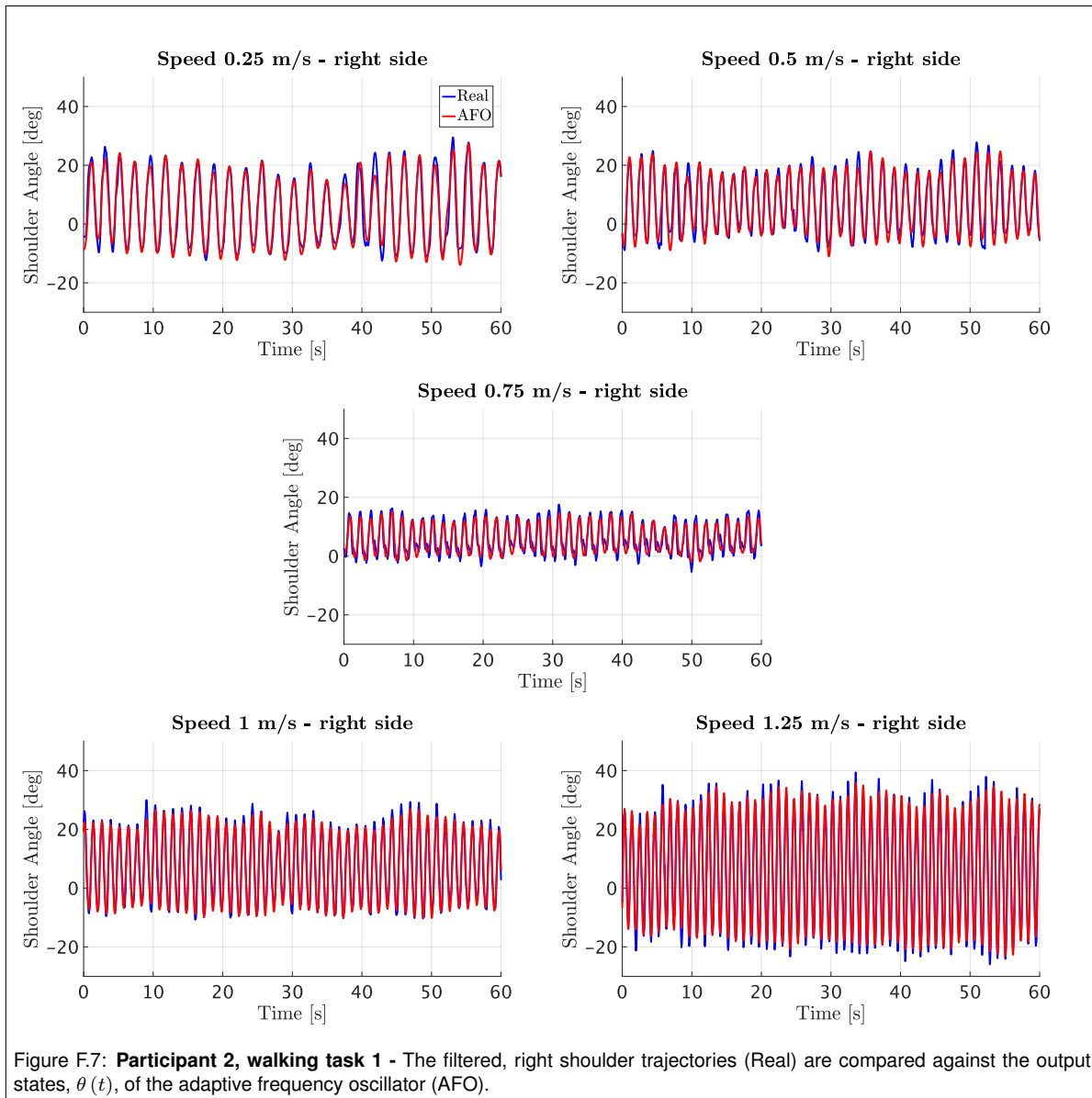
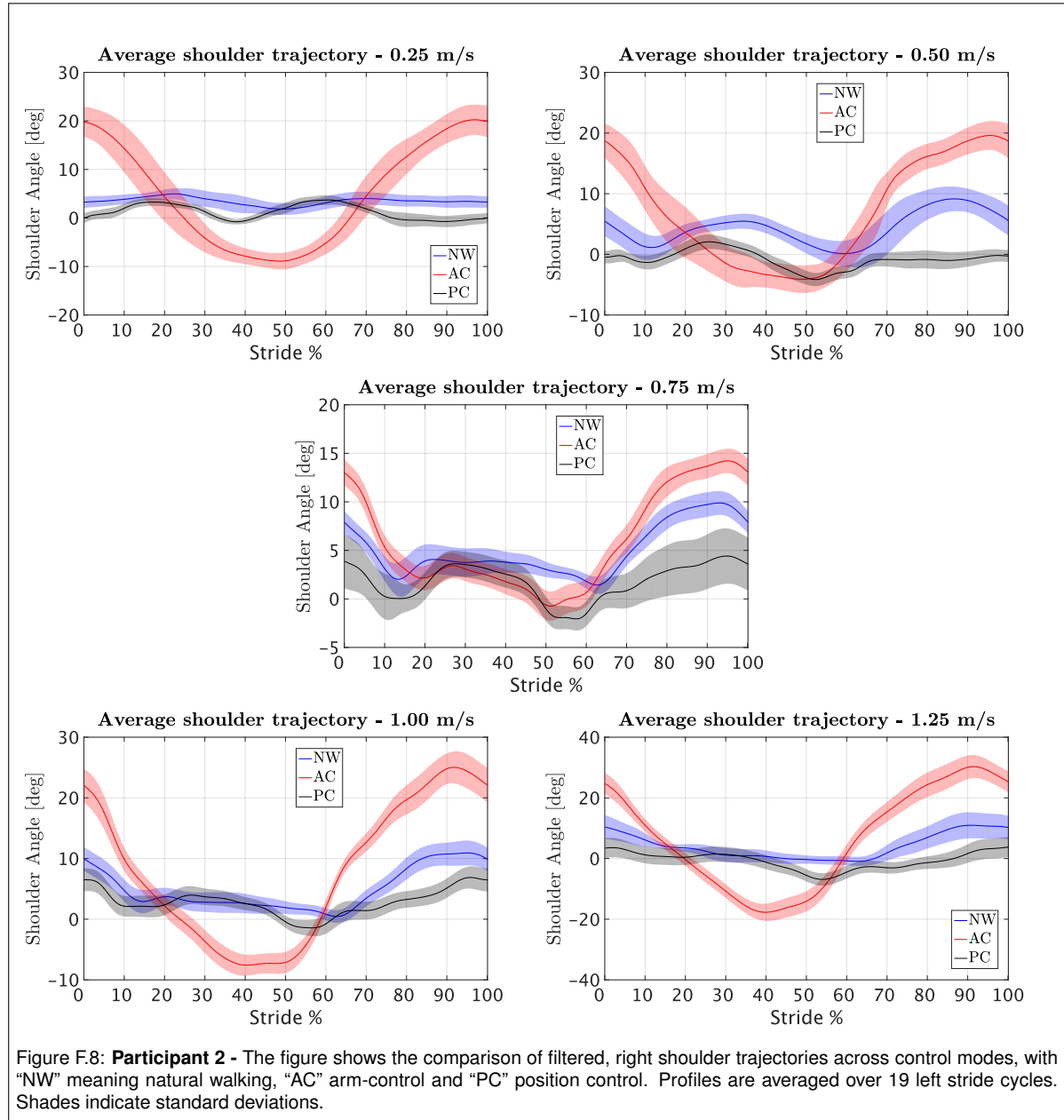


Figure F.5: **Participant 2, natural walking** - The filtered trajectories of each shoulder (Real) are compared against the output states, $\theta(t)$, of the associated adaptive frequency oscillator (AFO).







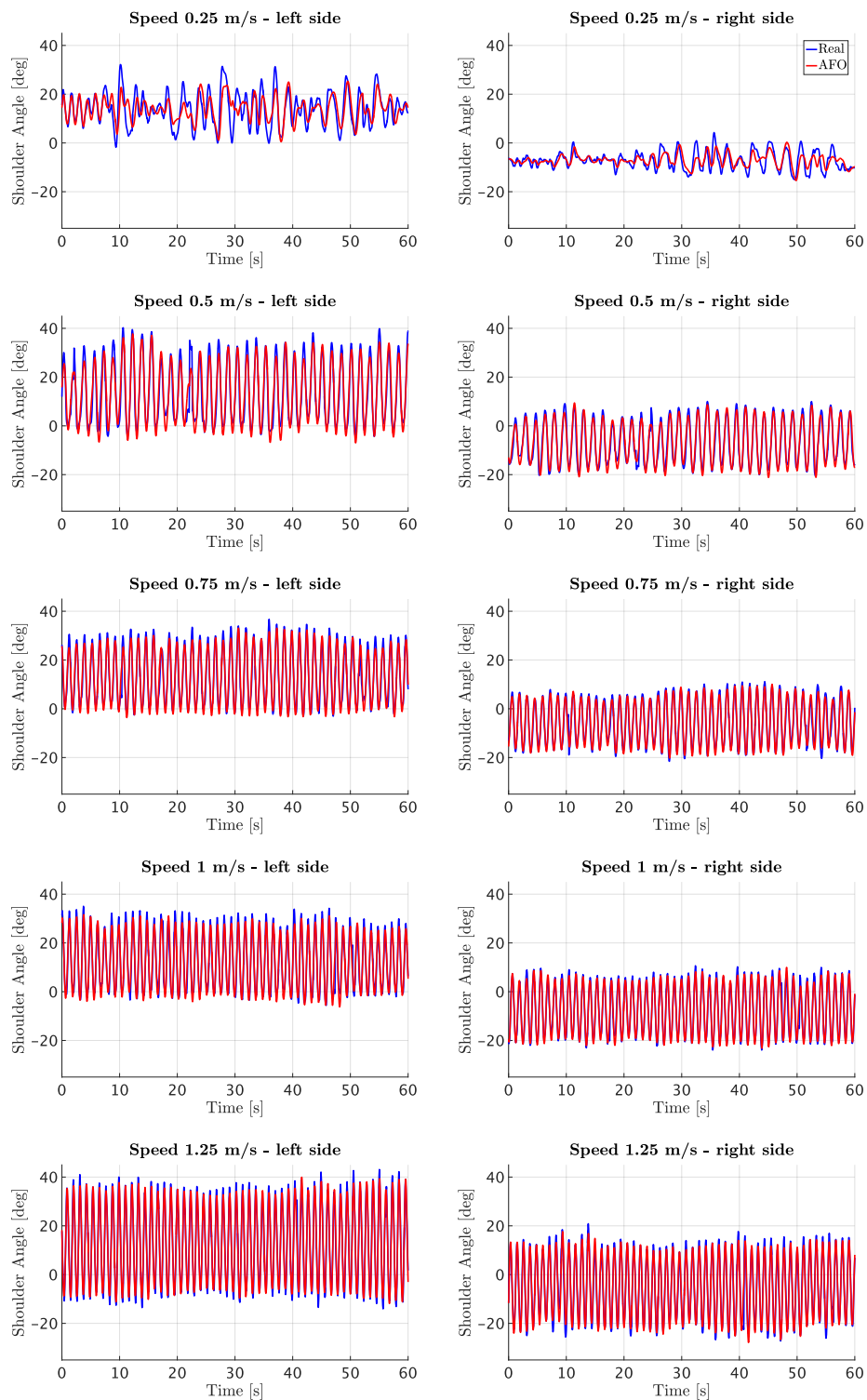
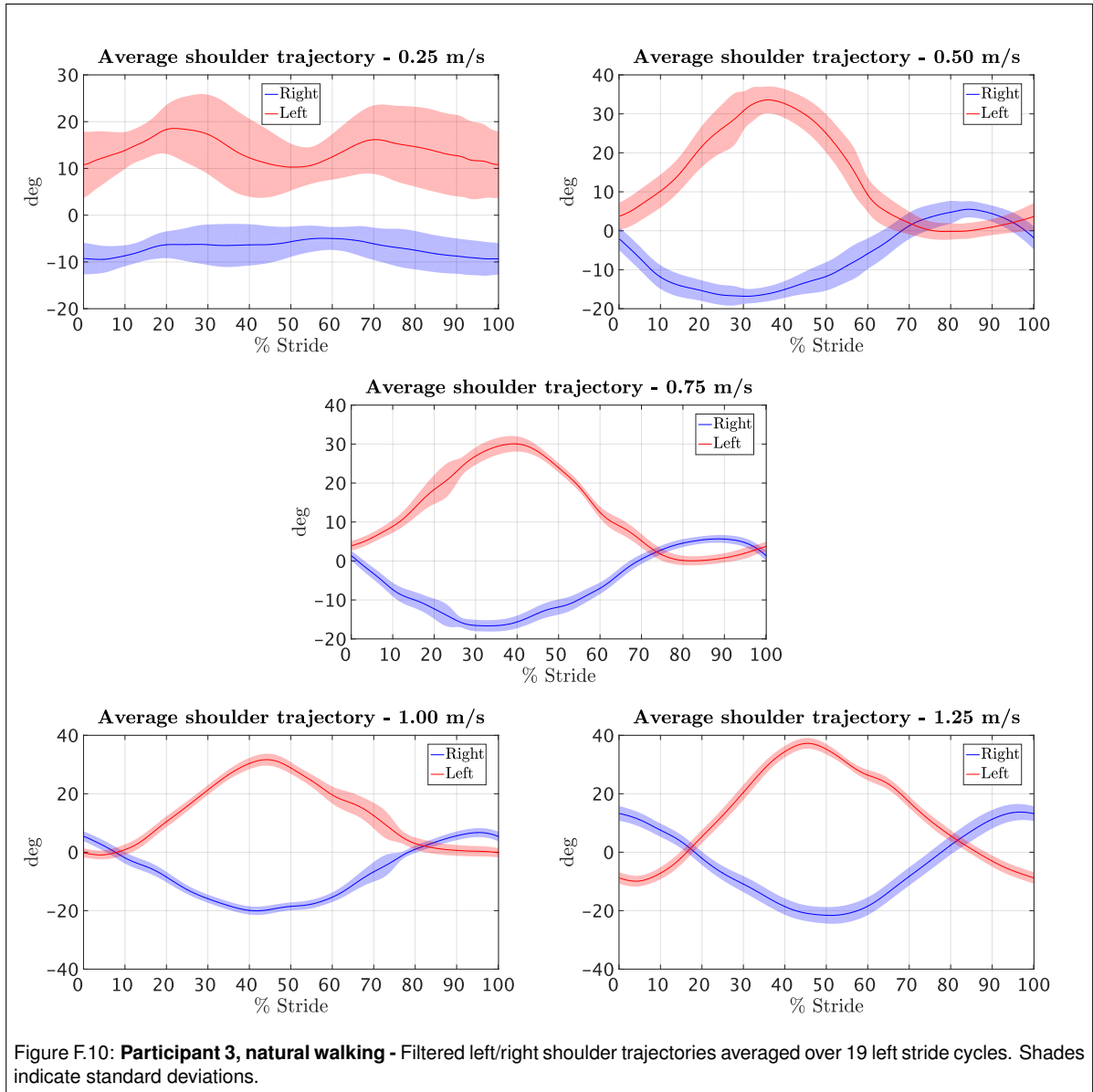
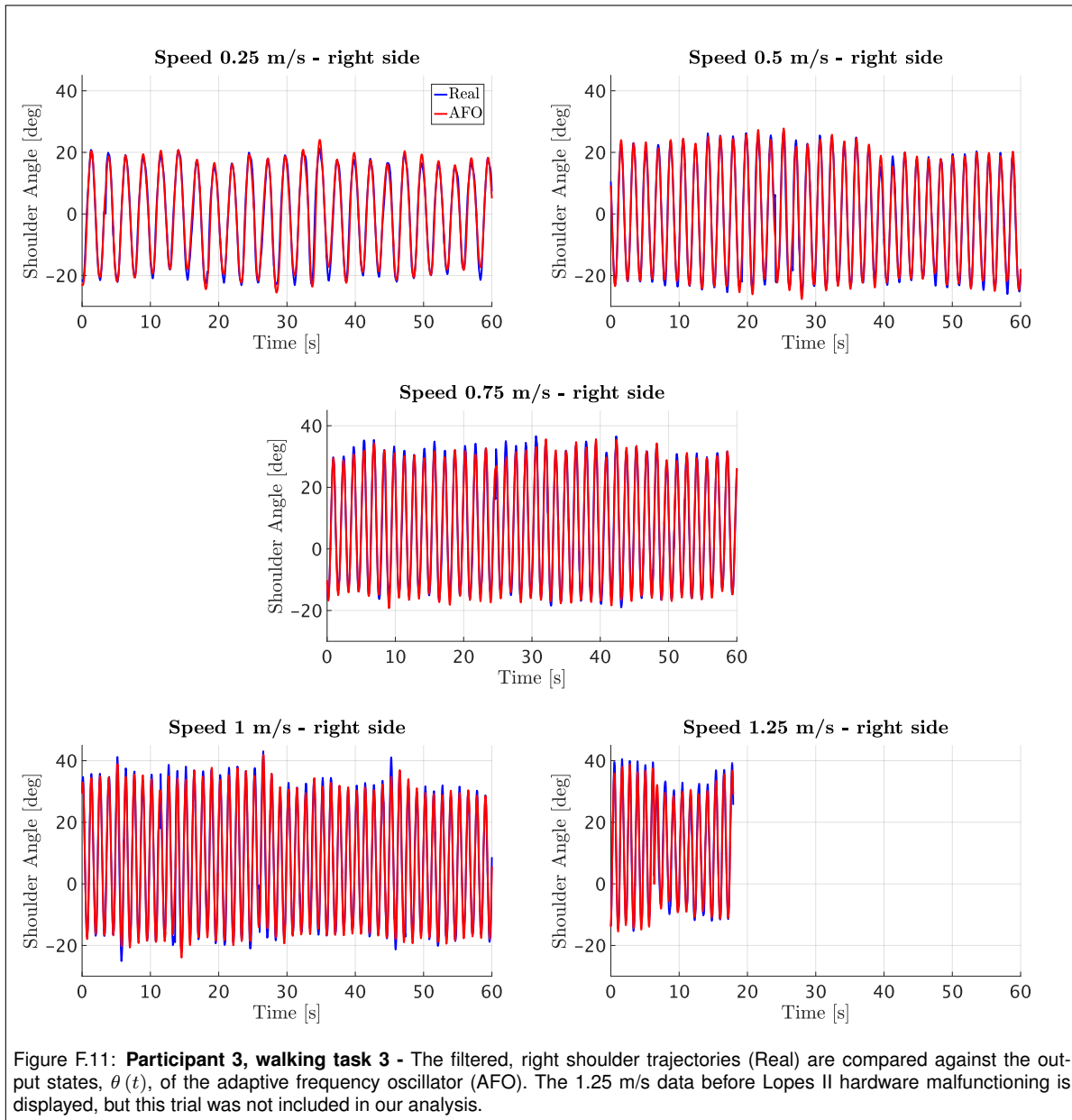
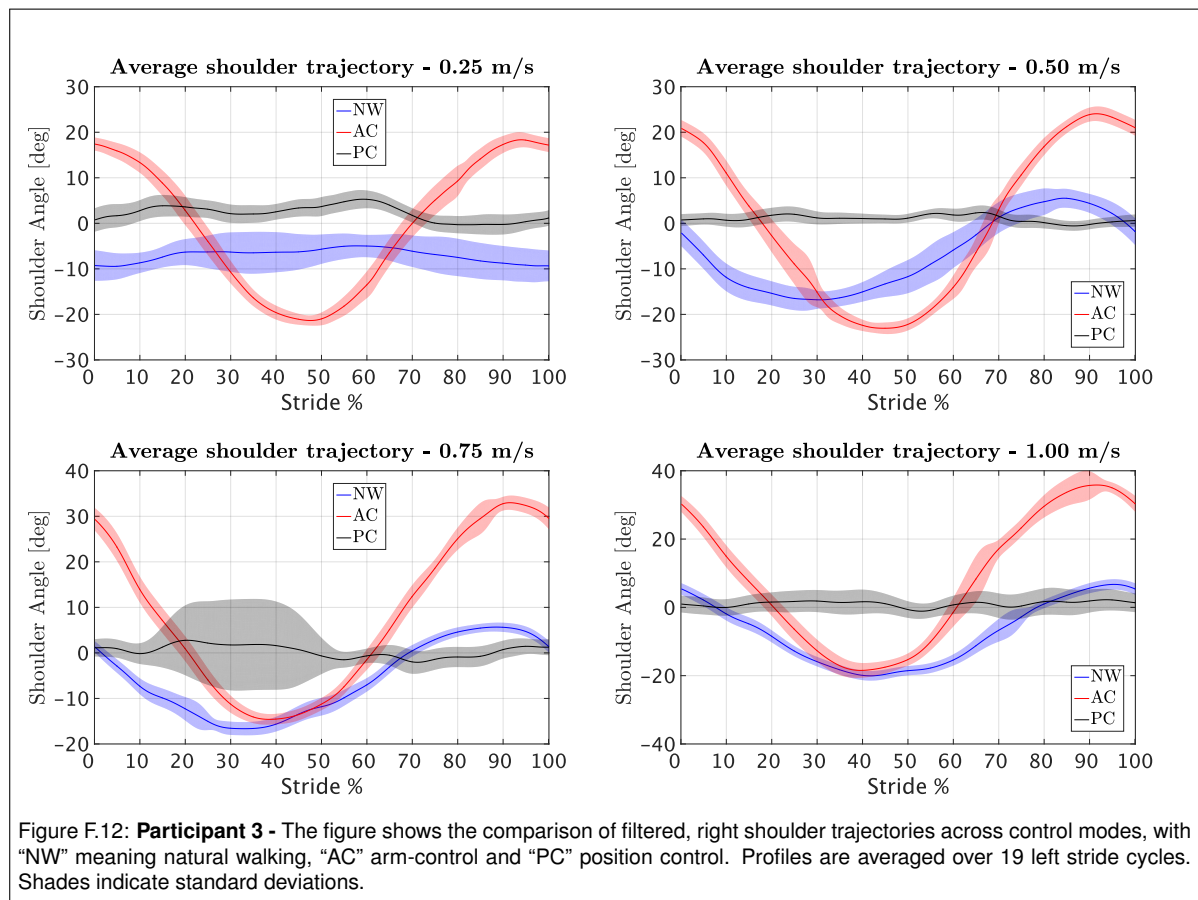


Figure F.9: **Participant 3, natural walking** - The filtered trajectories of each shoulder (Real) are compared against the output states, $\theta(t)$, of the associated adaptive frequency oscillator (AFO).







Bibliography

- [1] Maria L Fernandez Ballesteros, Fritz Buchthal, and Poul Rosenfalck. The pattern of muscular activity during the arm swing of natural walking. *Acta Physiologica Scandinavica*, 63(3):296–310, 1965.
- [2] Dustin A Bruening, Rebecca E Frimenko, Chuck D Goodyear, David R Bowden, and Adam M Fullenkamp. Sex differences in whole body gait kinematics at preferred speeds. *Gait & posture*, 41(2):540–545, 2015.
- [3] Ilaria Carpinella, Paolo Crenna, Marco Rabuffetti, and Maurizio Ferrarin. Coordination between upper-and lower-limb movements is different during overground and treadmill walking. *European journal of applied physiology*, 108(1):71–82, 2010.
- [4] Bing Chen, Hao Ma, Lai-Yin Qin, Fei Gao, Kai-Ming Chan, Sheung-Wai Law, Ling Qin, and Wei-Hsin Liao. Recent developments and challenges of lower extremity exoskeletons. *Journal of Orthopaedic Translation*, 5:26–37, 2016.
- [5] Guy Chéron, M Duvinage, C De Saedeleer, T Castermans, A Bengoetxea, M Petieau, K Seetharaman, T Hoellinger, B Dan, Thierry Dutoit, et al. From spinal central pattern generators to cortical network: integrated bci for walking rehabilitation. *Neural plasticity*, 2012, 2012.
- [6] Steven H Collins, Peter G Adamczyk, and Arthur D Kuo. Dynamic arm swinging in human walking. *Proceedings of the Royal Society of London B: Biological Sciences*, 276(1673):3679–3688, 2009.
- [7] Stella F Donker, Peter J Beek, RC Wagenaar, and Theo Mulder. Coordination between arm and leg movements during locomotion. *Journal of motor behavior*, 33(1):86–102, 2001.
- [8] Sunday Theophilus Eke-Okoro, M Gregoric, and Lars-Erik Larsson. Alterations in gait resulting from deliberate changes of arm-swing amplitude and phase. *Clinical Biomechanics*, 12(7-8):516–521, 1997.
- [9] Stefano Federici, Fabio Meloni, Marco Bracalenti, and Maria Laura De Filippis. The effectiveness of powered, active lower limb exoskeletons in neurorehabilitation: a systematic review. *NeuroRehabilitation*, 37(3):321–340, 2015.
- [10] Daniel P Ferris, Helen J Huang, and Pei-Chun Kao. Moving the arms to activate the legs. *Exercise and sport sciences reviews*, 34(3):113–120, 2006.
- [11] Matthew P Ford, Robert C Wagenaar, and Karl M Newell. Arm constraint and walking in healthy adults. *Gait & Posture*, 26(1):135–141, 2007.
- [12] B Gutnik, H Mackie, G Hudson, and C Standen. How close to a pendulum is human upper limb movement during walking? *HOMO-Journal of Comparative Human Biology*, 56(1):35–49, 2005.
- [13] Richard N Hinrichs. Whole body movement: coordination of arms and legs in walking and running. In *Multiple muscle systems*, pages 694–705. Springer, 1990.
- [14] Tim Killeen, Christopher S Easthope, Linard Filli, Lilla Lőrincz, Miriam Schrafl-Altermatt, Peter Brugger, Michael Linnebank, Armin Curt, Björn Zörner, and Marc Bolliger. Increasing cognitive load attenuates right arm swing in healthy human walking. *Royal Society open science*, 4(1):160993, 2017.
- [15] Marc D Klimstra, Evan Thomas, Rebecca H Stoloff, Daniel P Ferris, and E Paul Zehr. Neuromechanical considerations for incorporating rhythmic arm movement in the rehabilitation of walking. *Chaos: An Interdisciplinary Journal of Nonlinear Science*, 19(2):026102, 2009.

- [16] Bram Koopman, Edwin HF van Asseldonk, and Herman van der Kooij. Speed-dependent reference joint trajectory generation for robotic gait support. *Journal of biomechanics*, 47(6):1447–1458, 2014.
- [17] Masayoshi Kubo, Robert C Wagenaar, Elliot Saltzman, and Kenneth G Holt. Biomechanical mechanism for transitions in phase and frequency of arm and leg swing during walking. *Biological cybernetics*, 91(2):91–98, 2004.
- [18] Masayoshi Kubo, Kenneth G Holt, Elliot Saltzman, and Robert C Wagenaar. Changes in axial stiffness of the trunk as a function of walking speed. *Journal of biomechanics*, 39(4):750–757, 2006.
- [19] Johann P Kuhtz-Buschbeck and Bo Jing. Activity of upper limb muscles during human walking. *Journal of Electromyography and Kinesiology*, 22(2):199–206, 2012.
- [20] JP Kuhtz-Buschbeck, K Brockmann, R Gilster, A Koch, and H Stolze. Asymmetry of arm-swing not related to handedness. *Gait & Posture*, 27(3):447–454, 2008.
- [21] Valentina La Scaleia, Francesca Sylos-Labini, Thomas Hoellinger, Letian Wang, Guy Cheron, Francesco Lacquaniti, and Yuri P Ivanenko. Control of leg movements driven by emg activity of shoulder muscles. *Frontiers in human neuroscience*, 8:838, 2014.
- [22] Jason T Long, John B Groner, Dan C Eastwood, Timothy R Dillingham, Prateek Grover, and Gerald F Harris. Implications of arm restraint on lower extremity kinetics during gait. *Journal of Experimental & Clinical Medicine*, 3(5):200–206, 2011.
- [23] Jos Meuleman, Edwin van Asseldonk, Gijs van Oort, Hans Rietman, and Herman van der Kooij. Lopes ii—design and evaluation of an admittance controlled gait training robot with shadow-leg approach. *IEEE transactions on neural systems and rehabilitation engineering*, 24(3):352–363, 2016.
- [24] Pieter Meyns, Sjoerd M Bruijn, and Jacques Duysens. The how and why of arm swing during human walking. *Gait & posture*, 38(4):555–562, 2013.
- [25] M Pat Murray. Gait as a total pattern of movement: Including a bibliography on gait. *American Journal of Physical Medicine & Rehabilitation*, 46(1):290–333, 1967.
- [26] Justus D Ortega, Leslie A Fehlman, and Claire T Farley. Effects of aging and arm swing on the metabolic cost of stability in human walking. *Journal of biomechanics*, 41(16):3303–3308, 2008.
- [27] Tadej Petrič, Andrej Gams, Auke Jan Ijspeert, and Leon Žlajpah. On-line frequency adaptation and movement imitation for rhythmic robotic tasks. *The International Journal of Robotics Research*, 30(14):1775–1788, 2011.
- [28] Herman Pontzer, John H Holloway, David A Raichlen, and Daniel E Lieberman. Control and function of arm swing in human walking and running. *Journal of Experimental Biology*, 212(4):523–534, 2009.
- [29] Mamun Bin Ibne Reaz, MS Hussain, and Faisal Mohd-Yasin. Techniques of emg signal analysis: detection, processing, classification and applications. *Biological procedures online*, 8(1):11, 2006.
- [30] Ludovic Righetti, Jonas Buchli, and Auke Jan Ijspeert. Dynamic hebbian learning in adaptive frequency oscillators. *Physica D: Nonlinear Phenomena*, 216(2):269–281, 2006.
- [31] Melvyn Roerdink, Claudine JC Lamothe, Peter J Beek, et al. Online gait event detection using a large force platform embedded in a treadmill. *Journal of biomechanics*, 41(12):2628–2632, 2008.
- [32] Daniel Roetenberg, Henk Luinge, and Per Slycke. Xsens mvn: full 6dof human motion tracking using miniature inertial sensors. Xsens Motion Technologies BV, Tech. Rep, 1, 2009.
- [33] Jacqueline Romkes and Katrin Bracht-Schweizer. The effects of walking speed on upper body kinematics during gait in healthy subjects. *Gait & posture*, 54:304–310, 2017.

- [34] Renaud Ronsse, Nicola Vitiello, Tommaso Lenzi, Jesse van den Kieboom, Maria Chiara Carrozza, and Auke Jan Ijspeert. Human–robot synchrony: flexible assistance using adaptive oscillators. *IEEE Transactions on Biomedical Engineering*, 58(4):1001–1012, 2011.
- [35] Desney Tan and Anton Nijholt. Brain-computer interfaces and human-computer interaction. In *Brain-Computer Interfaces*, pages 3–19. Springer, 2010.
- [36] Samir K Trehan, Aviva L Wolff, Mandi Gibbons, Howard J Hillstrom, and Aaron Daluiski. The effect of simulated elbow contracture on temporal and distance gait parameters. *Gait & posture*, 41(3): 791–794, 2015.
- [37] Michael R Tucker, Jeremy Olivier, Anna Pagel, Hannes Bleuler, Mohamed Bouri, Olivier Lamercy, José del R Millán, Robert Riener, Heike Vallery, and Roger Gassert. Control strategies for active lower extremity prosthetics and orthotics: a review. *Journal of neuroengineering and rehabilitation*, 12(1):1, 2015.
- [38] Brian R Umberger. Effects of suppressing arm swing on kinematics, kinetics, and energetics of human walking. *Journal of biomechanics*, 41(11):2575–2580, 2008.
- [39] Heike Vallery and Martin Buss. Complementary limb motion estimation based on interjoint coordination using principal components analysis. In *2006 IEEE Conference on Computer Aided Control System Design, 2006 IEEE International Conference on Control Applications, 2006 IEEE International Symposium on Intelligent Control*, pages 933–938. IEEE, 2006.
- [40] Heike Vallery, Ralf Ekkelenkamp, Martin Buss, and Herman van der Kooij. Complementary limb motion estimation based on interjoint coordination: experimental evaluation. In *2007 IEEE 10th International Conference on Rehabilitation Robotics*, pages 798–803. IEEE, 2007.
- [41] Heike Vallery, Rainer Burgkart, Cornelia Hartmann, Jürgen Mitternacht, Robert Riener, and Martin Buss. Complementary limb motion estimation for the control of active knee prostheses. *Biomedizinische Technik/Biomedical Engineering*, 56(1):45–51, 2011.
- [42] RC Wagenaar and REA Van Emmerik. Resonant frequencies of arms and legs identify different walking patterns. *Journal of biomechanics*, 33(7):853–861, 2000.
- [43] David Webb, Russell H Tuttle, and Michael Baksh. Pendular activity of human upper limbs during slow and normal walking. *American Journal of Physical Anthropology*, 93(4):477–489, 1994.
- [44] Tingfang Yan, Marco Cempini, Calogero Maria Oddo, and Nicola Vitiello. Review of assistive strategies in powered lower-limb orthoses and exoskeletons. *Robotics and Autonomous Systems*, 64:120–136, 2015.
- [45] Ziva Yizhar, Spiro Boulos, Omri Inbar, and Eli Carmeli. The effect of restricted arm swing on energy expenditure in healthy men. *International journal of rehabilitation research*, 32(2):115–123, 2009.
- [46] Jungwon Yoon, Bondhan Novandy, Chul-Ho Yoon, and Ki-Jong Park. A 6-dof gait rehabilitation robot with upper and lower limb connections that allows walking velocity updates on various terrains. *IEEE/ASME Transactions on Mechatronics*, 15(2):201–215, 2010.
- [47] Aaron J Young and Daniel P Ferris. State of the art and future directions for lower limb robotic exoskeletons. *IEEE Transactions on Neural Systems and Rehabilitation Engineering*, 25(2):171–182, 2017.
- [48] E Paul Zehr. Neural control of rhythmic human movement: the common core hypothesis. *Exercise and sport sciences reviews*, 33(1):54–60, 2005.
- [49] E Paul Zehr and Jacques Duysens. Regulation of arm and leg movement during human locomotion. *The Neuroscientist*, 10(4):347–361, 2004.
- [50] E Paul Zehr, Sandra R Hundza, and Erin V Vasudevan. The quadrupedal nature of human bipedal locomotion. *Exercise and sport sciences reviews*, 37(2):102–108, 2009.